



SOFT AND HARD ELASTICITY OF  
LIQUID CRYSTAL ELASTOMERS



SOFT AND HARD ELASTICITY OF  
LIQUID CRYSTAL ELASTOMERS

John Simeon Biggins

CORPUS CHRISTI COLLEGE  
UNIVERSITY OF CAMBRIDGE



A DISSERTATION  
SUBMITTED FOR THE DEGREE  
OF DOCTOR OF PHILOSOPHY AT THE  
UNIVERSITY OF CAMBRIDGE

2010



# Contents

|   |       |
|---|-------|
| LIST OF FIGURES   | viii  |
| PREFACE   | xiii  |
| SUMMARY   | xvi   |
| NOMENCLATURE  | xviii |
| 1 INTRODUCTION  | 3     |
| 1.1 Describing Deformations   | 5     |
| 1.2 Polymers and Elastomers   | 7     |
| 1.3 Liquid Crystals   | 11    |
| 1.4 Liquid Crystal Polymers   | 14    |
| 1.5 Elastic Model of liquid crystal elastomers                          | 16    |
| 1.6 Soft Elasticity   | 18    |
| 1.7 Hints of complexity - stripe domains                                | 22    |
| 2 SEMISOFT ELASTIC RESPONSE OF MONO-DOMAIN NEMATIC<br>ELASTOMERS        | 27    |
| 2.1 The Compositional Fluctuations Model                                | 28    |
| 2.2 Predictions and successes of compositional fluctuations             | 29    |
| 2.3 Models of semi-softness   | 33    |
| 2.4 Soft elasticity in semi-soft elastomers                             | 39    |
| 2.5 General Consequences of Director Rotation                           | 44    |
| 2.6 Additional softness caused by texture                               | 48    |
| 2.7 Conclusions   | 49    |
| 2.8 Appendix: Algebraic Manipulations between eqn. (2.29)<br>and (2.30) | 51    |

## LIST OF FIGURES

|      |   |            |
|------|---|------------|
| 3    | STRAIN INDUCED POLARIZATION IN NON-IDEAL CHIRAL NE-<br>MATIC ELASTOMERS | <b>53</b>  |
| 3.1  | Introduction  | 53         |
| 3.2  | Phenomenological Approach   | 55         |
| 3.3  | Microscopic Minimal Model   | 60         |
| 3.4  | Example of a Polarization-Strain Curve                                  | 69         |
| 3.5  | Conclusions   | 72         |
| 3.6  | Appendix: Conformation Distribution of the Co-Polymer                   | 74         |
| 4    | CONVEXITY AND TEXTURED DEFORMATIONS                                     | <b>76</b>  |
| 4.1  | Formulating texture problems  | 77         |
| 4.2  | Geometric bound on the deformations made soft by tex-<br>ture           | 78         |
| 4.3  | Continuity of Textured Deformations                                     | 79         |
| 4.4  | Laminate Textures   | 82         |
| 4.5  | Laminates in Ideal Nematic Elastomers                                   | 83         |
| 4.6  | Relaxed Energy Functions  | 94         |
| 4.7  | Physical Interpretation of $W^{qc}$                                     | 98         |
| 4.8  | Length-scale of Textures  | 99         |
| 4.9  | The effect of Non-Ideality  | 100        |
| 4.10 | Smectic Elastomers  | 102        |
| 5    | ELASTICITY OF POLYDOMAIN LIQUID CRYSTAL ELASTOMERS                      | <b>113</b> |
| 5.1  | Models of Poly- and Monodomain Elastomers                               | 113        |
| 5.2  | Nematic Polydomains   | 121        |
| 5.3  | Smectic Polydomains   | 135        |
| 5.4  | Conclusions   | 145        |
| 6    | EPILOGUE  | <b>147</b> |
| 6.1  | Actuation of Polydomain Elastomers                                      | 147        |
| 6.2  | Length Scales in isotropic genesis polydomain nematic<br>elastomers     | 148        |
| 6.3  | Extremely Soft Polydomain elastomers                                    | 149        |
| 6.4  | Elastomers with imprinted director patterns                             | 149        |
| 6.5  | Imprinting of electric order  | 149        |
|      | BIBLIOGRAPHY  | <b>151</b> |

## List of Figures

|      |  |    |
|------|--|----|
| 1.1  | Deformation of a body described by a vector field  | 5  |
| 1.2  | Distortion of a body described by the gradient of a displacement field   | 6  |
| 1.3  | Replacing a polymer conformation with a discrete random walk   | 8  |
| 1.4  | Span vector of a random walk   | 9  |
| 1.5  | Diagrams of isotropic and nematic liquids  | 12 |
| 1.6  | Main chain and side chain nematic polymers   | 14 |
| 1.7  | Photograph of a monodomain elastomer cooling into a stretched aligned state  | 19 |
| 1.8  | Stretches of a nematic elastomer on cooling from the isotropic to the nematic  | 20 |
| 1.9  | Energetic cost of imposing a stretch on a nematic elastomer viewed from the isotropic reference state.                             | 23 |
| 1.10 | Stretching a nematic elastomer perpendicular to its director   | 24 |
| 1.11 | Diagram of the strains in a nematic stripe domain  | 26 |
| 1.12 | Photograph of a nematic stripe domain.   | 26 |
| 2.1  | Stretching a nematic monodomain perpendicular to its director causes sympathetic shears and director rotation                      | 30 |
| 2.2  | Director rotation in a semi-soft nematic elastomer stretched perpendicular to its director.  | 31 |
| 2.3  | Stress-strain plateau in a nematic elastomer stretched perpendicular to its director.  | 32 |
| 2.4  | Experiment to probe the modulus for an incremental shear compounded with an initial stretch perpendicular to the nematic director. | 40 |

LIST OF FIGURES

|      |   |     |
|------|---|-----|
| 2.5  | $C_5$ vs $\lambda$ and $\alpha$ calculated with the chain anisotropy parameter $r = 2$ .  | 45  |
| 2.6  | $C_5$ vs reduced extension ( $\lambda/\lambda_1$ ) calculated with the chain anisotropy parameter $r = 2$ and $\alpha = 0.1$ .                          | 45  |
|      |   |     |
| 3.1  | Applying a “right-hand-rule” to predict the electrical polarization of a stretched nematic elastomer.   | 57  |
| 3.2  | Two species on monomer in a chiral nematic chain.   | 61  |
| 3.3  | 2D Orientations of a chiral molecule in a nematic field.  | 63  |
| 3.4  | A stretched nematic elastomer can lower its energy by spontaneously shearing.   | 70  |
| 3.5  | Polarization strain curve for a chiral nematic elastomer.   | 72  |
| 3.6  | Diagram of a nematic stripe domain  | 73  |
|      |   |     |
| 4.1  | Compatible deformations and rank-1 connectivity   | 81  |
| 4.2  | Compatibility of shear across a plane boundary  | 82  |
| 4.3  | Nematic directors form equal and opposite angles on either side of plane boundaries in laminate textures  | 84  |
| 4.4  | Relaxed ideal nematic energy function   | 95  |
| 4.5  | Relaxed elastic energy functions in 1D are convex.  | 96  |
| 4.6  | Smectic-A and Smectic-C Liquid Crystals   | 103 |
| 4.7  | Laminates in SmA elastomers   | 104 |
| 4.8  | Laminates in SmC elastomers   | 107 |
| 4.9  | Class I SmC stripe domain   | 108 |
| 4.10 | Class II SmC stripe domain  | 109 |
| 4.11 | Shear angle associated with SmC stripe domains  | 110 |
|      |   |     |
| 5.1  | Visualizations of the set of deformations with a soft response in nematic elastomers, excluding and including the possibility of textured deformations. | 118 |
| 5.2  | Visualizations of the non-overlapping sets of soft deformations for different domains in a nematic genesis liquid crystal elastomer                     | 119 |
| 5.3  | Bounds on the free energy density of an isotropic genesis polydomain nematic elastomer  | 130 |
| 5.4  | Upper and lower bounds on the stress-strain curve for a non-ideal isotropic genesis polydomain  | 131 |

## LIST OF FIGURES

|     |   |     |
|-----|---|-----|
| 5.5 | Mechanically incompatible nematic director field  | 135 |
| 5.6 | Bounds on the free energy density of an ideal nematic genesis polydomain                | 136 |
| 5.7 | Estimate of stress vs strain for an ideal nematic genesis polydomain elastomer          | 137 |
| 5.8 | Spontaneous distortion of an elastomer cooling from a SmA to a SmC liquid crystal phase | 140 |



## Preface

IT HAS BEEN a privilege and a pleasure to spend the last three years thinking about liquid crystal elastomers. The richness of their behavior and the comparative simplicity of its description have made this field an extremely engaging and enjoyable one in which to learn the art of research. I have also been consistently comforted to know that liquid crystal elastomers are real macroscopic materials that one can see, touch and stretch. I have been extremely lucky to have been supervised on this journey by Mark Warner who is in many ways the father of the field and who's deep understanding has guided me through many intellectual quagmires. Mark has also been an exceptional and dedicated teacher, and I hope that I have learnt from him not only his field but something of his insightful and intuitive approach to physical reasoning.

This thesis documents my first steps into the world of research, taken mainly in the Theory of Condensed Matter Group in Cambridge University's Cavendish Laboratory where I have been enrolled as a Ph.D. student. However, I have also been closely supervised by Kaushik Bhattacharya, first during an extended visit by me to the California Institute of Technology's Mechanical Engineering department and then during his sabbatical in Cambridge. Kaushik's experience with martensitic metals has provided an invaluable guide for my thoughts about polydomain elastomers. Kaushik also taught me about elasticity, and, perhaps as importantly, convinced me that formal mathe-

matics can really be helpful in physical problems.

Many other people have guided and supported me during the last three years. I have had occasional but highly informative discussions with Eugine Terentjev, Kenji Urayama, James Adams, Daniel Corbett, Carl Modes and David Khemelinski, and it has always been reassuring to know that my second supervisor, Mike Payne, would help if I encountered difficulties. I have also enjoyed some highly engaging if unrelated supervision from Ben Simons. I would like to thank Tracey Ingham and Micheal Rutter for keeping TCM and its computers running, and Thomas Fink and Rob Farr for producing the style-sheet for this thesis. I acknowledge financial support from the Cambridge University Sims Fund and the Powell Foundation who supported me in Cambridge and Caltech respectively, and Corpus Christi College, which has provided a stimulating community, a beautiful home and many friends. Finally I thank my family for supporting and nurturing my interest in science, and my fellow Ph.D. students Alex Silver, Jamie Blundel, David O'Regan, Jonathan Edge and Robert Lee for providing intellectual and emotional support throughout the last three years.

This thesis is the result of my own work and includes nothing which is the outcome of work done in collaboration or which has been submitted for a previous degree except where specifically indicated in the text. It is also less than 60,000 words in length. Most of the results in this thesis have already been published as papers in scientific journals on which I am first or sole author. The results in Chapter 2 were published in [14], and those in Chapter 3 in [11]. Chapter 4 combines ideas from a review paper [12] and a research paper [13], while the main ideas in Chapter 5 were presented in a short letter [16], and a longer manuscript [15] has been prepared for publication but not yet submitted to a journal. However, I hope that in this thesis these ideas

PREFACE

form a coherent narrative with consistent notation, recurring themes and minimal repetition.

John Simeon Biggins  
Corpus Christi College  
May 2010

## Summary

L IQUID CRYSTAL ELASTOMERS (LCEs) are rubber like materials formed by cross-linking liquid crystal polymers that combine the mobile orientational order of liquid crystals with the extreme stretchiness of rubber. A powerful symmetry argument introduced by Golubovic and Lubensky suggests that LCEs should permit certain deformations to be imposed without energetic cost. These “soft” deformations are associated with Goldstone like rotations of the liquid crystal director inside the elastomer, and consequently depend on the existence of an isotropic state accessed when the elastomer is heated to destroy the liquid crystal order.

In this thesis I discuss the limitations of the above symmetry argument and consider the elastic behavior of less idealized but more realistic models. If an elastomer is prepared by cross-linking a nematic polymer in a high temperature isotropic state then, on cooling, the rods align locally but choose different liquid crystal directors at different points in the elastomer, resulting in the formation of a polydomain that is macroscopically isotropic. If the elastomer is to be prepared as a monodomain then a preferred alignment direction must be imprinted at cross-linking, breaking the isotropy of the state and limiting the softness of the elasticity. I present phenomenological arguments showing that the resulting monodomain will still show qualitatively soft behavior, and, at some stretches, the modulus for additional extension will vanish altogether. Furthermore, chiral nematic monodomains will

## SUMMARY

exhibit strain-induced electrical polarization, unlike nematic liquids or conventional elastomers.

One of the most dramatic consequences of soft and “semi-soft” elasticity is the formation of textured deformations. These are deformations in which the elastomer breaks into many small regions each of which undergoes a different low energy deformation, allowing the elastomer to undergo some macroscopic deformations softly that would have been energetically expensive to impose affinely. In this thesis I review our current understanding of textured deformations in liquid crystal elastomers and present new results about the morphology of some textured deformations in both nematic and smectic monodomain LCEs. I also consider the polydomains, both nematic and smectic, formed in the absence of imprinting and show that, through the formation of textured deformations, these elastomers can deform very softly. However, polydomains cross-linked in an aligned polydomain state rather than the isotropic state will be as hard as a conventional elastomer. This is in marked contrast to monodomain samples which display the same “semi-soft” behavior irrespective of the cross-linking state.

# Nomenclature

**T**HIS THESIS ASSUMES THAT the reader is familiar with standard mathematical notation at a level commensurate with a numerate undergraduate degree. A few conventions that will be followed throughout are recorded here to avoid confusion. Vectors will be set in bold, while second rank tensors will be double underlined. The individual components of either may be referenced using suffix notation, so  $u_i$  refers to the  $i$ th component of  $\mathbf{u}$  and  $\lambda_{xz}$  refers to the  $x - z$  component of  $\underline{\lambda}$ . The indices  $i$ ,  $j$  and  $k$  will be used following the Einstein summation convention, while the more explicit  $x$ ,  $y$  and  $z$  indices will not. A list of commonly used symbols is given below.

## COMMONLY USED SYMBOLS

- $a$  Persistence length of a polymer, and the step length of the corresponding random walk
- $\mathbf{a}$  Vector in the plane separating two deformations in a textured deformation in the reference state.
- $\mathbf{a}'$  Vector in the plane separating two deformations in a textured deformation in the final state.
- $b$  Length of the smaller arm in an L shaped monomer
- $\hat{\mathbf{c}}$  Electrical Polarization in SmC\*
- $\mathbf{d}$  Dipole of a chiral nematic monomer
- $F$  Free energy density and Free energy
- $k_b$  Boltzmann's constant

## NOMENCLATURE

- k** Smectic layer normal
- $K^{qc}$  The set of all deformations made soft after full, possibly textured, relaxation of the energy
- $K^0$  The set of all soft affine deformations
- $K^m$  The set of all deformations made soft after the use of  $m$ th rank laminates
- $\underline{\underline{\ell}}$  Step length tensor for liquid crystal polymer in the final state
- $\underline{\underline{\ell}}_0$  Step length tensor for liquid crystal polymer in the cross-linking/reference state
- $L$  Arc length of a polymer
- m** Boundary normal between two deformations in a textured deformation in the reference state.
- m'** Boundary normal between two deformations in a textured deformation in the final state.
- $\hat{\mathbf{n}}$  Liquid crystal director in the final state
- $\hat{\mathbf{n}}_0$  Liquid crystal director in the cross-linking/reference state
- $n_s$  Number density of cross-links in an elastomer
- $N$  Number of steps of length  $a$  in the random walk describing a polymer
- p** Electrical Polarization
- $\underline{\underline{Q}}$  Liquid crystal order parameter tensor
- $Q$  Liquid crystal scalar order parameter
- $\underline{\underline{R}}$  Rotation Matrix
- R** Polymer Strand Vector and vector between points embedded in elastic solid
- $r$  Anisotropy ratio of  $\underline{\underline{\ell}}$
- $\underline{\underline{S}}$  Symmetric Matrix
- $T$  Absolute temperature

## NOMENCLATURE

- $\hat{\mathbf{u}}$  Vector pointing along a liquid crystal rod
- $\mathbf{V}$  Polymer binormal
- $W$  Generic energy function/cost function
- $\alpha$  Parameter of semi-softness
- $\underline{\gamma}$  Deformation gradient from the cross-linking state
- $\underline{\underline{\delta}}$  Identity matrix
- $\lambda_1, \lambda_2, \lambda_3$  The principal values of the matrix  $\underline{\underline{\lambda}}$ , with  $\lambda_1 \leq \lambda_2 \leq \lambda_3$ . In some contexts  $\lambda_1$  is also used as a threshold extension.
- $\lambda$  A scalar extension ratio
- $\underline{\lambda}$  Deformation gradient tensor
- $\underline{\Lambda}$  Deformation from an unstable state
- $\mu$  Shear modulus of rubber, normally  $n_s k_b T$
- $\Omega$  Region of space occupied by an undeformed elastic body
- $\sigma$  Engineering stress  $\sigma = \frac{dF}{d\lambda}$

SOFT AND HARD ELASTICITY OF  
LIQUID CRYSTAL ELASTOMERS



# Chapter 1

## INTRODUCTION

L IQUID CRYSTAL ELASTOMERS are remarkable materials that sit at the interface between solids and liquids. A causal observer presented with a sample would conclude that it was a fairly ordinary piece of rubber, and most certainly a solid. However, if our observer probed the sample more carefully, they would discover that their rubber changed length dramatically when heated past a certain temperature, and that, while in one direction it stretched just like a elastic band, in the other two directions it offered scarcely any resistance to stretching at all. We are familiar with many substances that do not resist deformation, but we usually call them liquids and say that they are flowing. Liquid crystal elastomers, which resist some deformations and not others, are a completely novel type of material that truly does blur the distinction between a solid and a liquid.

It is perhaps less surprising to find liquid crystal elastomers occupying a space between solids and liquids when we consider their two constituents. Liquid crystals are liquids of rod shaped molecules in which the rods point in the same direction, so although they flow like a liquid, they are anisotropic and have long range orientational order like a solid crystal. Elastomers, in contrast, are melts of polymer molecules in which chemical cross-links between the polymer strands

have been introduced, turning the liquid melt into a solid rubber. Although elastomers resist deformation like a solid, they have no long range order and the individual polymer strands are in thermal motion just like in a liquid polymer melt. Liquid crystal elastomers, which are a hybrid of these two ideas achieved by cross-linking liquid-crystal-polymer melts, therefore combine two elements that already mix the properties of liquids and solids.

This thesis is an exploration of the elastic theory of liquid crystal elastomers focussing on the two questions “when do liquid crystal elastomers deform without resistance?” and “what limits how small the resistance they offer actually is?” The remainder of this chapter will be devoted to the essential building blocks of the subject: elasticity, liquid-crystals, polymers rubbers, and symmetry breaking soft elasticity. Chapter 2 will examine deformation without resistance in monodomain nematic elastomers, providing a phenomenological description of the terms in the free energy that limit their softness but that still predict true zeroes in the shear modulus at certain extensions. Chapter 3 will show that, although idealized perfectly soft mono-domain nematic elastomers cannot show strain induced electrical polarizations, real non-ideal samples can. Chapter 4 describes how the addition of a few soft modes of deformation into an otherwise solid energy function can result in the formation of rich microstructures in response to imposed deformations and describe the morphology of some such microstructures, while Chapter 5 will use results originating in the study of textured deformations to show that some polydomain elastomers can deform even more softly than their monodomain counterparts.

Except where explicitly marked, the work in this thesis is the result of my own original research. The introduction and chapter 4 necessar-

ily include extended descriptions of older results that my work builds upon.

### 1.1 DESCRIBING DEFORMATIONS

Elasticity is rich and venerable subject, and over the years many complimentary approaches to the subject have been developed and many excellent books have been written [6, 43]. Here we will use a description based on the deformation gradient  $\underline{\lambda}$  which is well suited to liquid crystal elastomers because it can describe the full geometric effect of arbitrarily large strains and rotations of both the final and target state.

To study elasticity problems we must first consider a body in a reference configuration to deform. We consider an elastic body at rest in a reference configuration, and define the region of space it occupies to be  $\Omega$  and each point in the body to be labeled by a position vector  $\mathbf{x}$ . Any deformation of the body can be described by a vector function  $\mathbf{x}'(\mathbf{x})$  that gives the new position vector of each point in the body, the result of which will be to cause the body to occupy a different region of space  $\Omega'$ . This is illustrated in Fig. 1.1.

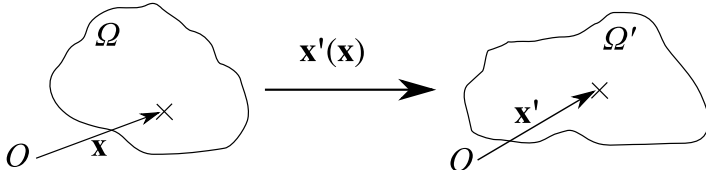


Figure 1.1: Left: An undeformed solid body occupying a region of space  $\Omega$ . Each point on the body is labeled by its position vector  $\mathbf{x}$ . Right: The same body after a deformation has been applied, now occupying the region  $\Omega'$ . A point at  $\mathbf{x}$  in the old body is now at position  $\mathbf{x}'(\mathbf{x})$ . The crosses in both diagrams correspond to the same point in the material.

To characterize the distortion of the above body caused by this deformation we imagine embedding a small vector  $\mathbf{R}$  between two points in the reference state and calculating what it becomes in the deformed state. If the vector spans between  $\mathbf{x}_1$  and  $\mathbf{x}_2$  in the reference state ( $\mathbf{R} = \mathbf{x}_1 - \mathbf{x}_2$ ) then in the deformed state it will be  $\mathbf{R}' = \mathbf{x}'(\mathbf{x}_1) - \mathbf{x}'(\mathbf{x}_2)$ . This configuration is drawn in Fig. 1.2. Taylor expanding  $\mathbf{x}'$  about  $\mathbf{x}'(\mathbf{x}_1)$  and keeping only the first order term (because  $\mathbf{x}_2$  is near  $\mathbf{x}_1$ ) we see that  $\mathbf{R}' = \frac{d\mathbf{x}'}{d\mathbf{x}} \mathbf{R}$ . We define this important first derivative that characterizes the local distortion of the body as the deformation gradient  $\underline{\lambda}(\mathbf{x}) = \frac{d\mathbf{x}'}{d\mathbf{x}}$ . A deformation is called homogenous if  $\underline{\lambda}$  is constant throughout the body. In this case there are no higher order terms in the Taylor expansion of  $\mathbf{x}'(\mathbf{x})$  so any vector  $\mathbf{R}$  embedded between two points in the reference configuration will become  $\underline{\lambda} \cdot \mathbf{R}$  in the deformed configuration.

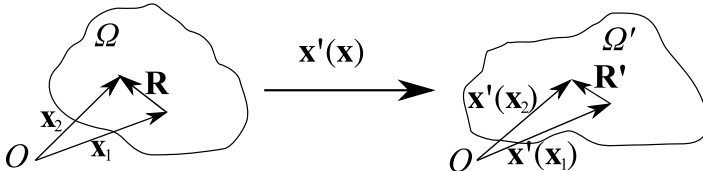


Figure 1.2: A vector connecting two material points,  $\mathbf{R}$  becomes  $\mathbf{R}'$  after the deformation  $\mathbf{x}'(\mathbf{x})$  is applied. The two vectors are related by  $\mathbf{R}' = \underline{\lambda} \cdot \mathbf{R}$  where  $\underline{\lambda}(\mathbf{x}) = \frac{d\mathbf{x}'}{d\mathbf{x}}$  if the two points are very close to each other.

The deformation gradient tensors for homogenous deformation are the same as the transformation matrices met in elementary mathematics — if the deformation was a rotation it is a rotation matrix, if it was a shear it is a shear matrix etc. If a second deformation is applied to the deformed state the total deformation gradient is simply the matrix product of the two separate deformations. Elasticity in elastomers often involves very large deformations so, unlike in many other systems,

## INTRODUCTION

these matrix products cannot be expanded and linearized about the identity matrix.

We can gain great insight into the nature of homogenous deformations by applying the polar decomposition theorem to the second rank tensor  $\underline{\lambda}$ . This tells us that we can always write  $\underline{\lambda} = \underline{R} \cdot \underline{S}$  where  $\underline{R}$  is a rotation matrix, and  $\underline{S}$  is a symmetric matrix and hence in some frame diagonal. This means that any deformation can be thought of as a simple stretch, with three orthogonal principal axes, followed by a body rotation. Since only the former involves any distortion of the body, the amount of distortion is completely described by the three (positive) eigenvalues of  $\underline{S}$ ,  $\lambda_1 \leq \lambda_2 \leq \lambda_3$ , which are called the principal values of the deformation  $\underline{\lambda}$ . The volume of the deformed body is simply the volume of the body in the reference state multiplied by  $\det \underline{\lambda} = \lambda_1 \lambda_2 \lambda_3$ , which can easily be visualized by imagining a unit cube in the reference state whose edges align with the principal axes of  $\underline{S}$  — after deformation the cube will be a cuboid with edges of length  $\lambda_1$ ,  $\lambda_2$  and  $\lambda_3$  so its total volume has increased by a factor of  $\det \underline{\lambda}$ .

Although the deformation gradient tensor  $\underline{\lambda}(\mathbf{x})$  contains all the information about a deformation, there is one important consideration that must not be forgotten, namely that  $\underline{\lambda}$  is the gradient of a vector field, so that a  $\underline{\lambda}(\mathbf{x})$  only corresponds to a legitimate deformation if it is curl free.

## 1.2 POLYMERS AND ELASTOMERS

The most basic question one might ask about an elastic deformation is how much energy it cost to impose. To answer this question we need to express the energy of the system as a function of the deformation gradient, that is we need to find  $E(\underline{\lambda})$ , and if we can construct  $E(\underline{\lambda})$

from microscopic considerations then it will connect our microscopic understanding of the material with its macroscopic elastic properties. In this section we will recall how this is done for the simple case of gaussian rubber, before extending this to liquid-crystal rubbers in later sections.

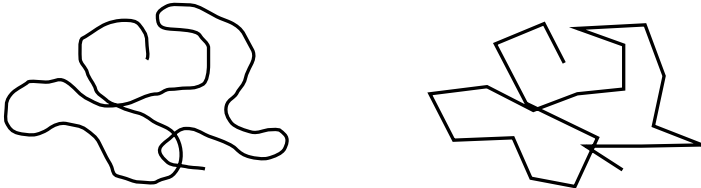


Figure 1.3: A polymer conformation in 2D with a characteristic length  $a$  over which the tangent vector does not change (left) can be modeled as a random walk with step length  $a$  (right).

Polymers are molecules that are characterized by being very long and thin. They are synthesized in polymerization reactions in which many copies of an underlying monomer are joined together in a long string, so the resulting polymer may be thousands of times longer than it is wide. In a melt of many such polymer strands the individual strands undergo a great deal of thermal motion, causing them not only to move past each other, but to wrap round each other and buffet each other. This overall result of this motion is that the conformation of a given strand is constantly changing. Polymers have a certain amount of rigidity which makes them difficult to bend over small arc distances, so we define a characteristic distance  $a$  (corresponds to the length of one monomer for many systems) which marks the division between length scales the polymer does and does not bend over in the melt. If we then divide the length of the polymer strand into  $N$  pieces of length  $a$ , we expect each piece to be essentially straight, but the adjacent pieces to be pointing in different completely uncorrelated directions, so we can model the conformations of the polymer by a

## INTRODUCTION

random walk with  $N$  steps each of length  $a$ , as illustrated in Fig. 1.3. If the direction of the  $i$ th step is given by the vector  $\mathbf{v}_i$  then the end to end span vector associated with a given conformation  $\mathbf{R}$  (see Fig. 1.4) is simply

$$\mathbf{R} = \sum_{i=1}^N a\mathbf{v}_i. \quad (1.1)$$

In the limit of large  $N$  we can apply the central limit theorem to

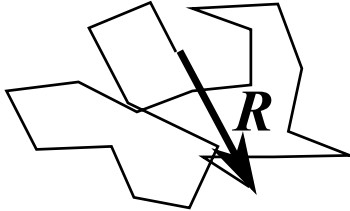


Figure 1.4: The vector  $\mathbf{R}$  is the span of the polymer conformation.

each of the three spatial dimensions of this sum, remembering that  $\langle \mathbf{v}_x \cdot \mathbf{v}_x \rangle = \frac{1}{3}$  in 3D, to conclude that

$$P(\mathbf{R}) \propto \exp\left(-\frac{3\mathbf{R} \cdot \mathbf{R}}{2Na^2}\right). \quad (1.2)$$

Recognizing  $Na = L$ , the contour length of the chain, we can rewrite this as

$$P(\mathbf{R}) \propto \exp\left(-\frac{3\mathbf{R} \cdot \mathbf{R}}{2La}\right). \quad (1.3)$$

As with any random walk, typical strands have span vectors that are proportional to the square root of their total arc length. If we have a melt of such polymer strands, their span vectors will be following this distribution. We turn such a melt into a rubber by introducing cross-linking molecules that form chemical links between the chains, preventing the strands from macroscopically flowing. Provided there are enough cross-links that every strand is cross-linked into the net-

work, but few enough cross-links that the span between cross-links is still very much larger than  $a$ , then the distribution of span vectors between cross-links will also follow the above distribution, where  $N$  is now the number of steps between cross-links rather than between ends.

We bridge the gap between these probability distributions and an energy function by using statistical mechanics. The partition function  $Z$  for a chain constrained to a span vector  $\mathbf{R}$  is simply proportional to  $P(\mathbf{R})$  since all conformations have the same energy, so the free energy of such a strand is given by  $F = -k_B T \ln Z$ , giving

$$F(\mathbf{R}) = k_b T \frac{3\mathbf{R} \cdot \mathbf{R}}{2La} + C, \quad (1.4)$$

where  $C$  is an irrelevant additive constant that we will subsequently ignore. If we now consider applying a deformation  $\underline{\underline{\lambda}}$  to our solid rubber, then a span between cross-links that was previously  $\mathbf{R}$  will become  $\underline{\underline{\lambda}} \cdot \mathbf{R}$ , and the free energy associated with the span will be  $F(\underline{\underline{\lambda}} \cdot \mathbf{R})$ . Averaging  $F(\underline{\underline{\lambda}} \cdot \mathbf{R})$  over initial span vectors  $\mathbf{R}$ , using the above distribution for the initial span vectors, we get the average free energy per cross-link of the deformed rubber

$$\langle F_s \rangle = \frac{1}{2} k_b T \text{Tr} (\underline{\underline{\lambda}} \cdot \underline{\underline{\lambda}}^T). \quad (1.5)$$

Multiplying this by the number density of cross-links  $n_s$  and defining the shear modulus  $\mu = n_s k_b T$ , the energy density of our rubber is simply

$$F = \frac{1}{2} \mu \text{Tr} (\underline{\underline{\lambda}} \cdot \underline{\underline{\lambda}}^T). \quad (1.6)$$

This is the energy function that allows us to calculate the cost of imposing a deformation. We notice it has two important symmetries, if we replace  $\underline{\underline{\lambda}}$  by either  $\underline{\underline{R}} \cdot \underline{\underline{\lambda}}$  or  $\underline{\underline{\lambda}} \cdot \underline{\underline{R}}$ , where  $\underline{\underline{R}}$  is a rotation matrix,

## INTRODUCTION

then the energy of the system is unchanged. This corresponds to the energy not changing if we rotate the sample after we apply the deformation, reflecting the isotropy of space, and not changing if we rotate the sample before deformation, reflecting the isotropy of the rubber.

The above energy appears to be minimized at  $\underline{\lambda} = \text{diag}(0, 0, 0)$ , which would correspond to the rubber collapsing to a point. This is because we have neglected to include the energetic cost associated with the monomers being squeezed on top of each other, which in reality is very high. This causes rubber to have a bulk modulus several orders of magnitude higher than  $\mu$ , so rather than include it explicitly in the energy, it is better to replace it by the constraint that  $\det \underline{\lambda} = 1$ .

### 1.3 LIQUID CRYSTALS

Liquid crystal phases are also mixtures of long thin molecules, but in this case the molecules are rigid rods rather than floppy chains, and the molecules typically have fairly modest aspect ratios (3-10) rather than the huge aspect ratios of polymers. An extensive understanding of liquid crystals has been developed over the last 50 years, and, as with elasticity, they are the subject of several books [26], but here the briefest of overviews will suffice. In an isotropic fluid made of rod shaped molecules, if we associate each molecule with a vector  $\hat{\mathbf{u}}$  which points along its length, then the average of  $\hat{\mathbf{u}}$  over all the rods in the liquid,  $\langle \hat{\mathbf{u}} \rangle$ , will certainly be zero, if it was not then the fluid would have some preferred direction and not be isotropic. If we calculate the expectation of the next moment of the rod distribution,  $\langle u_i u_j \rangle$  (where the subscripts denote the spatial components of  $\hat{\mathbf{u}}$  and the average is once again over all the rods), then this is simply  $\frac{1}{3}\delta_{ij}$ , since the average of  $\cos^2 \theta$  in 3 dimensions is a third. Reassuringly, this is also

isotropic.

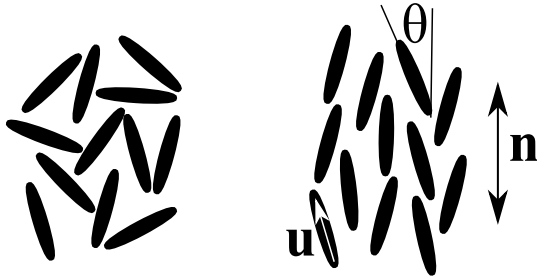


Figure 1.5: In an isotropic liquid the rods have no average alignment (right) while in a nematic liquid (right) they do.

Nematic order arises when a fluid of rods is cooled down. Below some temperature the rods tend to align in an average direction, although they do not have any positional ordering and the resulting material is still a liquid. Nematic phases are quadropolar, meaning that although the phases distinguishes one axis — the alignment axis — it does not distinguish up from down along this axis, so reflecting the whole phase in a plane perpendicular to this axis does not appear to change the phase at all. This means that in the nematic state  $\langle \hat{\mathbf{u}} \rangle$  is still zero. However, if each rod makes an angle  $\theta$  with the axis of average alignment, illustrated in Fig. 1.5, and we assume the azimuthal directions are evenly distributed the next moment,  $\langle u_i u_j \rangle$ , is given by

$$\langle u_i u_j \rangle = \left\langle \begin{pmatrix} \frac{1-\cos^2(\theta)}{2} & 0 & 0 \\ 0 & \frac{1-\cos^2(\theta)}{2} & 0 \\ 0 & 0 & \cos^2(\theta) \end{pmatrix} \right\rangle. \quad (1.7)$$

As we have already observed, if the distribution is isotropic then this collapses to  $\frac{1}{3}\delta$ . We can make a good order parameter that is zero in the isotropic state and finite in the nematic state by subtracting  $\frac{1}{3}\delta$

## INTRODUCTION

from this average to make it traceless. Convention dictates that the actual order parameter  $\underline{\underline{Q}}$  is then three-halves of this quantity, giving

$$Q_{ij} = \left\langle \frac{3}{2}u_i u_j - \frac{1}{2}\delta_{ij} \right\rangle, \quad (1.8)$$

which can be represented in terms of the scalar order parameter  $Q = \left\langle \frac{1}{2}(3\cos^2(\theta) - 1) \right\rangle$ , which expresses the magnitude of the ordering, and  $\hat{\mathbf{n}}$  which captures the direction of the alignment, as

$$\underline{\underline{Q}} = Q \left( \frac{3}{2}\hat{\mathbf{n}}\hat{\mathbf{n}} - \frac{1}{2}\underline{\underline{\delta}} \right). \quad (1.9)$$

The isotropic phase then corresponds to  $Q = 0$ , while the nematic phase is specified by a finite values of  $Q$  and a direction of alignment  $\hat{\mathbf{n}}$ .

Having identified the correct order parameter, we can now conduct a Landau expansion of the free energy (called a Landau de-Gennes expansion in this context) to study the mean field behavior of the phase transition, writing

$$F(\underline{\underline{Q}}) = A \text{Tr} \left( \underline{\underline{Q}} \cdot \underline{\underline{Q}} \right) + B \text{Tr} \left( \underline{\underline{Q}} \cdot \underline{\underline{Q}} \cdot \underline{\underline{Q}} \right) + C \text{Tr} \left( \underline{\underline{Q}} \cdot \underline{\underline{Q}} \cdot \underline{\underline{Q}} \cdot \underline{\underline{Q}} \right) + \dots \quad (1.10)$$

For the purposes of this thesis, it is sufficient to note that this contains odd powers of  $Q$  so the transition from the isotropic to the nematic will be first order. Furthermore, it is possible to construct microscopic theories of the isotropic-nematic transition that predict the values of these coefficients and consequently the transition temperature. Again, for the purposes of this thesis, such development is not necessary, except to note that the characteristic scale of the free energy is  $k_B T$  per rod.

## 1.4 LIQUID CRYSTAL POLYMERS

The ideas of liquid crystals and polymers collide in liquid crystal polymers [29]. These are polymer melts which incorporate rigid liquid crystal rods either directly into the main chain of the polymer or as pendent like side chains. These two possibilities are illustrated in Fig. 1.6. The effect of the liquid crystal phase is to bias the polymer so

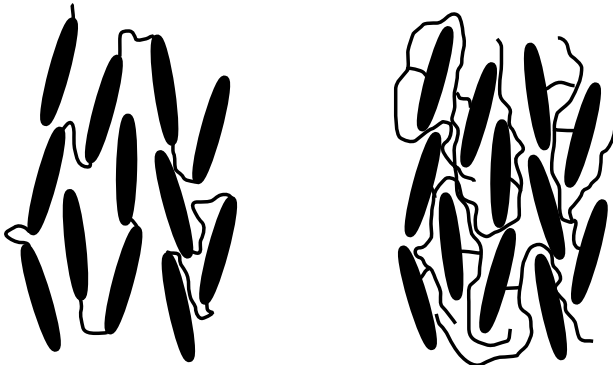


Figure 1.6: Liquid crystal rods can be incorporated into polymer strands either as constituents of the main chain (left) or side chains (right)

that any given segment is more likely to be aligned with the nematic direction than any other. We can include this in our random walk model of polymer distributions by biasing the walk, either by making it more likely to take steps along the nematic director or, equivalently, by making the effective step length for steps along the director longer than steps taken in perpendicular directions. Taking this latter view, the new span vector distribution can be derived exactly as before, but the variance is now different in the directions parallel and perpendicular to the nematic director, giving

$$P(\mathbf{R}) \propto \exp\left(-\frac{3R_{\perp}^2}{2Na_{\perp}^2}\right) \exp\left(-\frac{3R_{\parallel}^2}{2Na_{\parallel}^2}\right). \quad (1.11)$$

## INTRODUCTION

We can write this in a form very reminiscent of eqn. (1.3) — if the total contour length of the chain in  $L$  then we can introduce a step length tensor  $\underline{\ell} = (N/L)(a_{\perp}^2 \underline{\delta} + (a_{\parallel}^2 - a_{\perp}^2)\hat{\mathbf{n}}\hat{\mathbf{n}})$  and write this as

$$P(\mathbf{R}) \propto \exp\left(-\frac{3\mathbf{R} \cdot \underline{\ell}^{-1} \cdot \mathbf{R}}{2L}\right). \quad (1.12)$$

In the isotropic phase  $a_{\perp} = a_{\parallel} = a$ ,  $L = Na$  and  $\underline{\ell} = a\underline{\delta}$ , so we recover the original isotropic distribution. In the nematic phase the average length of the component of the span along the director is longer than the perpendicular components, so the polymer tends to adopt oblate conformations that are extended along the nematic director.

The characteristic length over which a polymer can change direction is not changed by the presence of a liquid crystal phase, so the underlying persistence length  $a = L/N$  is still an important and unchanging quantity. This makes it sensible to define  $\underline{\ell} = a(\underline{\delta} + (r-1)\hat{\mathbf{n}}\hat{\mathbf{n}})$ , where  $r$  is a dimensionless number that records the coupling between the nematic phase and the polymer conformations. In our previous notation  $r = (a_{\parallel}/a_{\perp})^2$ .

Although the above discussion is rather phenomenological in nature, one can easily develop microscopic models of this type of behavior which relate  $r$  to  $\underline{\underline{Q}}$  and link  $a$  and  $N$  to the microscopics of the polymer in question. The very simplest example would be to replace the liquid crystal polymer by chains built out of  $N$  freely jointed rods of length  $a$  which are forming a nematic field with order parameter  $\underline{\underline{Q}}$ . This model then leads to the relation [64]

$$r = \frac{1 + 2\underline{\underline{Q}}}{1 - \underline{\underline{Q}}}. \quad (1.13)$$

## 1.5 ELASTIC MODEL OF LIQUID CRYSTAL ELASTOMERS

We have now developed all the tools to build the free energy that governs the elasticity of liquid crystal elastomers. The derivation, first published in [17], follows exactly the same route as the gaussian rubber derivation in section 1.2, but now we must include the possibility that as well as deforming the rubber, the liquid crystal order may also have changed since cross-linking. Liquid-crystal elastomers are the subject of a recent book [64] which discusses more fully this and many other topics introduced briefly in this thesis. Returning to the derivation, as before, the free energy per strand is simply  $-k_B T \ln P(\mathbf{R})$  giving

$$F_s(\mathbf{R}) = k_B T \frac{3\mathbf{R} \cdot \underline{\underline{\ell}}^{-1} \cdot \mathbf{R}}{2L} + C. \quad (1.14)$$

If a strand was cross-linked into the network with a span  $\mathbf{R}$  and then a deformation  $\underline{\lambda}$  was applied, causing the span to change to  $\underline{\lambda} \cdot \mathbf{R}$ , then the new free energy of the strand will be

$$F_s(\mathbf{R}) = k_B T \frac{3(\underline{\lambda} \cdot \mathbf{R}) \cdot \underline{\underline{\ell}}^{-1} \cdot (\underline{\lambda} \cdot \mathbf{R})}{2L} + C \quad (1.15)$$

where  $\underline{\underline{\ell}}$  is the step length tensor caused by the nematic phase in the final state. To get the free energy of the whole sample we must average this over initial span vectors  $\mathbf{R}$ , remembering that the probability distribution of initial span vectors is fixed at cross-linking as

$$P(\mathbf{R}) \propto \exp\left(-\frac{3\mathbf{R} \cdot \underline{\underline{\ell}_0}^{-1} \cdot \mathbf{R}}{2L}\right). \quad (1.16)$$

where  $\underline{\underline{\ell}_0}$  is the step length tensor caused by the nematic phase in the cross-linking state. Performing the average over  $\mathbf{R}$ , the average free

## INTRODUCTION

energy per strand is

$$\langle F_s \rangle = \frac{1}{2} k_b T \text{Tr} \left( \underline{\underline{\lambda}} \cdot \underline{\ell}_0 \cdot \underline{\underline{\lambda}}^T \cdot \underline{\underline{\ell}}^{-1} \right). \quad (1.17)$$

Multiplying this by the number density of strands  $n_s$  and once again defining the shear modulus  $\mu = n_s k_B T$ , this gives a free energy density of

$$F = \frac{1}{2} \mu \text{Tr} \left( \underline{\underline{\lambda}} \cdot \underline{\ell}_0 \cdot \underline{\underline{\lambda}}^T \cdot \underline{\underline{\ell}}^{-1} \right). \quad (1.18)$$

As in the gaussian rubber case, the bulk modulus of nematic elastomers is several orders of magnitude higher than the shear modulus, so rather than include it explicitly in the model, it is better to add the constraint  $\det \underline{\underline{\lambda}} = 1$ .

The above free energy is caused by the conformational entropy of the polymer chains, and has magnitude  $\sim k_b T$  per cross-link. This polymer free energy should really be supplemented by the free energy of the nematic rods. However, this term will have magnitude  $k_b T$  per rod, and since there are many rods per chain, it will be very much larger than the chain free energy. This means that when minimizing the energy over  $\underline{\underline{Q}}$  to find the behavior of the nematic field, the chain free energy will have almost no influence on the magnitude of  $Q$  which will be fixed by the far larger liquid crystal free energy. Since the liquid crystal free energy has no dependence on the direction of  $\hat{\mathbf{n}}$  or  $\underline{\underline{\lambda}}$ , it is therefore sufficient to regard the liquid crystal free energy as imposing a magnitude of  $Q$ , and therefore  $r$ , and then study the elasticity of liquid crystal elastomers by considering just the elastic part of the energy.

## 1.6 SOFT ELASTICITY

Consider a liquid crystal elastomer cross-linked in the isotropic state but then cooled to the nematic state after cross-linking. In the isotropic state  $r = 1$  giving  $\underline{\underline{\ell}} = a\underline{\delta}$ , while in the nematic state  $\underline{\underline{\ell}} = a(\underline{\underline{\delta}} + (r - 1)\hat{\mathbf{n}}\hat{\mathbf{n}})$ . The elastic energy of the liquid crystal elastomer is

$$F = \frac{1}{2}\mu a \text{Tr} (\underline{\underline{\lambda}} \cdot \underline{\underline{\lambda}}^T \cdot \underline{\underline{\ell}}^{-1}). \quad (1.19)$$

We notice that this energy is unchanged by replacing  $\underline{\underline{\lambda}}$  by  $\underline{\underline{\lambda}} \cdot \underline{\underline{R}}$ , where  $\underline{\underline{R}}$  is a rotation matrix, reflecting the fact that rotation of the cross-linking state does not cost any energy since it is isotropic. We also expect it to be unchanged under a rotation of the final state, since body rotation of the whole sample should not cost any energy. This is indeed the case, but to perform this rotation we must replace  $\underline{\underline{\lambda}}$  by  $\underline{\underline{R}} \cdot \underline{\underline{\lambda}}$  and  $\hat{\mathbf{n}}$  by  $\underline{\underline{R}} \cdot \hat{\mathbf{n}}$  so that we have rotated both the body and the liquid crystal field. To minimize this energy over  $\underline{\underline{\lambda}}$  we use the polar decomposition theorem to write  $\underline{\underline{\lambda}} = \underline{\underline{S}} \cdot \underline{\underline{R}}$ , where  $\underline{\underline{S}}$  is a symmetric matrix and  $\underline{\underline{R}}$  is a rotation matrix. As discussed, the energy does not depend on  $\underline{\underline{R}}$  since the cross-linking state was isotropic, and since  $\underline{\underline{\ell}}^{-1}$  is uniaxial, we expect the energy to be minimized by a uniaxial choice of  $\underline{\underline{S}}$  that is coaxial with  $\underline{\underline{\ell}}$ . Volume conservation requires  $\det(\underline{\underline{S}}) = 1$  so we can write  $\underline{\underline{S}} = 1/\sqrt{\lambda}\underline{\underline{\delta}} + (\lambda - 1/\sqrt{\lambda})\hat{\mathbf{n}}\hat{\mathbf{n}} = \text{diag}(\lambda, 1/\sqrt{\lambda}, 1/\sqrt{\lambda})$  in a frame with  $\hat{\mathbf{n}}$  along the  $x$  axis. Substituting this into the free energy gives

$$F = \frac{1}{2}\mu \left( \frac{\lambda^2}{r} + \frac{2}{\sqrt{\lambda}} \right), \quad (1.20)$$

which is minimized at  $\frac{3}{2}\mu r^{1/3}$  by  $\lambda = r^{1/3}$ . This means that when the elastomer cools from the isotropic to the nematic, it must stretch by a factor of  $r^{1/3}$  along the nematic director. This is one of the most dramatic behaviors of nematic elastomers, and is shown in the photos

## INTRODUCTION

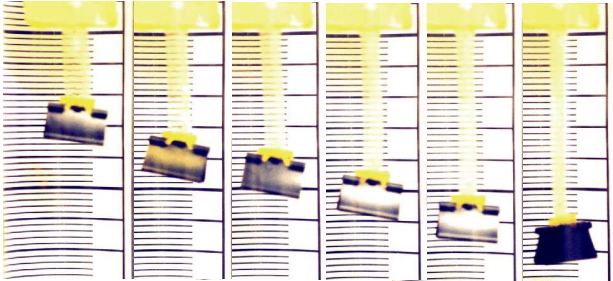


Figure 1.7: Photos of a nematic elastomer cooling from a high temperature isotropic state (left) to a low temperature aligned and stretched state (right).

in Fig. 1.7. Elastomers that spontaneously stretch by 400% have been synthesized, suggesting that systems can be made with  $r$  anywhere between 1 and 50.

The spontaneous extension on cooling has a second dramatic consequence. Since the cross-linking state was isotropic, on cooling the nematic director could have formed in any direction, causing the elastomer to stretch in any direction, as illustrated in Fig. 1.8. This means that there are many equivalent low energy nematic states, each of which has a different nematic director and a different deformation with respect to the cross-linking state. If one deforms one such aligned stretched energy minimizing state into another, equivalent to moving around the arc in Fig. 1.8, this second deformation cannot cost any energy to impose — it must be completely soft. Therefore we see that, as a result of the symmetry breaking nature of the isotropic-nematic transition, we must have a set of completely soft deformations. This symmetry argument for soft elasticity was first proposed by Golubovic and Lubensky [36], and is one of the cornerstones of the theory of nematic elastomers.

We can observe the existence of soft elastic modes in our elastic

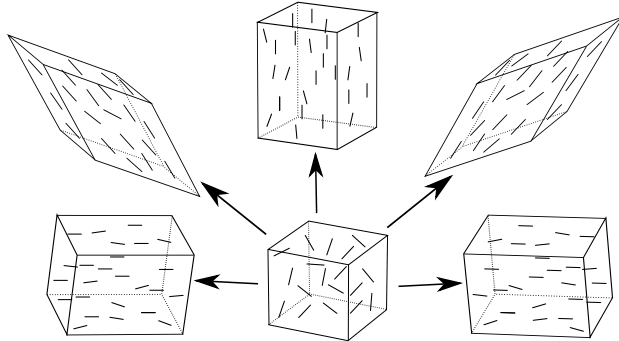


Figure 1.8: A liquid crystalline polymer is cross-linked in the high temperature isotropic state - centre, bottom row. On cooling, a nematic phase is formed and the elastomer stretches along the new nematic director. Since any director could have been chosen there are many equivalent low energy states, shown in an arc around the isotropic state. Deformations around the arc will not cost energy.

energy by considering deformations from the aligned stretched state. Substituting  $\underline{\lambda} = \underline{\lambda}_2 \cdot \left(1/\sqrt{\lambda}\underline{\delta} + (\lambda - 1/\sqrt{\lambda})\hat{\mathbf{n}}\hat{\mathbf{n}}\right)$  into eq. (1.19), so that  $\underline{\lambda}_2$  is the deformation from the aligned stretched state, gives,

$$F = \frac{1}{2}\mu r^{-1/3} \text{Tr} \left( \underline{\lambda}_2 \cdot \underline{\ell}_0 \cdot \underline{\lambda}_2^T \cdot \underline{\ell}^{-1} \right). \quad (1.21)$$

In the above energy  $\underline{\ell}_0$  points along the nematic director in the relaxed aligned state that  $\underline{\lambda}_2$  is the deformation from, and is constructed out of the two spontaneous deformation terms, while  $\underline{\ell}$  is defined in the final state, after the application of  $\underline{\lambda}_2$ <sup>1</sup>. To see soft modes in the above free energy, we observe that not only is it minimized by  $\underline{\lambda}_2 = \underline{\delta}$  and

---

<sup>1</sup>That the energy takes on this form, which is functionally identical to eq. 1.18, is extremely useful, since it means that it is not necessary to keep track of the cross-linking state and complex cross-linking history of a nematic elastomer — the energy function for deformations from a given relaxed state is as if the elastomer had been cross-linked directly in that state.

## INTRODUCTION

$\underline{\underline{\ell}} = \underline{\underline{\ell}}_0$ , it is also minimized by

$$\underline{\lambda}_2 = \underline{\ell}^{1/2} \cdot \underline{\underline{R}} \cdot \underline{\underline{\ell}}_0^{-1/2}, \quad (1.22)$$

with any choice of director for  $\underline{\ell}$  and any choice of rotation matrix  $\underline{\underline{R}}$ . This is a continuous set of deformations that can be applied to the aligned nematic state without energy cost. These microscopic arguments for soft elasticity, pioneered in [48, 61], go beyond the purely symmetry based arguments in one important respect. Although we have been considering a system cross-linked in the isotropic state and for which the symmetry argument for the existence of soft modes is very compelling, the above energy, eqn. (1.21), is the same as that for a system cross-linked in the nematic state. Therefore, at least within the approximation of homogenous gaussian chains, soft elasticity also arises if the system is cross-linked in the nematic state. This is because, on heating such an elastomer a completely isotropic state is formed, with no memory of the original cross-linking director, and the symmetry arguments can then be applied to this state.

The nematic elastomer energy takes on a particularly simple form if we take the isotropic state as the elastic reference state, then consider cooling the sample to the nematic state, which fixes the value of  $Q$  and hence  $r$ , and then imposing a deformation  $\underline{\lambda}$ . The nematic director  $\hat{\mathbf{n}}$  will then adopt the direction that results in the minimal free energy, so the energy we wish to consider is

$$F = \frac{1}{2}\mu a \min_{\hat{\mathbf{n}}} \text{Tr} (\underline{\lambda} \cdot \underline{\lambda}^T \cdot \underline{\underline{\ell}}^{-1}). \quad (1.23)$$

Once again using the polar decomposition theorem to write  $\underline{\lambda} = \underline{\underline{S}} \cdot \underline{\underline{R}}$ , and defining the principal values of  $\underline{\underline{S}}$  as  $\lambda_1 \leq \lambda_2 \leq \lambda_3$ , we can straightforwardly conduct the minimization over  $\hat{\mathbf{n}}$ , which will result in  $\hat{\mathbf{n}}$  pointing along the principal direction of  $\underline{\underline{S}}$  with the largest principal

value, giving

$$F = \frac{1}{2}\mu \left( \lambda_1^2 + \lambda_2^2 + \frac{\lambda_3^2}{r} \right). \quad (1.24)$$

This energy is minimized by  $\lambda_3 = r^{1/3}$  and  $\lambda_2 = \lambda_1 = r^{-1/6}$ , however, since these are the principal stretches of  $\underline{\underline{\lambda}}$ , this corresponds to a stretch by  $r^{1/3}$  in any direction. We can easily add the requirement of volume conservation into this form of the energy by writing

$$F(\underline{\underline{\lambda}}) = \begin{cases} \frac{1}{2}\mu (\lambda_1^2 + \lambda_2^2 + \lambda_3^2/r) & \text{if } \lambda_1\lambda_2\lambda_3 = 1 \\ \infty & \text{otherwise.} \end{cases} \quad (1.25)$$

A two dimensional slice of this energy function is plotted in Fig. 1.9 for both  $r = 1$  (conventional rubber) and a  $r = 8$ . The latter nematic case clearly shows a ring of minima, corresponding to a degenerate set of low energy states.

## 1.7 HINTS OF COMPLEXITY - STRIPE DOMAINS

The elastic energy described in the previous sections is extremely rich and underpins our understanding of many exotic behaviors found in liquid crystal elastomers. We will conclude this introduction by examining one of the most subtle — the formation of textured deformations. Consider stretching a well aligned nematic elastomer in a direction perpendicular to the alignment direction. Taking the initial alignment direction as the  $z$  direction, the initial state can be thought of as a deformation from the isotropic state of  $\underline{\underline{\lambda}}_1 = \text{diag}(r^{-1/6}, r^{-1/6}, r^{1/3})$ . The elastomer would also be in a low energy state if the deformation applied to the isotropic state had been  $\underline{\underline{\lambda}}_3 = \text{diag}(r^{1/3}, r^{-1/6}, r^{-1/6})$ , and in this case the alignment would be in the  $x$  direction. If we take the elastomer aligned in the  $z$  direction and stretch in the  $x$  direction then we will be applying stretches of the form  $\underline{\underline{\lambda}}_2 = \text{diag}(\lambda_{xx}, 1/(\lambda_{xx}\lambda_{zz}), \lambda_{zz})$ ,

## INTRODUCTION

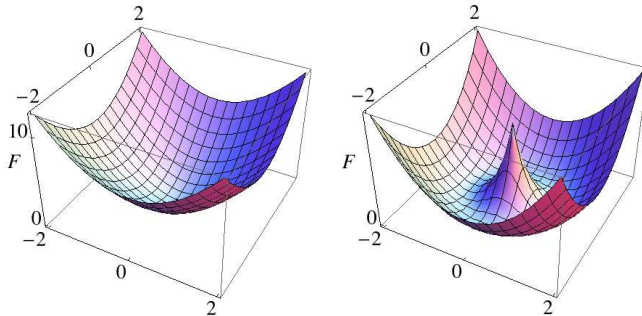


Figure 1.9: Energetic cost of imposing a uniaxial stretch on an isotropic elastomer (left) and nematic elastomer from the isotropic reference state (right) given by eqn. (1.24). The plots are as a function of the two dimensional vector  $\rho$ , and the value of the function at  $\rho$  is the cost of imposing a uniaxial stretch of magnitude  $|\rho| + 1$  in the direction of  $\rho$ . We see that in the nematic state, the isotropic reference configuration is unstable, and the function is minimized by a uniaxial deformation by  $r^{1/3}$  in any direction, and that deformations that move the elastomer around the ring of minima will be soft.

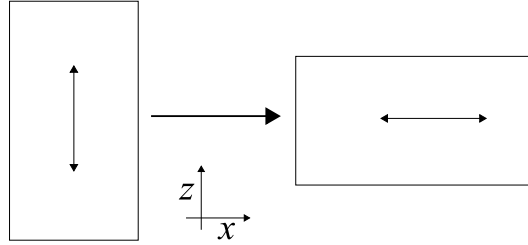


Figure 1.10: A nematic elastomer with its director aligned with the  $z$  axis (left) can be stretched along the  $x$ , causing the director to rotate to the  $x$  axis (right).

and the total deformation from the isotropic will be  $\underline{\underline{\lambda}}_2 \cdot \underline{\underline{\lambda}}_1$ . This is equal to  $\underline{\underline{\lambda}}_3$  when  $\lambda_{xx} = \sqrt{r}$  and  $\lambda_{zz} = 1/\sqrt{r}$ , so after the elastomer has been stretched this far, the director will have swung round by  $90^\circ$  to lie along the  $x$  axis, and the energy of the elastomer will not have changed. The geometry of this situation is shown in Fig. 1.10.

The above analysis raises the question what happens at intermediate stretches between  $\underline{\underline{\lambda}}_2 = \underline{\underline{\delta}}$  and  $\underline{\underline{\lambda}}_2 = \text{diag}(\sqrt{r}, 1, 1/\sqrt{r})$ . If we consider stretches of the form  $\underline{\underline{\lambda}}_2 = \text{diag}(\lambda, 1, 1/\lambda)$ , and substitute  $\underline{\underline{\lambda}} = \underline{\underline{\lambda}}_2 \cdot \underline{\underline{\lambda}}_1$ , which is the total deformation from the isotropic, into eqn. (1.25), then, we get

$$F(\lambda) = \begin{cases} \frac{1}{2}\mu \left( r^{-1/3} + \lambda^2 r^{-1/3} + \frac{1}{r^{1/3}\lambda^2} \right) & \text{if } \lambda \leq r^{1/4} \\ \frac{1}{2}\mu \left( r^{-1/3} + \frac{\lambda^2}{r^{4/3}} + \frac{r^{2/3}}{\lambda^2} \right) & \text{if } \lambda \geq r^{1/4}. \end{cases} \quad (1.26)$$

This is only minimized by the two values of  $\lambda$  we have already identified, namely  $\lambda = 1$  and  $\lambda = \sqrt{r}$ , so it would appear that the elastomer must cross an energy barrier to get between the two aligned low energy states. However, it is possible to pass between these states softly by adopting a textured deformation. If we consider deformations of

## INTRODUCTION

the form

$$\underline{\underline{\lambda}}_2^{\pm} = \begin{pmatrix} \lambda & 0 & \pm\lambda_{xz} \\ 0 & 1 & 0 \\ 0 & 0 & 1/\lambda \end{pmatrix}, \quad (1.27)$$

then it is clear that  $\frac{1}{2}\underline{\underline{\lambda}}_2^+ + \frac{1}{2}\underline{\underline{\lambda}}_2^- = \underline{\underline{\lambda}}_2$ . Furthermore, substituting  $\underline{\underline{\lambda}}_2^{\pm} \cdot \underline{\lambda}_1$  into eqn. (1.25), it is possible to find a  $\lambda_{xz}$  such that the energy is minimized for both of these deformations for every value of  $\lambda$  between 1 and  $\sqrt{r}$ . The required value of  $\lambda_{xz}$  is zero at 1 and  $\sqrt{r}$  but finite between them. This means that if the elastomer can split into equal volume fractions that have undergone  $\frac{1}{2}\underline{\underline{\lambda}}_2^+$  and  $\frac{1}{2}\underline{\underline{\lambda}}_2^-$  then the average deformation will be the desired  $\underline{\underline{\lambda}}_2$  but the deformation will be soft. Furthermore, if the oscillations between the two deformations happens on a small enough scale then the discrepancy between the actual and desired shape of the elastomer will be very small. However, finding two soft deformations that average to the required deformation is only half the problem, we must also show that the two deformations can be fitted together in such a way as to make a legitimate, compatible deformation field, that is the gradient of a displacement. To do this, we notice that vectors in the  $x - y$  plane are mapped to the same vectors under both deformations. This means that if we apply the deformations in two adjacent regions separated by a plane with normal  $\hat{\mathbf{z}}$  then, since each vector in the plane is mapped to the same vector under both deformations, the plane will not fracture, so the two deformations will form a compatible deformation field. This is not true of any other plane, and for two general deformations this may be true of no planes at all. In this case, if the sample splits into very fine stripes separated by boundaries which are  $x - y$  planes then the two deformations can alternate between stripes, forming a compatible soft textured deformation that allows the elastomer to deform softly throughout the reorientation process. A complete diagram of

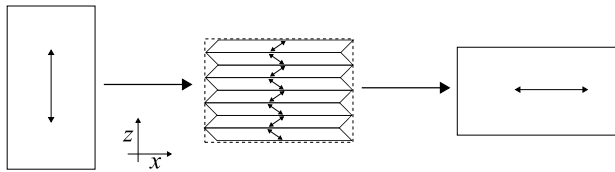


Figure 1.11: Intermediate strains that do not form cause full re-orientation result in the formation of stripe-patterns of alternating director rotation and shear.

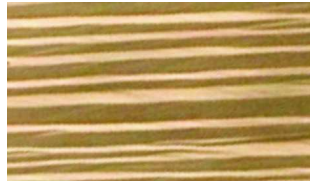


Figure 1.12: A view of the cloudy stripe phase though cross-polars, the alternating stripes of director rotation are clearly visible. The length scale of the stripes is of the order of 10 microns.

the process is shown in Fig. 1.11.

The stripe patterns discussed above are one example of the complex elastic responses induced by the introduction of a set of soft modes to a material. The stripes were first observed by Kundler and Finklemann [39], and explained theoretically shortly afterwards [32]. In the experiment the stripes were just micrometers wide, and introduced lots of light scattering into the sample, so that the clear mono-domain elastomer becomes cloudy on stretching and then clear again when the stripe domain is replaced by the perpendicular mono-domain. A photograph of a real stripe domain taken between crossed linear polarizers is shown in Fig. 1.12.

## Chapter 2

# SEMISOFT ELASTIC RESPONSE OF MONO-DOMAIN NEMATIC ELASTOMERS

DESPITE THE SYMMETRY ARGUMENTS made in the introduction, real nematic elastomers do not deform completely softly — there is always a preferred alignment direction and small restoring force. This is because, in order to synthesize a mono-domain elastomer with a homogenous director orientation throughout the sample, a preferred direction for this alignment must be imprinted on the sample using magnetic, electric or stress fields. This imprinted direction breaks the symmetry of the isotropic state, allowing the material to provide a weak resistance to deformation.

This chapter is an exploration of the free energies that describe semi-soft elasticity. A simple microscopic model of semi-soft behavior, called the compositional fluctuations model, has enjoyed almost universal success in describing the behavior of real nematic elastomers, despite the fact that the microscopic model itself is very specific and rather implausible. In this chapter we will show that this is because the form of the free energy predicted is in fact very general. We will then show that, although this energy is semi-soft, there are certain points in the energy landscape where the modulus for an incremental deformation is zero. Finally, we will show that these zeroes in

the shear modulus are even more general than the original model, depending only on the symmetry of the system and the possibility of director rotation coupled to strain. These latter results are equivalent to those obtained by Lubensky *et al.* by consideration of a Landau theory equivalent to a nematic liquid crystal in crossed electric and magnetic fields [65, 66].

## 2.1 THE COMPOSITIONAL FLUCTUATIONS MODEL

The essential idea behind the compositional fluctuations model is that different polymer strands will couple to the nematic field with different strengths, so the constant value for  $r$  used in the ideal model must be replaced by different values for each strand. One simple way this could come about is if the strands incorporate different numbers of rod like units in their backbones. If we cross-link such a melt in the nematic state then each chain will be sampling its optimal conformation distribution, but when we try to deform the resultant rubber, strains that are soft for chains with one value of  $r$  will not be soft for all values of  $r$  so the deformation will cost energy.

Following [57], we turn this idea into a free energy by averaging the free energy per strand, eqn. (1.17), across all the different strands, which now have different values for  $r$ , giving,

$$\begin{aligned} \langle F_s \rangle &= \left\langle \frac{1}{2} k_b T \text{Tr} \left( \underline{\lambda} \cdot \underline{\ell}_0 \cdot \underline{\lambda}^T \cdot \underline{\ell}^{-1} \right) \right\rangle_r \\ &= \frac{1}{2} k_b T \text{Tr} \left( \underline{\lambda} \cdot \underline{\ell}_0 \cdot \underline{\lambda}^T \cdot \underline{\ell}^{-1} \right) \\ &\quad + \frac{1}{2} k_b T \left( \left\langle \frac{1}{r} \right\rangle - \frac{1}{\langle r \rangle} \right) \text{Tr} \left( (\underline{\delta} - \hat{\mathbf{n}}_o \hat{\mathbf{n}}_o) \cdot \underline{\lambda}^T \cdot \hat{\mathbf{n}} \hat{\mathbf{n}} \cdot \underline{\lambda} \right), \end{aligned} \quad (2.1)$$

where the step length tensors are defined with the average anisotropy,  $\langle r \rangle$ , and  $\hat{\mathbf{n}}$  is the liquid crystal director in the final state and  $\hat{\mathbf{n}}_0$  is

the director in the cross-linking state. Defining the coefficient of non-ideality

$$\alpha = \left\langle \frac{1}{r} \right\rangle - \frac{1}{\langle r \rangle}, \quad (2.2)$$

and, once again multiplying by the number density of cross-links  $n_s$  and defining the shear modulus  $\mu = n_s k_b T$ , this energy takes the form

$$F = \frac{1}{2} \mu \text{Tr} \left( \underline{\underline{\ell}}_0 \cdot \underline{\underline{\lambda}}^T \cdot \underline{\underline{\ell}}^{-1} \cdot \underline{\underline{\lambda}} \right) + \frac{1}{2} \mu \alpha \text{Tr} \left( (\underline{\delta} - \hat{\mathbf{n}}_0 \hat{\mathbf{n}}_0) \cdot \underline{\underline{\lambda}}^T \cdot \hat{\mathbf{n}} \hat{\mathbf{n}} \cdot \underline{\underline{\lambda}} \right), \quad (2.3)$$

which is the compositional fluctuations free energy. The semi-soft term introduces a penalty for rotations of the director away from  $\hat{\mathbf{n}}_0$ , which makes the previously soft deformations cost energies of magnitude  $\alpha \mu$ .

## 2.2 PREDICTIONS AND SUCCESSES OF COMPOSITIONAL FLUCTUATIONS

The response of the compositional fluctuations model has been extensively studied in the context of the experiment described in Fig. 1.11 in which a nematic monodomain is stretched perpendicular to its initial alignment. As discussed in the introduction, the ideal model predicts the formation of a striped-textured state that allows the elastomer to stretch completely softly until director reorientation is complete, by which time a stretch  $\sqrt{r}$  has been imposed. The compositional fluctuations model of semi-softness predicts that the response of an elastomer to a finite elongation perpendicular to the initial director will be one of three possibilities depending on the amount of elongation. The full forms for the deformation responses ( $\underline{\underline{\lambda}}_i$ ) and director rotations that result from applying the stretch  $\lambda_{xx} = \lambda$ , which are stated below, were derived in [58] and are discussed in [64]. The ge-

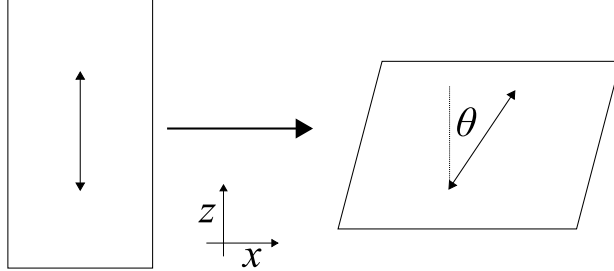


Figure 2.1: Experiment in which an elastomer is prepared with the director aligned in the  $z$  direction then stretched in the  $x$  direction causing director rotation and the formation of sympathetic shears.

ometry used in these expressions is illustrated in Fig. 2.1. Introducing the threshold strain

$$\lambda_1 = \left( \frac{r - 1}{r - 1 - \alpha r} \right)^{1/3}, \quad (2.4)$$

if  $\lambda \leq \lambda_1$  the director does not rotate, ( $\theta = 0$ ) and the deformation tensor ( $\underline{\underline{\lambda}}$ ) is simply that expected from a classical rubber:

$$\underline{\underline{\lambda}} = \begin{pmatrix} \lambda & 0 & 0 \\ 0 & 1/\sqrt{\lambda} & 0 \\ 0 & 0 & 1/\sqrt{\lambda} \end{pmatrix}. \quad (2.5)$$

If  $\lambda_1 \leq \lambda \leq \sqrt{r}\lambda_1$  then the director starts to rotate and the deformation tensor includes sympathetic  $\lambda_{xz}$  shears:

$$\sin^2 \theta = \frac{r(\lambda^2 - \lambda_1^2)}{(r - 1)\lambda^2}, \quad \underline{\underline{\lambda}} = \begin{pmatrix} \lambda & 0 & \lambda_{xz} \\ 0 & 1/\sqrt{\lambda_1} & 0 \\ 0 & 0 & \sqrt{\lambda_1}/\lambda \end{pmatrix}. \quad (2.6)$$

See Fig. 2.2 for a comparison of this prediction for  $\theta(\lambda)$  with experimental data. The shear is

## SEMISOFT ELASTIC RESPONSE

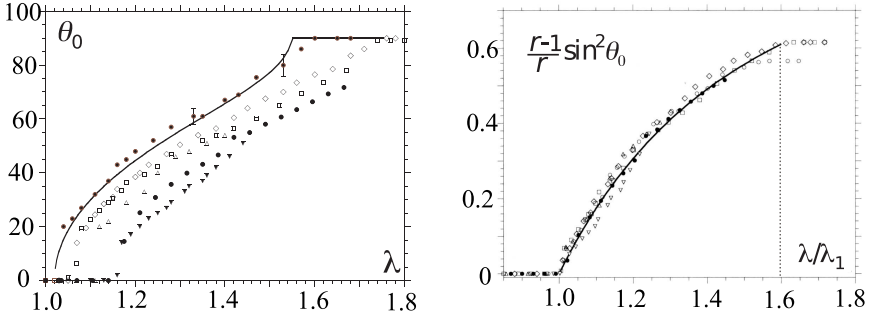


Figure 2.2: Left: Director rotation ( $\theta_0$ ) as a function of stretch ( $\lambda$ ) for samples prepared by several different groups. The solid line is a theoretical curve (from eq. (2.6)) fitted to the data for one sample. Right: Plotting reduced rotation against reduced extension causes all the data sets to collapse onto one master curve. The solid line is the theoretical prediction derived from eq. (2.6). Figure adapted from [64], see also [32] for the original analysis.

$$\lambda_{xz}^2 = \frac{(\lambda^2 - \lambda_1^2)(r\lambda_1^2 - \lambda^2)}{r\lambda^2\lambda_1^3}. \quad (2.7)$$

If  $\sqrt{r}\lambda_1 \leq \lambda$  then the director rotation is complete ( $\theta = \pi/2$ ) and the elastomer once again deforms as a classical rubber would:

$$\underline{\underline{\lambda}}_1 = \begin{pmatrix} \lambda & 0 & 0 \\ 0 & r^{1/4}/\sqrt{\lambda} & 0 \\ 0 & 0 & 1/(r^{1/4}\sqrt{\lambda}) \end{pmatrix}. \quad (2.8)$$

The model also predicts that the stress strain curve for the elastomer should have a different gradients in these three regions, with a much lower gradient in the middle region forming a stress plateau (see [64]). This stress prediction is confirmed over a huge range of strains; typical data is shown in Fig 2.3. Since the model predicts all three stress gradients and also the position of the two kinks in the curve (five quantities) in terms of three underlying constants, it

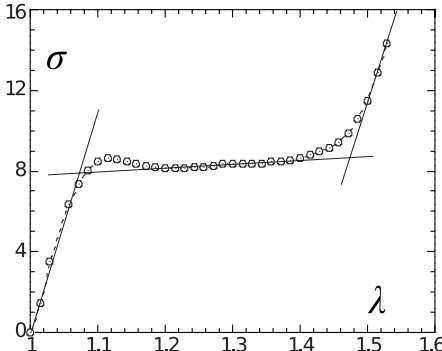


Figure 2.3: Stress-strain data for an elastomer showing a threshold to a subsequent stress-strain plateau and then final classical behaviour. The solid lines show the stress curves predicted by the compositional fluctuations model. Data provided by S. M. Clarke.

is already highly non-trivial. These 5 quantities have already been shown to match the model predictions by several groups [32, 42, 55], as has the form of the director rotation, as shown in Fig. 2.2. We must therefore conclude that the compositional fluctuations free energy is a very good model. However, as noted in [58], if we take the microscopic model literally and try to predict  $\alpha$ , which can be done for example by considering chains that are random mixtures of two types of rods with different couplings to the nematic field, then the predicted values of the semisoftness parameter are  $\alpha \sim 10^{-5}$ , which is several magnitudes smaller than the observed values, which are typically around 0.1. It also seems implausible semi-softness in all the different elastomers, with very different syntheses and imprinting techniques, has the same microscopic origin. This motivates us to consider a phenomenological description of the compositional fluctuations free energy, to understand the observed universal behavior.

## 2.3 MODELS OF SEMI-SOFTNESS

In this section we consider the scope for models of semi-softness other than the compositional fluctuations model. We first show that, despite its initial derivation, the compositional fluctuations free energy is in fact the most general quadratic free energy that only manifestly contains one direction in both the initial and final states. We then show how recovering the ideal model amounts to assuming that there is an isotropic reference state. Finally we consider the scope for other models that contain more directions and are not quadratic in the deformation tensor.

### 2.3.1 GENERALITY OF THE COMPOSITIONAL FLUCTUATIONS FORM OF THE SEMI-SOFT FREE ENERGY DENSITY

The compositional fluctuations model of semi-softness breaks ideality by introducing a distribution of coupling strengths between the polymer backbone chains and the nematic mean field. Since there are other ways (for instance by introducing aligned rigid-rod crosslinks) one could imagine breaking ideality, the success of this particular model in describing experimental data raises a question — is it simply the case that compositional fluctuations are the dominant cause of non-ideality or is there an underlying reason why, whatever the microscopic cause of non-ideality, the same or similar form of the semi-soft free energy results? To address this question, we consider a sample of non-ideal nematic elastomer that is subject to a deformation  $\Lambda_{ij} \equiv \partial R_i / \partial x_j$  that takes it from a reference state ( $\mathbf{x}$ ) to a target state ( $\mathbf{R}$ ). Here we use  $\underline{\underline{\Lambda}}$  rather than  $\underline{\underline{\lambda}}$  because we reserve  $\underline{\underline{\lambda}}$  for deformations from relaxed states, and this reference state may not be relaxed. If it is not relaxed, there will be a spontaneous relaxing deformation,  $\underline{\underline{\Lambda}}_r$ , to a relaxed state. Functions of  $\underline{\underline{\Lambda}}$  can be recast in terms of deformations

from the relaxed state ( $\underline{\underline{\Lambda}}$ ) by substituting

$$\underline{\underline{\Lambda}} = \underline{\underline{\lambda}} \cdot \underline{\underline{\Lambda}}_r. \quad (2.9)$$

The first subscript on  $\Lambda_{ij}$  ( $i$ ) is clearly a target state subscript and should only be contracted with subscripts from other target state variables. The second ( $j$ ) is a reference state subscript which must be contracted only with reference state subscripts if rotational invariance is to be observed. Therefore the most general free energy we can write down that is quadratic in  $\Lambda$  is of the form

$$F = \sum_{i,j} \text{Tr} \left( \underline{\underline{A}}_i \cdot \underline{\underline{\Lambda}}^T \cdot \underline{\underline{B}}_j \cdot \underline{\underline{\Lambda}} \right), \quad (2.10)$$

where the matrices  $\underline{\underline{A}}_i$  are constructed out of reference state vectors and scalars, while the matrices  $\underline{\underline{B}}_j$  are constructed out of target state scalars and vectors. If we assume that the reference state is characterised by a single direction  $\hat{\mathbf{n}}_0$  and the final state by a single direction  $\hat{\mathbf{n}}$  (so both states are uniaxial), this becomes

$$\begin{aligned} F = & \text{Tr}(\mathbf{H} \underline{\underline{\Lambda}}^T \underline{\underline{\Lambda}} + \mathbf{J} \hat{\mathbf{n}}_0 \hat{\mathbf{n}}_0 \underline{\underline{\Lambda}}^T \underline{\underline{\Lambda}} \\ & + K \hat{\mathbf{n}}_0 \hat{\mathbf{n}}_0 \underline{\underline{\Lambda}}^T \hat{\mathbf{n}} \hat{\mathbf{n}} \underline{\underline{\Lambda}} + L \underline{\underline{\Lambda}}^T \hat{\mathbf{n}} \hat{\mathbf{n}} \underline{\underline{\Lambda}}). \end{aligned} \quad (2.11)$$

In general this free energy will not be relaxed and will undergo a spontaneous deformation to a relaxed state. The relaxing deformation,  $\underline{\underline{\Lambda}}_r$ , must also be volume-preserving so it must have determinant of 1. For the resulting free energy not to have any soft deformations, this spontaneous deformation must not break the uniaxial symmetry of the reference state. If it were to break this symmetry, there would be other equivalent deformations that break the same symmetry differently, leading to multiple relaxed states and soft deformations

mapping between them. Experimentally, the spontaneous distortions of monodomain elastomers on changing conditions are always along the original director. Therefore,  $\hat{\mathbf{n}}$  must be equal to  $\hat{\mathbf{n}}_o$  and  $\underline{\underline{\Lambda}}$  must be of the form

$$\underline{\underline{\Lambda}}_r = a \left( \underline{\underline{\delta}} + \left( \frac{1}{a^3} - 1 \right) \hat{\mathbf{n}}_o \hat{\mathbf{n}}_o \right), \quad (2.12)$$

where  $a$  is a constant to be determined. Substituting this deformation into eqn. (2.11) and taking the trace gives

$$F = a^2 \left( 2H + \frac{H + J + K + L}{a^6} \right). \quad (2.13)$$

Minimising this with respect to  $a$  we obtain the preferred value:

$$a^6 = \frac{H + J + K + L}{H}. \quad (2.14)$$

We can now recast the original free energy in terms of deformations away from the relaxed state,  $\underline{\underline{\lambda}}$ , by substituting  $\underline{\underline{\Lambda}} = \underline{\underline{\lambda}} \cdot \underline{\underline{\Lambda}}_r$ , giving

$$\begin{aligned} F = & a^2 \text{Tr} \left( H \underline{\underline{\lambda}}^T \underline{\underline{\lambda}} + L \underline{\underline{\lambda}}^T \hat{\mathbf{n}} \hat{\mathbf{n}} \underline{\underline{\lambda}} + \left( \frac{J + H}{a^6} - H \right) \hat{\mathbf{n}}_o \hat{\mathbf{n}}_o \underline{\underline{\lambda}}^T \underline{\underline{\lambda}} \right. \\ & \left. + \left( \frac{K + L}{a^6} - L \right) \hat{\mathbf{n}}_o \hat{\mathbf{n}}_o \underline{\underline{\lambda}}^T \hat{\mathbf{n}} \hat{\mathbf{n}} \underline{\underline{\lambda}} \right). \end{aligned} \quad (2.15)$$

Inspecting this form, we see that relaxation has reduced the number of unknown constants in the theory from four to three because we can write

$$\begin{aligned} F = & a^2 \text{Tr} \left( H \underline{\underline{\lambda}}^T \underline{\underline{\lambda}} + L \underline{\underline{\lambda}}^T \hat{\mathbf{n}} \hat{\mathbf{n}} \underline{\underline{\lambda}} + M \hat{\mathbf{n}}_o \hat{\mathbf{n}}_o \underline{\underline{\lambda}}^T \underline{\underline{\lambda}} \right. \\ & \left. - (M + L) \hat{\mathbf{n}}_o \hat{\mathbf{n}}_o \underline{\underline{\lambda}}^T \hat{\mathbf{n}} \hat{\mathbf{n}} \underline{\underline{\lambda}} \right). \end{aligned} \quad (2.16)$$

where  $M = (J + H)/a^6 - H$ . The coefficients in this free energy can be rewritten without loss of generality as

$$\begin{aligned} a^2 H &= \frac{1}{2}\mu \\ a^2 L &= \frac{1}{2}\mu \left( \alpha + \frac{1}{r} - 1 \right) \\ a^2 M &= \frac{1}{2}\mu(r - 1). \end{aligned} \quad (2.17)$$

Substituting these forms into  $F$  we recover the form of the free energy identical to the expression stemming from the compositional fluctuations model, eqn. (2.3). Since this derivation is not microscopic, it does not provide microscopic interpretations of the quantities in  $F$ , in particular the identification of  $r$  as the degree of anisotropy of the second moment of the chain shape distribution is not strictly justified. However, since this identification is exact for the ideal model (Gaussian chains all with the same anisotropic second moment),  $r$  is likely to retain a very similar meaning in any microscopic non-ideal model that tends to the ideal model (as opposed to just the ideal free energy) in its  $\alpha \rightarrow 0$  limit.

### 2.3.2 RECOVERING IDEALITY

The above equations can easily be inverted to find  $\alpha$ ,  $r$  and  $\mu$  in terms of  $H$ ,  $J$ ,  $K$  and  $L$  giving

$$\begin{aligned} \mu &= 2(H + J + K + L)^{\frac{1}{3}} H^{\frac{2}{3}}, \\ r &= \frac{H + J}{H + J + K + L}, \\ \alpha &= \frac{L}{H} - \frac{K + L}{H + J}. \end{aligned} \quad (2.18)$$

Interestingly, if  $K = J = 0$  then  $\alpha = 0$  and the ideal elastomer free energy is recovered. Inspecting the original form of the free energy, we see that this corresponds to the reference state being isotropic because the terms that depend on  $\hat{\mathbf{n}}_o \hat{\mathbf{n}}_o$  have been set to zero. This is a manifestation of the Golubovic-Lubensky theorem [36] that an isotropic state leads to soft modes of deformation. In this case, the spontaneous deformation does break symmetry because it introduces a direction  $\hat{\mathbf{n}}_o$  into an otherwise isotropic system. More generally,  $\alpha = 0$  if

$$\frac{J}{H} = \frac{K}{L}, \quad (2.19)$$

which is equivalent to demanding that  $F$  factorises to the generic form

$$F = \text{Tr} \left( (N\underline{\underline{\delta}} + P\hat{\mathbf{n}}_o \hat{\mathbf{n}}_o) \underline{\underline{\Lambda}}^T (R\underline{\underline{\delta}} + U\hat{\mathbf{n}} \hat{\mathbf{n}}) \underline{\underline{\Lambda}} \right). \quad (2.20)$$

This  $F$  also has an isotropic state which can be demonstrated by substituting  $\underline{\underline{\Lambda}} = \underline{\underline{\lambda}} (N\underline{\underline{\delta}} + P\hat{\mathbf{n}}_o \hat{\mathbf{n}}_o)^{-1/2}$ , giving

$$F = \text{Tr} \left( \underline{\underline{\lambda}}^T (R\underline{\underline{\delta}} + U\hat{\mathbf{n}} \hat{\mathbf{n}}) \underline{\underline{\lambda}} \right) \quad (2.21)$$

which has no  $\hat{\mathbf{n}}_o$  dependence. This means that any directions that can be defined in the state obtained by applying  $\underline{\underline{\Lambda}} = (N\underline{\underline{\delta}} + P\hat{\mathbf{n}}_o \hat{\mathbf{n}}_o)^{-1/2}$  do not enter into the free energy of deformations imposed from this state. Therefore this state is in effect isotropic.

### 2.3.3 ROUTE TO SEMI-SOFTNESS BY INTRODUCING ANOTHER DIRECTION

The above argument demonstrates that non-ideal elastomer theories are made by destroying the existence of an isotropic state, in accordance with the Golubovic-Lubensky theorem. Further, it shows that if this is done simply by introducing a *single* direction, typically  $\hat{\mathbf{n}}$ , into

the reference state one must end up with the generic model, eqn. (2.3), or remain with the ideal model. However, this does not mean that there are no other non-ideal models; it only means that in order to find them we must introduce new directions into the theory or deviate from the quadratic form in (2.11) by introducing terms that depend on symmetry-allowed variants of  $\underline{\Lambda}$ . We can introduce a new direction straightforwardly by defining a new reference state direction  $\mathbf{k}_o$ , and a corresponding final state vector  $\mathbf{k}$ . The vector  $\mathbf{k}$  can either be a free direction that we minimise over for a given deformation (like  $\hat{\mathbf{n}}$ ) or can be defined as a final state vector derived from the initial state vector through variants of  $\underline{\Lambda}$  such as  $\underline{\Lambda}\mathbf{k}_o$  or  $\underline{\Lambda}^{-T}\mathbf{k}_o$ . This last possibility is how a vector area expressed by a normal to the plane would be expected to transform, provided  $\det\underline{\Lambda} = 1$ . This is discussed at length under the theory of smectic elastomers in [64].

Having introduced a new direction into the problem it becomes much harder to write down a general form for  $F$  because, not only do we have to consider cross terms between the two direction in both states, we can also define various scalars (such as  $\hat{\mathbf{n}} \cdot \mathbf{k}$  and  $\mathbf{k} \cdot \mathbf{k}$ ) the coefficients of which could be functions of  $\underline{\Lambda}$ . Also allowing terms that are not quadratic in  $\underline{\Lambda}$  leads to even more possible terms. Since relaxation only removes one degree of freedom from a system, these considerations lead us to conclude that, by including such terms, a large number of alternative models could be constructed if physical phenomena were to be found that the above generic semi-soft free energy can not explain.

A very simple example would be introducing a new direction  $\mathbf{k}_o$  that is initially aligned with  $\hat{\mathbf{n}}_o$  but, unlike  $\hat{\mathbf{n}}$ , transforms under the deformation  $\underline{\Lambda}$  as  $\mathbf{k} = \underline{\Lambda}^{-T}\mathbf{k}_o$ . One possible relaxed free energy (because it is relaxed, we use  $\underline{\lambda}$  rather than  $\underline{\Lambda}$ ) constructed using this

direction is

$$F = \frac{1}{2}\mu\text{Tr} \left( \underline{\underline{\ell}}_o \cdot \underline{\underline{\lambda}}^T \cdot \underline{\underline{\ell}}^{-1} \cdot \underline{\underline{\lambda}} \right) - \alpha \left( \frac{\hat{\mathbf{n}} \cdot \underline{\underline{\lambda}}^{-T} \mathbf{k}_o}{|\underline{\underline{\lambda}}^{-T} \mathbf{k}_o|} \right)^2 \quad (2.22)$$

which has a simple physical interpretation — the elastomer is semi-soft because it contains regions of weakly ordered SmA phase. For weak smectic order there would be a small energy penalty for rotating the director away from the current layer normal,  $\hat{\mathbf{k}} \propto \lambda^{-T} \mathbf{k}_o$ . Thus the semi-soft term in eqn. (2.22) is effectively  $-\alpha(\hat{\mathbf{n}} \cdot \hat{\mathbf{k}})^2$ .

Kundler and Finkelmann have observed (using X-rays) embryonic regions of smectic order in macroscopically nematic elastomers, and have termed such specimens cybotactic nematic elastomers [40]. However, it has been observed in such systems with smectic fluctuations that the semi-soft behavior — that is, the precise form of the director rotation (from 0 to 90 degrees, along with singular edges), the correlation between the length of the semi-soft plateau and the magnitude of spontaneous thermal distortions, and the variation of semi-softness (and hence the initial threshold) with degree of smectic ordering — was well described [40] by the generic model.

## 2.4 SOFT ELASTICITY IN SEMI-SOFT ELASTOMERS

Having established that real elastomers conform very well to the compositional fluctuations free energy, and understood that this is because, on phenomenological grounds, this is the simplest possible non-ideal energy, it might appear that truly soft deformation has been ruled out. However, in this section we will show that at certain points the generic compositional fluctuations type free energy does predict incremental deformations without elastic cost. To do this we consider a two step experiment, illustrated in Fig. 2.4, in which a monodomain

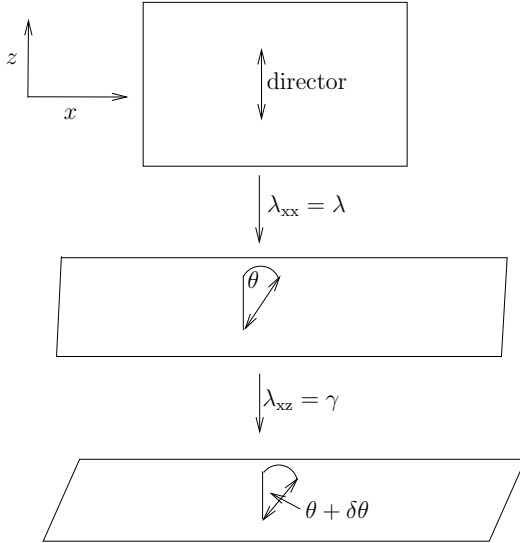


Figure 2.4: A two step experiment in which the sample is prepared with the director along the  $z$  axis, then a stretch  $\lambda_{xx} = \lambda$  is imposed (which may lead to director rotation (shown) and sympathetic shears (not shown)), then a small  $\lambda_{xz} = \gamma$  shear is imposed at constant stretch.

elastomer prepared with its director aligned with the  $z$  axis is first stretched by some amount in the  $x$  direction before a small additional  $x - z$  shear is applied. We will see that the modulus associated with the incremental  $x - z$  shear vanishes at the onset and end of director rotation.

In general small-shear ( $\lambda_{xz} \lesssim 10^{-4}$ ) mechanical experiments offer a much more limited route to exploring constitutive relations of liquid crystal elastomers than large strain experiments ( $\lambda_{xx} \lesssim 5$ ) which at the same time induce large (90 degree) rotations of nematic order upon which the new properties of nematic elastomers are predicated. Experiments of the type discussed here which compound small strain rheology with large pre-stretches can explore a much wider range of

the elastomer's response. This type of experiment was first considered by Lubensky and Ye [66]. They analyzed the elastomers response using a phenomenological lagrangian-strain minimal model of nematic elastomers in which the director had been integrated out, so that the energy only depended on the strain. However, the calculation that follows is the first to consider such experiments using the full and experimentally verified compositional-fluctuations form of the free energy.

#### 2.4.1 SEMI-SOFT RESPONSE TO SMALL SHEARS COMPOUNDED WITH LARGE STRAINS

Using the geometry described in figure 2.4, we wish to calculate the apparent shear modulus for the final infinitesimal shear ( $C_5$ ) as a function of the arbitrary finite stretch  $\lambda$  imposed during the first stage of the experiment. If after applying the initial stretch  $\lambda$ , causing an initial deformation  $\underline{\underline{\lambda}}_1$  and the director to make an angle  $\theta_o$  with the  $z$  axis, we then impose an additional infinitesimal shear  $\underline{\underline{\lambda}}_2 = \underline{\underline{\delta}} + \gamma \hat{\mathbf{x}} \hat{\mathbf{z}}$ , which causes  $\theta_o$  to change to  $\theta_o + \delta\theta$ , then, since both perturbations are small, we can expand the resulting free energy in powers of  $\delta\theta$  and  $\gamma$ ,

$$F = D\gamma^2 + E\delta\theta^2 + G\delta\theta\gamma. \quad (2.23)$$

There are no linear terms in this expansion because there is no spontaneous shear or director rotation. Minimising this energy with respect to  $\delta\theta$  gives  $\delta\theta = -G\gamma/2E$ . Putting this value back into  $F$  we can read off the apparent shear modulus,  $C_5$ , as twice the coefficient of the quadratic term in  $\gamma$ ,

$$C_5 = 2 \left( D - \frac{G^2}{4E} \right). \quad (2.24)$$

In order to calculate  $C_5$  we must evaluate eqn. (2.3) at a total deformation  $\underline{\lambda} = \underline{\lambda}_2 \cdot \underline{\lambda}_1$  and director angle  $\theta = \theta_o + \delta\theta$ , expand the result to second order in  $\gamma$  and  $\delta\theta$  and then read off the coefficients ( $D$ ,  $G$  and  $E$ ) we need for eqn. (2.24). Since the  $\underline{\lambda}_i$  are large deformations, we must compound rather than add the two consecutive deformations (multiply the tensors). In the first region (below the strain threshold —  $\lambda \leq \lambda_1$ ) we have

$$F = \frac{\mu}{2\lambda} \left[ (\lambda^3 + \gamma^2 r) \left( 1 + \left( \frac{1}{r} - 1 \right) \sin^2 \theta \right) + \alpha \lambda^3 \sin^2 \theta + 2\gamma r \left( \frac{1}{r} - 1 \right) \sin \theta \cos \theta + r \left( 1 + \cos^2 \theta \left( \frac{1}{r} - 1 \right) \right) + 1 \right]. \quad (2.25)$$

Expanding this out around  $\theta = 0$  we can read off the coefficients we need for  $C_5$  as

$$\begin{aligned} D &= \frac{\mu r}{2\lambda}, \\ E &= \frac{\mu}{2\lambda} \left( \lambda^3 \left( \frac{1}{r} - 1 + \alpha \right) - 1 + r \right), \\ G &= \frac{\mu}{\lambda} (1 - r). \end{aligned} \quad (2.26)$$

Substituting these expressions into (2.24) gives the apparent shear modulus before the semi-soft threshold,

$$C_5(\lambda) = \frac{\mu r}{\lambda} \left( \frac{\lambda^3 - \lambda_1^3}{\lambda^3 - r\lambda_1^3} \right). \quad (2.27)$$

The calculation in the second region of the semisoft plateau ( $\lambda_1 \leq \lambda \leq \sqrt{r}\lambda_1$ ) is more involved because of the more complicated deformations. Substituting the appropriate form for  $\underline{\lambda}_i$  (eqn. (2.6)) into the free

energy we find an  $F$  that is valid for arbitrary  $\theta$ :

$$F = \frac{\mu}{2\lambda} \left[ \sin^2 \theta (1-r) \left( \frac{\lambda^3}{r\lambda_1^3} + \left( \sqrt{\lambda} \lambda_{xz} + \gamma \sqrt{\frac{\lambda_1}{\lambda}} \right)^2 \right) + \lambda^3 + \frac{\lambda}{\lambda_1} + r \left( \sqrt{\lambda} \lambda_{xz} + \gamma \sqrt{\frac{\lambda_1}{\lambda}} \right)^2 + (r + (1-r) \cos^2 \theta) \frac{\lambda_1}{\lambda} + 2(1-r) \sin \theta \cos \theta \sqrt{\frac{\lambda_1}{\lambda}} \left( \sqrt{\lambda} \lambda_{xz} + \gamma \sqrt{\frac{\lambda_1}{\lambda}} \right) \right] \quad (2.28)$$

Expanding out about  $\theta_o$  we can extract the coefficients to calculate  $C_5$ :

$$\begin{aligned} \frac{2\lambda D}{\mu} &= \sin^2 \theta_o (1-r) \frac{\lambda_1}{\lambda} + r \frac{\lambda_1}{\lambda} \\ \frac{2\lambda E}{\mu} &= \cos 2\theta_o (1-r) \left( \frac{\lambda^3}{\lambda_1^3 r} + \lambda \lambda_{xz}^2 - \frac{\lambda_1}{\lambda} \right) \\ &\quad - 2 \sin 2\theta_o (1-r) \sqrt{\lambda_1} \lambda_{xz} \\ \frac{2\lambda G}{\mu} &= 2 \sin 2\theta_o (1-r) \sqrt{\lambda_1} \lambda_{xz} + 2 \cos 2\theta_o (1-r) \frac{\lambda_1}{\lambda}. \end{aligned} \quad (2.29)$$

Calculating  $C_5$  is now simply a matter of using eqns. (2.6) and (2.7) to replace  $\theta_o$  and  $\lambda_{xz}$  by  $\lambda$  in these expressions then compiling the expressions into  $C_5$  using eqn. (2.24). The details of this manipulation can be found in the Appendix (section 2.8), the result is

$$C_5 = \frac{4\mu r (\beta^2(1+r) - \beta^4 - r)}{\lambda \beta^3(r-1)^2}. \quad (2.30)$$

where  $\beta = \lambda/\lambda_1$ .

In the region after the semi-soft plateau, when the director rotation is complete, ( $\lambda > \sqrt{r}\lambda_1$ ), substituting the appropriate  $\underline{\underline{\lambda}}$  (eqn. (2.8))

into the free energy gives,

$$F = \frac{\mu}{2\lambda} \left[ (\lambda^3 + \gamma^2 \sqrt{r}) \left( 1 - \frac{r-1}{r} \sin^2 \theta \right) + \alpha \lambda^3 \sin^2 \theta - \gamma \sqrt{r} \frac{r-1}{r} \sin 2\theta + \sqrt{r} \left( 1 - \frac{r-1}{r} \cos^2 \theta \right) + 1 \right]. \quad (2.31)$$

Expanding this about  $\theta = \pi/2$  gives the coefficients

$$\begin{aligned} D &= \frac{\mu}{2\sqrt{r}\lambda}, \\ E &= \frac{\mu}{2\sqrt{r}\lambda} \left( \frac{\lambda^3}{\sqrt{r}} \left( 1 - \frac{1}{r} - \alpha \right) + 1 - r \right), \\ G &= \frac{\mu}{\sqrt{r}\lambda} (1 - r), \end{aligned} \quad (2.32)$$

which, when substituted into eqn. (2.24) give

$$C_5 = \frac{\mu}{\sqrt{r}\lambda} \left( \frac{\lambda^3 - r^{\frac{3}{2}}\lambda_1^3}{\lambda^3 - \sqrt{r}\lambda_1^3} \right). \quad (2.33)$$

The full graph of the apparent shear modulus ( $C_5$ ) variation with  $\lambda$  and the strength of semi-softness  $\alpha$  is shown in Fig. 2.5. A slice through this graph at constant  $\alpha$  is shown in Fig. 2.6. The graphs clearly show kinks in  $C_5$  along the zeroes at the beginning and end of director rotation. Differentiating the form for  $C_5(\lambda)$ , it is straightforward to show that at the first kink  $C_5 \propto |\lambda - \lambda_1|$  and at the second kink  $C_5 \propto |\lambda - \sqrt{r}\lambda_1|$ . The constants of proportionality in these relations are different on each side of each kink.

## 2.5 GENERAL CONSEQUENCES OF DIRECTOR ROTATION

Although we have argued that the compositional fluctuations form of the free energy is very generic, it is possible to construct models

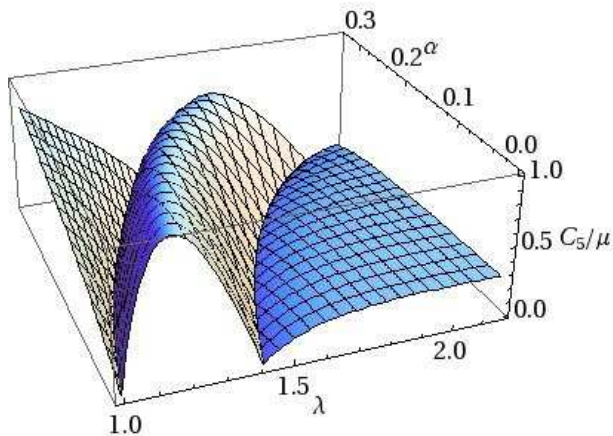


Figure 2.5:  $C_5$  vs  $\lambda$  and  $\alpha$  calculated with the chain anisotropy parameter  $r = 2$ .

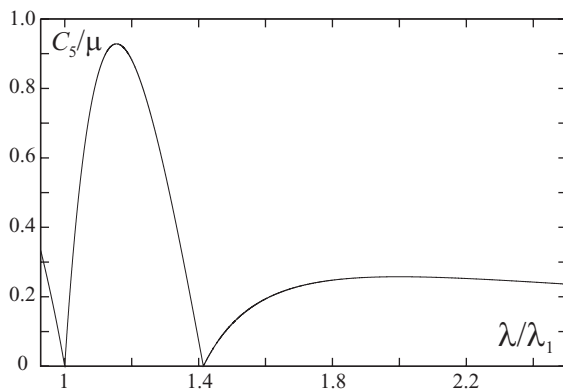


Figure 2.6:  $C_5$  vs reduced extension ( $\lambda/\lambda_1$ ) calculated with the chain anisotropy parameter  $r = 2$  and  $\alpha = 0.1$ .

that go beyond it. Not only might there be additional directions, as considered earlier in the chapter, but if the chains deviate from gaussian distributions, there may be higher powers of  $\underline{\lambda}$  in the free energy. In this section we will give general arguments that none of these effects can alter the key signature of semi-soft elastomers, the stress-plateau, or eradicate the zeroes in the shear modulus discussed in the previous section.

If we once again consider an experiment such as that described in Fig. 2.4, any model of a non ideal elastomer will predict a free energy density for the elastomer as a function of the imposed stretch,  $\theta$  and all the other components of the deformation tensor:

$$F = F(\lambda, \theta, \lambda_{xz}, \dots). \quad (2.34)$$

Before we impose the incremental shear, the behavior of the elastomer will be given by minimising  $F$  over all the variables except  $\lambda$ . We define  $F_\theta$  to be the free energy after minimising over all variables except  $\lambda$  and  $\theta$ . Both before director rotation, and when  $\theta$  is still very small, we can expand  $F_\theta$  in powers of  $\theta$ . Since nothing in the setup distinguishes  $\pm x$  only even powers of  $\theta$  can appear, giving:

$$F_\theta = A(\lambda) + B(\lambda)\theta^2 + C(\lambda)\theta^4 + \dots \quad (2.35)$$

This is minimised by taking

$$\theta = \begin{cases} 0, & B \geq 0, \\ \pm\sqrt{-B/2C}, & B < 0. \end{cases} \quad (2.36)$$

Since before any strain was applied  $\theta = 0$ , the sample must start with  $B \geq 0$ . When the director rotates,  $\theta$  becomes non-zero, and so  $B$  must become negative. Thus at the onset of director rotation,  $B$

must pass through  $B = 0$  and, if this happens at a threshold  $\lambda = \lambda_1$ , then  $B$  generically behaves as  $B \sim \lambda_1 - \lambda$ . We thus expect  $\theta$  to grow as  $\theta \propto \sqrt{-B} \propto \pm\sqrt{\lambda - \lambda_1}$ . We can calculate the gradient of the stress-strain curve (the apparent extension modulus at high strains) on either side of this point as the second derivative of the minimised free energy with respect to  $\lambda$ :

$$\frac{d^2F}{d\lambda^2} = \begin{cases} A'', & B = 0^+ \\ A'' - B'^2/2C & B = 0^-, \end{cases} \quad (2.37)$$

where ' indicates derivative with respect to  $\lambda$ . Since  $C$  is positive definite (to ensure the theory gives finite values for  $\theta$ ) the stress-strain curve has a discontinuous reduction in gradient at the onset of rotation, which reflects the start of a stress-strain plateau.

The onset of rotation occurs when the quadratic term in the free energy vanishes ( $B = 0$ ) making  $F_\theta$  quartic to leading order in  $\theta$ . In nematic elastomers the director couples to the elastomer network, that is changes in the director cause deformations of the elastomer and vice-versa. As  $\theta$  is adjusted slightly to explore this quartic well there is an accompanying deformation,  $\underline{\lambda}$ . The only component of  $\underline{\lambda}$  that can reflect the sign of  $\theta$  is the  $\lambda_{xz}$  shear component. Since  $F_\theta$  is quartic in  $\theta$ , the energy cost of imposing such a shear will also be quartic in  $\lambda_{xz}$ , so the corresponding shear modulus disappears at this point.

Because nematic order is of quadrupolar symmetry,  $F_\theta$  must be  $\pi$ -periodic in  $\theta$  and is in fact more properly expressed as a power series in  $\sin 2\theta$ . At the end of director rotation  $\theta = \pm\pi/2$  so  $\sin 2\theta$  is again vanishing and  $F$  can again be truncated at 4th order. This means that the cessation of director rotation can be described as the reverse of the onset director rotation, so the transition is again accompanied

by a vanishing apparent shear modulus (for  $x$ - $z$  shear) and a discontinuity (this time an increase) in the gradient of the stress-strain curve marking the end of the plateau.

## 2.6 ADDITIONAL SOFTNESS CAUSED BY TEXTURE

The preceding analysis predicting a vanishing shear modulus at the onset and end of director rotation assumed that the elastomer deformed in the lowest energy affine way, whereas in fact we know that monodomains subject to extension perpendicular to their director deform in a textured way, forming stripes of equal and opposite shear and director rotation. It is likely that the timescales for the adoption of such textures are rather long — observations of the stress-strain plateau often requires the elastomer to relax for minutes or even longer between measurements — which may place such calculations outside the spirit of rheological investigation, but analysis of the true lowest energy equilibrium response is certainly interesting in its own right.

If we allow for the formation of the lowest energy textured state then the modulus for an incremental shear compounded with a finite extension vanishes not only at the onset and end of director rotation, but at every point in between. This is simply because the stretch imposed between the onset and end of director rotation is associated with a non-zero sympathetic  $\lambda_{xz}$  shear — see eqn. (2.6). The sense of these shears follow the sense of the director rotation, but switching the sense of both, that is setting  $\lambda_{xz}$  to  $-\lambda_{xz}$  and  $\theta$  to  $-\theta$ , gives an exactly equivalent state which must have the same energy. This symmetry underpins the zeroes in shear modulus already observed. The elastomer can form a stripe domain exactly like the one described in Fig. 1.11 using these two equivalent states with the same  $x$  extension ( $\lambda$ ) but different senses of shear  $\lambda_{xz}$ . In the introduction 50:50

stripe-fractions were considered, resulting in a state with no macroscopic shear, but by changing this volume fraction a state with a shear anywhere between  $+\lambda_{xz}$  and  $-\lambda_{xz}$  can be achieved without changing the free energy density. Accordingly, the shear modulus associated with  $\lambda_{xz}$  shear, the  $C_5$  modulus, must be zero. Furthermore, it is not just zero to first order because the elastomer is in fact exploring some quartic rather than quadratic well, rather it is truly zero for all shears between  $\pm\lambda_{xz}$  because the free energy function between these shears is completely flat.

## 2.7 CONCLUSIONS

We have shown that the success of the compositional-fluctuations model of non-ideal nematic elastomers it in fact predicted a very generic form for the free energy. We have further shown that any theory including director rotation will lead to zeroes in the apparent shear modulus ( $C_5$ ) and kinks in the stress-strain curve (forming a stress-strain plateau) at the onset and end of director rotation. We have calculated this modulus as a function of pre-imposed strain for the compositional-fluctuations model of semi-softness, and shown it does predict these zeros, but also predicts other features which could form the basis of further experimental tests. Furthermore, we predict that in sufficiently slow experiments, the shear modulus should also vanish between the onset and conclusion of rotation, and for finite as well as small shears.

The zeroes in the shear modulus that have been the main focus of the latter part of this chapter were first proposed by Lubensky at the International Liquid Crystal Elastomer Conference in 2007, and were the cause of much controversy. Since then several authors have examined the issue [28, 44, 65] and a consensus has emerged that the

## HARD AND SOFT LCEs

zeroes must indeed occur, and they have been observed experimentally [50].

## 2.8 APPENDIX: ALGEBRAIC MANIPULATIONS BETWEEN EQN. (2.29) AND (2.30)

Introducing  $\beta = \lambda/\lambda_1$  we see immediately that substituting the expression for  $\sin \theta_o$  (2.6) into the expression for C gives

$$\frac{2\lambda C}{\mu} = \frac{r}{\beta^3}. \quad (2.38)$$

The expressions for E and F are more complicated, so it is worth considering them one part at a time. First we calculate  $\sin 2\theta$  and  $\cos 2\theta$ :

$$\sin 2\theta = 2 \sin \theta \sqrt{1 - \sin^2 \theta} \quad (2.39)$$

$$= \frac{2\sqrt{r}}{r-1} \sqrt{\left(1 - \frac{1}{\beta^2}\right) \left(\frac{r}{\beta^2} - 1\right)} \quad (2.40)$$

and,

$$\cos 2\theta = 1 - 2 \sin^2 \theta = 1 - \frac{2r}{r-1} \left(1 - \frac{1}{\beta^2}\right). \quad (2.41)$$

Second, we reexpress  $\lambda_{xz}$  as

$$\lambda_{xz}^2 = \frac{1}{r\lambda\beta} (\beta^2 - 1)(r - \beta^2). \quad (2.42)$$

We can now calculate two larger expressions needed for G:

$$2 \sin 2\theta (1-r) \sqrt{\lambda_1} \lambda_{xz} = -\frac{4}{\beta^3} (\beta^2 - 1) (r - \beta^2) \quad (2.43)$$

and,

$$\frac{\lambda_1}{\lambda} 2 \cos 2\theta (1-r) = \frac{2+2r}{\beta} - \frac{4r}{\beta^3}. \quad (2.44)$$

Adding these two expressions to find  $G$ , we get

$$\frac{2\lambda G}{\mu} = 4\beta - 2\frac{r+1}{\beta}. \quad (2.45)$$

To find  $E$  we need to first compute one more fragment:

$$\begin{aligned} & \cos 2\theta(1-r) \left( \frac{\beta^3}{r} + \lambda \lambda_{xz}^2 \right) \\ &= \frac{1}{r}(1+r-\frac{2r}{\beta^2}) \left( \beta^3 + \frac{1}{\beta}(\beta^2-1)(r-\beta^2) \right), \end{aligned} \quad (2.46)$$

which multiplies out to give

$$= \beta \left( 2 + \frac{1}{r} + r \right) - \frac{3}{\beta}(r+1) + \frac{2r}{\beta^3}. \quad (2.47)$$

Substituting these results for the three fragments back into (2.29) we see that

$$\frac{2\lambda E}{\mu} = \beta \left( r + \frac{1}{r} - 2 \right). \quad (2.48)$$

We can now substitute these expressions for  $E$   $C$  and  $G$  into (2.24) to find  $C_5$ ,

$$C_5 = \frac{\mu}{\lambda} \left( \frac{r}{\beta^3} - \frac{(2\beta^2 - r - 1)^2}{\beta^3(r + \frac{1}{r} - 2)} \right), \quad (2.49)$$

which simplifies to

$$C_5 = \frac{4\mu}{\lambda\beta^3} \left( \frac{\beta^2(1+r) - \beta^4 - r}{r + \frac{1}{r} - 2} \right), \quad (2.50)$$

the result stated in the chapter.

# Chapter 3

## STRAIN INDUCED POLARIZATION IN NON-IDEAL CHIRAL NEMATIC ELASTOMERS

NEMATIC LIQUIDS do not exhibit electrical polarizations, and nor do conventional elastomers, although spontaneous polarizations in chiral SmC elastomers are common. In this chapter we will show that, although ideal chiral nematic elastomers cannot exhibit strain induced polarizations, non-ideal ones, which is to say all real ones, can. This result will first be argued on symmetry grounds, then confirmed by a microscopic model. We will also calculate an example of a polarization-strain curve for a typical experimental geometry. In this geometry the polarization is exactly zero at both small and large strain but pronounced for a large set of intermediate strains corresponding to the strains that cause incremental rotation of the nematic director.

### 3.1 INTRODUCTION

In this chapter we depart briefly from the elastic response of nematic elastomers to consider their electrical response to imposed strains. Our understanding that the key difference between the ideal nematic elastomer model and the more realistic non-ideal model relates to the

existence of a completely isotropic reference state [36] in the former and not in the latter will allow us to establish that while ideal systems cannot exhibit strain induced polarization, non-ideal ones can. Two previous papers have looked at polarizations in nematic elastomers. Warner and Terentjev [52,63] developed a microscopic theory of Gaussian chains of chiral rod like monomers to model chiral ideal elastomers. It was found that although polarizations did arise in the model if the nematic director and imposed strain were specified separately, if, as would really happen in an experiment, the director was allowed to rotate to the lowest energy direction, then the polarizations disappeared. Here we argue this is because ideal elastomers have an isotropic reference state rather than because of the details of the model. The microscopic model developed in this paper will be a non-ideal counterpart of the model in this work. Adams [1] explored several mechanisms to circumvent this relaxation including non equilibrium dynamics, smectic ordering and a specially prepared semi-soft elastomer. Here we argue that in fact all semi-soft chiral nematic elastomers, and hence all real life chiral nematic elastomers, will show strain-induced polarizations that will not relax to zero on holding the strain.

Rubbers are much softer than conventional piezoelectric materials such as quartz, so they will exhibit polarizations at much higher strains but much lower stresses. Their low mechanical impedance will also help them couple to liquid and gaseous systems rather more efficiently than ceramic and crystalline transducers. These properties may eventually lead to applications as sensors in high strain, low stress environments.

This chapter will be presented in three sections. In the first, symmetry arguments will be used to show that ideal elastomers cannot show electrical polarization, but non-ideal ones can. These will then

be developed to predict the full form of the polarization as a function of strain. In the second section a microscopic minimal model of chiral non-ideal elastomers — Gaussian chains with main-chain chiral liquid-crystal rods and compositional fluctuations — will be constructed and shown to exhibit the form of strain-induced polarization predicted by the phenomenological analysis. Finally, in the third section, an example of a polarization-strain curve will be calculated for a specific geometry, namely stretching a nematic elastomer perpendicular to its director.

### 3.2 PHENOMENOLOGICAL APPROACH

In the liquid state chiral nematic liquid crystals form helical phases called cholesterics. Several authors have used a phenomenological approach to study strain induced polarization in cholesteric elastomers [18, 49, 53], although the subtleties of the symmetry cholesteric phases lead to incorrect conclusions in at least two of these papers [18, 53]. This work differs from all the above in that it describes strain using the full (non-linear) deformation gradient tensor, and works directly with the polarization pseudovector rather than the free energy, and, more importantly, because it deals with the chiral nematic monodomain state. This is not a state accessible to fluid liquid-crystals, but can easily be achieved in an elastomer by cross-linking in the presence of a stress-field, just like a conventional nematic monodomain.

#### 3.2.1 SYMMETRY ARGUMENTS FOR THE EXISTENCE OF A POLARIZATION

Ideal nematic elastomers have an isotropic reference state which is found by applying the deformation  $\underline{\lambda} \propto \underline{\ell}_o^{-\frac{1}{2}}$  to the relaxed state, in effect compressing it along the nematic director so that the poly-

mers follow an isotropic conformation distribution. An isotropic state clearly cannot show any polarization since every direction is equal, so no one direction can be distinguished for the polarization to point along. If a deformation  $\underline{\Lambda}$  applied to this state (breaking the isotropy) were to cause a strain induced polarization  $\mathbf{p}$ , we would like to be able to write  $\mathbf{p}$  as a function of  $\underline{\Lambda}$  so that we could predict what polarization a given deformation would cause. Unfortunately there is no function that can map deformations onto vectors. Intuitively this is because a deformation from an isotropic state is completely characterized by three double headed perpendicular vectors (the principal stretches), and even with a handedness and hence the ability to take cross products, this does not uniquely define any single headed axial or polar vectors. We can easily prove this more formally by considering (without loss of generality) a diagonal deformation  $\underline{\Lambda}$  from the isotropic state. If the function  $f$  maps  $\underline{\Lambda}$  onto a polarization  $\mathbf{p}$ ,

$$f(\underline{\Lambda}) = \mathbf{p}, \quad (3.1)$$

then, for any rotation  $\underline{\underline{R}}$  it must satisfy

$$f(\underline{\Lambda} \cdot \underline{\underline{R}}) = \mathbf{p}, \quad (3.2)$$

because the reference state is isotropic. Similarly

$$f(\underline{\underline{R}} \cdot \underline{\Lambda}) = \underline{\underline{R}}\mathbf{p}, \quad (3.3)$$

because a final state rotation should rotate a final state vector. If  $\underline{\underline{R}}$  is a  $\pi$  rotation about one of the principal directions of  $\underline{\Lambda}$  then  $\underline{\underline{R}} \cdot \underline{\Lambda} \cdot \underline{\underline{R}} = \underline{\Lambda}$  but

$$f(\underline{\underline{R}} \cdot \underline{\Lambda} \cdot \underline{\underline{R}}) = \underline{\underline{R}}\mathbf{p} = f(\underline{\Lambda}) = \mathbf{p}, \quad (3.4)$$

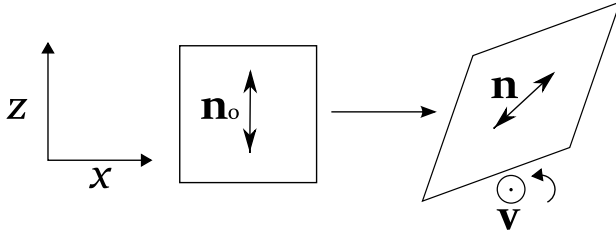


Figure 3.1: An elastomer prepared with director  $\hat{\mathbf{n}}_o$  is subject to pure shear that causes the director to rotate to  $\hat{\mathbf{n}}$ . If the elastomer was allowed to relax, the director would rotate anticlockwise. Applying a “right-hand rule” (derived from the handedness of the chiral nematic rods) to this rotational sense allows an axial vector  $\mathbf{v}$  to be defined.

which is only possible if  $\mathbf{p}$  is along the axis of  $\underline{\underline{R}}$ . However, we could have chosen the axis of  $\underline{\underline{R}}$  to be any of the three perpendicular principle stretches of  $\underline{\underline{\Lambda}}$ , and  $\mathbf{p}$  cannot be parallel to all of them, so the function  $f$  and hence an electrical polarization cannot exist.

The above argument relies crucially on the existence of an isotropic reference state, eqn. (3.2), which is the hallmark of an ideal elastomer. However, non-ideal elastomers do not have an isotropic reference state so the above reasoning does not apply. Indeed it is easy to see that a non-ideal elastomer does have low enough symmetry to exhibit polarization. Consider a strip of non-ideal elastomer prepared with its director,  $\mathbf{n}_o$ , parallel to the  $z$  axis, that is then subject to pure shear causing the director to rotate to  $\mathbf{n}$  as shown in Fig. 3.1. Since the elastomer is non ideal, the energy of the elastomer increases. In this state the director “knows” about a definite rotational sense — the direction in which it would rotate if the elastomer were allowed to relax — so if the system also has a handedness, caused by the chiral nature of the nematic rods, a right hand rule can be applied to the director and its turning sense to define a single headed pseudovector  $\mathbf{v}$  along

which a polarization could lie. This argument fails if the elastomer is ideal because the elastomer can relax to a zero energy state with director  $\mathbf{n}$  so relaxation does not define a rotational sense. There is also no rotational sense before any strain is imposed, so the relaxed state is not polarized. More subtly, there is no rotational sense after some very large strains have been imposed — if a large  $x$  stretch had been imposed the director would lie along the  $x$  axis so, on relaxation, it could rotate back clockwise or anticlockwise to relax to  $z$ . However, the reasoning does apply to all states where the director has started rotating and applying further deformation causes further rotation.

### 3.2.2 STRAIN DEPENDENCE OF THE POLARIZATION

Any polarization in a semi-soft chiral nematic elastomer must be built out of the following ingredients,  $\hat{\mathbf{n}}_o$ ,  $\hat{\mathbf{n}}$ ,  $\underline{\lambda}$  and  $\epsilon_{ijk}$ . To be properly rotationally invariant the polarization must be constructed by contracting these objects correctly, that is by only contracting final state indexes (the  $i$  on  $\lambda_{ij}$  and the  $i$  on  $n_i$ ) with other final state indexes, and likewise for reference state indexes (the  $j$  on  $\lambda_{ij}$  and the  $j$  on  $n_{oj}$ ). Finally, since  $\hat{\mathbf{n}}$  and  $\hat{\mathbf{n}}_o$  are nematic directors, they are quadrupolar (double headed) vectors so they must only appear in even numbers so that the polarization is invariant under the transformations  $\hat{\mathbf{n}} \mapsto -\hat{\mathbf{n}}$  and  $\hat{\mathbf{n}}_o \mapsto -\hat{\mathbf{n}}_o$ . At zeroth order in  $\underline{\lambda}$  the only permissible term is

$$\epsilon_{ijk} n_j n_k \quad (3.5)$$

which is zero because contracting a symmetric tensor with  $\epsilon_{ijk}$  gives zero. Similarly at first order in  $\underline{\lambda}$  the only possible term,  $\lambda_{ij} \epsilon_{jkl} n_{ok} n_{ol}$  is also zero. At second order in  $\underline{\lambda}$  there are 5 permissible terms that

are listed below:

$$\epsilon_{jkl} [\underline{\lambda} \underline{\lambda}^T, \underline{\lambda} \hat{\mathbf{n}}_o \hat{\mathbf{n}}_o \underline{\lambda}^T, \underline{\lambda} \underline{\lambda}^T \hat{\mathbf{n}} \hat{\mathbf{n}}, \underline{\lambda} \hat{\mathbf{n}}_o \hat{\mathbf{n}}_o \underline{\lambda}^T \hat{\mathbf{n}} \hat{\mathbf{n}}, \hat{\mathbf{n}} \hat{\mathbf{n}} \underline{\lambda} \underline{\lambda}^T]_{kl}. \quad (3.6)$$

The first and second of these give zero. The third and fifth are parallel because both  $\hat{\mathbf{n}} \hat{\mathbf{n}}$  and  $\underline{\lambda} \underline{\lambda}^T$  are symmetric tensors. Therefore we only have two potentially independent vectors left,

$$\epsilon_{jkl} [\underline{\lambda} \underline{\lambda}^T \hat{\mathbf{n}} \hat{\mathbf{n}}]_{kl} \text{ and } \epsilon_{jkl} [\underline{\lambda} \hat{\mathbf{n}}_o \hat{\mathbf{n}}_o \underline{\lambda}^T \hat{\mathbf{n}} \hat{\mathbf{n}}]_{kl}. \quad (3.7)$$

We expect the elasticity of a chiral nematic elastomer to be governed by the compositional fluctuations free energy studied at length in the previous chapter, and that  $\hat{\mathbf{n}}$  will rotate to the direction that minimized this energy. The terms in the compositional fluctuations model involving  $\hat{\mathbf{n}}$  are

$$\text{Tr} \left( \left( \left\langle \frac{1}{r} - 1 \right\rangle \underline{\lambda} \underline{\lambda}^T + \left\langle 2 - r - \frac{1}{r} \right\rangle \underline{\lambda} \hat{\mathbf{n}}_o \hat{\mathbf{n}}_o \underline{\lambda}^T \right) \hat{\mathbf{n}} \hat{\mathbf{n}} \right). \quad (3.8)$$

The matrix pre-multiplying  $\hat{\mathbf{n}} \hat{\mathbf{n}}$  is clearly symmetric and hence, in some frame, diagonal. Therefore the energy is minimized when  $\hat{\mathbf{n}}$  lies along the eigenvector of this matrix with smallest eigenvalue, giving the relaxation condition that

$$\left( \left\langle \frac{1}{r} - 1 \right\rangle \underline{\lambda} \underline{\lambda}^T + \left\langle 2 - r - \frac{1}{r} \right\rangle \underline{\lambda} \hat{\mathbf{n}}_o \hat{\mathbf{n}}_o \underline{\lambda}^T \right) \hat{\mathbf{n}} \hat{\mathbf{n}} = A \hat{\mathbf{n}} \hat{\mathbf{n}} \quad (3.9)$$

for the smallest eigenvalue  $A$ . Contracting this relaxation condition with the  $\epsilon_{ijk}$  we see that both the above terms (eq. (3.7)) are also parallel, so the only admissible vector at quadratic order in  $\underline{\lambda}$  is

$$\mathbf{p} \propto \epsilon_{jkl} [\underline{\lambda} \underline{\lambda}^T \hat{\mathbf{n}} \hat{\mathbf{n}}]_{kl}. \quad (3.10)$$

However, elasticity in nematic elastomers is typically large strain, so there is little reason to truncate this series at quadratic order. At higher orders there are other admissible vectors that can be constructed. However, rubber-elasticity, particularly Gaussian rubber elasticity, is extremely well described by just the low order terms even at large strain, motivating the consideration of just the lowest order terms.

### 3.3 MICROSCOPIC MINIMAL MODEL

The phenomenological analysis above suggests a simple and universal form for the direction and strain-dependence of polarization in chiral nematic elastomers — eq. (3.10). In the following section we develop a microscopic minimal model that also predicts the same form. The use of this is threefold, it lends weight to the phenomenological analysis, yields an overall magnitude for the polarization (which tends to zero as the elastomer becomes ideal) and illustrates a possible microscopic mechanism for the effect. The model developed is a non-ideal counterpart of that studied in [63].

#### 3.3.1 SETTING UP THE MODEL

The model is based on two different rigid rod monomers. The first, species 1, we model as a rigid rod of length  $a$ . The second, species 2, we model as an L shaped molecule with dimensions  $a$  and  $b$  and an electrical dipole  $\mathbf{d}$  assigned using a “right-hand rule” — see Fig. 3.2. The two monomers are polymerized to make random co-polymers, which we model as freely jointed (Gaussian) chains of  $N$  monomers, with binomially distributed compositions between species one and two. The rigid rod nature of the monomers allows them to form a joint nematic phase, which results in the polymers having anisotropic conformation

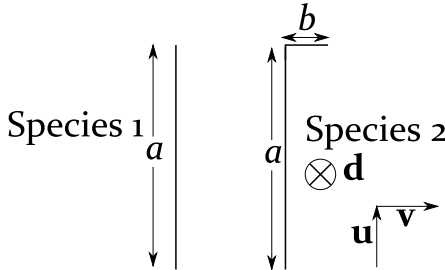


Figure 3.2: Dimensions of the two species of rigid rod monomers. The electrical dipole  $d$  is assigned using a “right-hand rule”,  $\mathbf{d} \propto \mathbf{u} \wedge \mathbf{v}$ , making the second species chiral.

distributions. However, the two monomers couple to the nematic order with different strengths, so a polymer made entirely of species 1 would have step length tensor  $\underline{\underline{\ell}}_1 \propto \underline{\underline{\delta}} + (r_1 - 1)\hat{\mathbf{n}}\hat{\mathbf{n}}$  with anisotropy  $r_1$  and one made of species two would have step length tensor  $\underline{\underline{\ell}}_2 \propto \underline{\underline{\delta}} + (r_2 - 1)\hat{\mathbf{n}}\hat{\mathbf{n}}$  with anisotropy  $r_2$ . For simplicity we assume that the constants of proportionality for both these tensors is the same. The random copolymers have different overall anisotropies depending on their composition. The polymers are cross linked in the nematic state to form a chiral non-ideal nematic liquid crystal elastomer, which we will show exhibits strain induced polarization.

This model captures the two essential ingredients for a nematic elastomer to show electrical polarization, non-ideality (introduced via compositional fluctuations) and chirality, introduced by the right hand rule used to assign the electrical dipoles to the L shaped monomers.

The assumptions that both species of monomer have the same length, and that both step length tensors have the same constants of proportionality (i.e. the same components perpendicular to  $\hat{\mathbf{n}}$ ) are somewhat unrealistic. However, these assumptions significantly simplify the algebra. The model can be solved without these assumptions in the same manner as outlined below, with the end result being sim-

ply that the coefficient of polarization is slightly altered.

### 3.3.2 POLYMERS WITH HOMOGENEOUS COMPOSITION

If a polymer is constructed out of freely jointed monomers of species 2, numbered by  $\alpha = 1, \dots, N$ , and each monomer has end to end vector  $\mathbf{w}^\alpha = a\mathbf{u}^\alpha + b\mathbf{v}^\alpha$  (see Fig. 3.2) then the total end to end vector for the chain is

$$\mathbf{R} = \sum_{\alpha} \mathbf{w}^\alpha \quad (3.11)$$

and, defining the binormal of the chain to be

$$\mathbf{V} = \sum_{\alpha} \mathbf{u}^\alpha \wedge \mathbf{w}^\alpha, \quad (3.12)$$

the electrical polarization of the chain is

$$\mathbf{p} = d\mathbf{V}. \quad (3.13)$$

If the monomers in the chain are freely jointed, their orientations are independent, and the probability of the chain being in a configuration with a given  $\mathbf{R}$  and  $\mathbf{V}$  is [63]

$$P_2(\mathbf{R}, \mathbf{V}) \propto \exp \left( -\frac{3}{2Na} \mathbf{R}^T \underline{\underline{\ell}}^{-1} \mathbf{R} - \frac{1}{N} \mathbf{V}^T \underline{\underline{M}}^{-1} \mathbf{V} \right) \times \quad (3.14)$$

$$\left( 1 + \frac{3b}{N^2 a^2} [\mathbf{R} \wedge \underline{\underline{\ell}}^{-1} \mathbf{R}] \underline{\underline{M}}^{-1} \mathbf{V} + O(R^4, R^2 V^2) + \dots \right).$$

where, if the nematic director is  $\mathbf{n}$  then  $\underline{\underline{\ell}} \propto \underline{\underline{\delta}} + (r_2 - 1)\mathbf{n}\mathbf{n}$  and  $\underline{\underline{M}} = \underline{\underline{\delta}} - \underline{\underline{\ell}}/3a$ . This model can give a non zero binormal for a chain if the spanning vector for the chain is not along the liquid-crystal director. An intuitive sense of this can be developed by considering a 2D system with perfect nematic order, so all long sides of all the

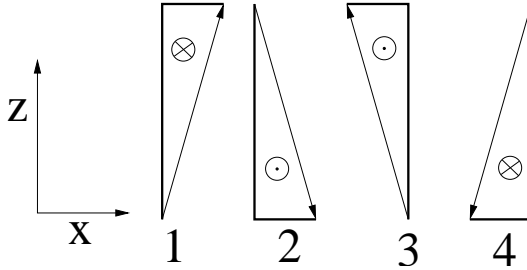


Figure 3.3: The four possible orientations for L shaped monomer units confined to 2D and by perfect nematic alignment in the  $z$  direction. The vector bi-normals, assigned with a right hand rule, are also shown pointing into out of the page.

Ls align perfectly along the nematic director,  $\mathbf{z}$ . This means each monomer can contribute one of 4 vectors to the chain path, shown in Fig. 3.3. If the overall conformation has a significant component along  $z$  then there must be many more monomers in the first and third orientations than the second and fourth. If the conformation also includes a component along  $x$  then there must be more monomers in the first orientation than the third, so an overall binormal is developed.

The equivalent result for a chain made entirely of species 1, and thus with no binormal, is simply

$$P_1(\mathbf{R}) \propto \exp\left(-\frac{3}{2Na}\mathbf{R}^T \underline{\underline{\ell}}_1^{-1} \mathbf{R}\right), \quad (3.15)$$

where  $\underline{\underline{\ell}}_1 \propto \underline{\underline{\delta}} + (r_1 - 1)\mathbf{n}\mathbf{n}$ .

### 3.3.3 RANDOM CO-POLYMERS

If a chain has  $N_1$  monomers of species 1 and  $N_2 = N - N_1$  monomers of species 2, since the chain is freely jointed, the order in which the monomers are arranged does not effect the conformation probability distribution. Therefore, the chain is equivalent to a chain of  $N_1$

monomers of species one connected to a chain of  $N_2$  monomers of species 2, so the new chains distribution is simply

$$P(\mathbf{R}, \mathbf{V}) = \int P_1(\mathbf{R}_1) P_2(\mathbf{R} - \mathbf{R}_1, \mathbf{V}) d\mathbf{R}_1. \quad (3.16)$$

This distribution can be calculated explicitly (see the appendix — section 3.6 — for details) by completing the square in the exponent. The resulting distribution is

$$\begin{aligned} P(\mathbf{R}, \mathbf{V}) \propto & \exp \left( -\frac{3}{2L} \mathbf{R}^T \underline{\underline{\ell}}^{-1} \mathbf{R} - \frac{1}{N_2} \mathbf{V}^T \underline{\underline{M}}^{-1} \mathbf{V} \right) \\ & \times \left( 1 + \frac{3b}{L^2} \frac{r_2 - 1}{r - 1} (\mathbf{R} \wedge \underline{\underline{\ell}}^{-1} \mathbf{R}) \underline{\underline{M}}^{-1} \mathbf{V} + \dots \right) \end{aligned} \quad (3.17)$$

where  $L = Na$  is the total contour length of the chain,  $r$  is the length weighted average of  $r_1$  and  $r_2$ , that is,

$$r = \frac{L_1 r_1 + L_2 r_2}{L_1 + L_2}, \quad (3.18)$$

and  $\underline{\underline{\ell}} \propto \underline{\underline{\delta}} + (r - 1)\mathbf{n}\mathbf{n}$ . We see that the distribution for the co-polymer is identical to that for a homogeneous chain but with modified coefficients.

### 3.3.4 POLARIZATION OF A STRAND OF CO-POLYMER

The polarization of a strand is given as  $d\langle \mathbf{V} \rangle$ . This is straightforward to calculate since

$$\langle \mathbf{V} | \mathbf{R} \rangle = \frac{\int \mathbf{V} P(\mathbf{R}, \mathbf{V}) d\mathbf{V}}{\int P(\mathbf{R}, \mathbf{V}) d\mathbf{V}}. \quad (3.19)$$

Evaluating this is a simple case of doing a Gaussian integral (using eqn. (3.17) as  $P(\mathbf{V})$  which has  $\langle \mathbf{VV} \rangle = \frac{1}{2} N_2 \underline{\underline{M}}$ ) and gives

$$\langle \mathbf{V} | \mathbf{R} \rangle = \frac{3N_2 b}{2L^2} \frac{r_2 - 1}{r - 1} \mathbf{R} \wedge \underline{\underline{\ell}}^{-1} \mathbf{R}. \quad (3.20)$$

If the polymer strand is cross-linked into a nematic elastomer with nematic director  $\hat{\mathbf{n}}_o$  and span vector  $\mathbf{R}_o$  between its crosslinked ends, and then a deformation  $\underline{\lambda}$  is applied to the system, causing the span to change to  $\mathbf{R} = \underline{\lambda} \mathbf{R}_o$  and the director to change to  $\hat{\mathbf{n}}$ , the new binormal will be

$$\langle \mathbf{V} | \mathbf{R}_o \rangle = \frac{3N_2 b}{2L^2} \frac{r_2 - 1}{r - 1} \underline{\lambda} \mathbf{R}_o \wedge \underline{\underline{\ell}}^{-1} \underline{\lambda} \mathbf{R}_o. \quad (3.21)$$

Averaging this expression over all possible initial spanning vectors using  $\langle \mathbf{R}_o \mathbf{R}_o \rangle = L \underline{\underline{\ell}} / 3$  gives

$$\langle \mathbf{V} \rangle = \frac{N_2 b}{2L^2} \frac{r_2 - 1}{r - 1} \epsilon_{ijk} [\underline{\underline{\ell}}^{-1} \underline{\lambda} \underline{\underline{\ell}} \underline{\lambda}^T]_{jk}, \quad (3.22)$$

which gives a polarization per strand of

$$\langle \mathbf{p} \rangle = \frac{bd}{2a} \frac{L_2}{L_1 + L_2} \frac{r_2 - 1}{r - 1} \epsilon_{ijk} [\underline{\underline{\ell}}^{-1} \underline{\lambda} \underline{\underline{\ell}} \underline{\lambda}^T]_{jk}. \quad (3.23)$$

### 3.3.5 MECHANICAL RESPONSE OF A SEMI-SOFT NEMATIC ELASTOMER

The arguments in section 3.2 show that a chiral non-ideal elastomer can develop a polarization under deformation. We thus consider a random co-polymer strand cross-linked into a nematic elastomer network. The mechanical part of its free energy is simply

$$F = \frac{1}{2} k_B T \text{Tr} (\underline{\underline{\ell}} \underline{\lambda}^T \underline{\lambda}^{-1} \underline{\lambda}), \quad (3.24)$$

the same as for a non-chiral strand in a nematic elastomer. However, in this case the anisotropy,  $r$ , is a function of the individual strands composition, so averaging across all the strands in the elastomer gives

$$\begin{aligned}\langle F \rangle &= \frac{1}{2} k_b T \langle \text{Tr} (\underline{\ell}_o \underline{\lambda}^T \underline{\ell}^{-1} \underline{\lambda}) \rangle \\ &= \frac{1}{2} k_b T \text{Tr} \left( \underline{\lambda} \bar{\underline{\ell}}_o \underline{\lambda}^T \bar{\underline{\ell}}^{-1} + \alpha \underline{\lambda} (\underline{\delta} - \hat{\mathbf{n}}_o \hat{\mathbf{n}}_o) \underline{\lambda}^T \hat{\mathbf{n}} \hat{\mathbf{n}} \right),\end{aligned}\quad (3.25)$$

where  $\bar{\underline{\ell}} \propto \underline{\delta} + (\langle r \rangle - 1) \hat{\mathbf{n}} \hat{\mathbf{n}}$  and  $\alpha = \langle \frac{1}{r} \rangle - \frac{1}{\langle r \rangle}$ . This is the usual non-ideal free energy for a nematic elastomer, so it will also follow the mechanical relaxation condition given in eq. (3.9).

### 3.3.6 POLARIZATION OF A SEMISOFT CHIRAL NEMATIC ELASTOMER

The polarization per strand given in (3.23) takes the form

$$\mathbf{p} = p(r) \epsilon_{ijk} [\underline{\ell}^{-1} \underline{\lambda} \underline{\ell}_o \underline{\lambda}^T]_{jk} \quad (3.26)$$

where the polarizability,  $p(r)$ , is a coefficient that depends on the composition of the strand, and hence its anisotropy ratio. To find the behavior of the whole elastomer we must average this result over all compositions (all strands in the elastomer). Introducing polarization-weighted averages as

$$\langle f(r) \rangle_p = \frac{\langle p(r) f(r) \rangle}{\langle p(r) \rangle} \quad (3.27)$$

we get the strand averaged polarization

$$\begin{aligned}\mathbf{p} &= \langle p(r) \rangle \epsilon_{ijk} \left[ \underline{\lambda} \underline{\lambda}^T + \left\langle \frac{1}{r} - 1 \right\rangle_p \hat{\mathbf{n}} \hat{\mathbf{n}} \underline{\lambda} \underline{\lambda}^T + \right. \\ &\quad \left. \left\langle 2 - r - \frac{1}{r} \right\rangle_p \hat{\mathbf{n}} \hat{\mathbf{n}} \underline{\lambda} \hat{\mathbf{n}}_o \hat{\mathbf{n}}_o \underline{\lambda}^T + \langle r - 1 \rangle_p \underline{\lambda} \hat{\mathbf{n}}_o \hat{\mathbf{n}}_o \underline{\lambda}^T \right]_{jk}.\end{aligned}\quad (3.28)$$

The first and last of these terms evaluate to zero since because they consist of a symmetric tensor contracted with  $\epsilon_{ijk}$ . The middle two terms are exactly the two terms related by the mechanical relaxation condition (3.9). Since  $A\hat{\mathbf{n}}\hat{\mathbf{n}}$  is also a symmetric tensor, we can use the relaxation condition to eliminate one of the two terms, giving

$$\mathbf{P} = \langle p(r) \rangle \left\langle \frac{1}{r} - 1 \right\rangle \left( \frac{\left\langle \frac{1}{r} - 1 \right\rangle_p}{\left\langle \frac{1}{r} - 1 \right\rangle} - \frac{\left\langle 2 - \frac{1}{r} - r \right\rangle_p}{\left\langle 2 - \frac{1}{r} - r \right\rangle} \right) \times \epsilon_{ijk} [\underline{\underline{\lambda}}^T \hat{\mathbf{n}}\hat{\mathbf{n}}]_{jk}. \quad (3.29)$$

This expression for the polarization has a simple vector part but quite a complex coefficient. Note that the coefficient gives zero for an ideal elastomer because then all strands have the same value of  $r$  so both types of average give the same result. They also give the same result (and hence the coefficient is zero) if all strands have the same polarizability.

### 3.3.7 EVALUATING THE COEFFICIENT FOR THE RANDOM CO-POLYMER MODEL

In the analysis of a random co-polymer strand we predicted the anisotropy of the strand,  $r$ , and the polarizability of the strand,  $p(r)$ , in terms of its composition. Assuming the strands for the elastomer were generated by randomly polymerizing a mixture of the two monomer units, a reasonable model for the compositional distribution of the chains is that all the chains have  $N$  monomers, of which  $N_1$  are of species 1, and  $N_1$  is distributed binomially with probability  $q$ ,

$$N_1 \sim B(N, q). \quad (3.30)$$

The effective anisotropy of the chain is given by

$$\langle r \rangle = \left\langle \frac{N_1 r_1 + N_2 r_2}{N} \right\rangle = qr_1 + (1 - q)r_2. \quad (3.31)$$

Defining  $\Delta = N_1 - Nq$ , in a large  $N$  limit we expect  $\Delta/N \sim 1/\sqrt{N}$  to be small, so we can expand the coefficient as a Taylor series in this quantity and then average and keep the leading term. We can easily use this method to evaluate  $\langle 1/r \rangle$ :

$$\left\langle \frac{1}{r} \right\rangle = \left\langle \frac{N}{N_1 r_1 + N_2 r_2} \right\rangle, \quad (3.32)$$

substituting  $N_2$  for  $N$  and  $N_1$  for  $q$  and  $\Delta$  gives

$$\left\langle \frac{1}{r} \right\rangle = \left\langle \frac{1}{r_2 + (q + \Delta/N)(r_1 - r_2)} \right\rangle, \quad (3.33)$$

$$= \left\langle \frac{1}{\langle r \rangle + \Delta(r_1 - r_2)/N} \right\rangle. \quad (3.34)$$

$$(3.35)$$

Expanding in  $\Delta/N$  to second order,

$$\left\langle \frac{1}{r} \right\rangle \approx \frac{1}{\langle r \rangle} \left\langle 1 - \frac{\Delta(r_1 - r_2)}{Nr} + \left( \frac{\Delta(r_1 - r_2)}{Nr} \right)^2 + \dots \right\rangle. \quad (3.36)$$

Finally, taking the average over  $\Delta$  we see that to leading order

$$\left\langle \frac{1}{r} \right\rangle \approx \frac{1}{\langle r \rangle} + \frac{q(1 - q)(r_1 - r_2)^2}{Nr^3} + \dots \quad (3.37)$$

so the semisoft parameter  $\alpha$  is given by

$$\alpha = \left\langle \frac{1}{r} \right\rangle - \frac{1}{\langle r \rangle} \approx \frac{q(1 - q)(r_1 - r_2)^2}{Nr^3}. \quad (3.38)$$

The full coefficient in eqn. (3.29) can be expanded out in a similar manner to give

$$\langle \mathbf{p} \rangle = \frac{bd}{2a} \frac{(r_1 - 1)(r_2 - 1)(r_1 - r_2)q(1 - q)}{Nr(r - 1)^2} \epsilon_{ijk} [\underline{\lambda} \underline{\lambda}^T \hat{\mathbf{n}} \hat{\mathbf{n}}]_{jk}, \quad (3.39)$$

which is non zero, so the model does predict a polarization. At first sight it may appear small because it contains a factor of  $1/N$ . However so does the measure of non-ideality,  $\alpha$ . In the compositional fluctuations model, non-ideality goes to zero as the chain length becomes infinite because the variance of the chain anisotropy vanishes. Therefore this coefficient is only small because our model is in fact almost ideal. Taking this at face value and replacing the small ( $1/N$ ) factor by  $\alpha$  we can (very crudely) estimate the magnitude of the polarization for a real non ideal elastomer as  $|\mathbf{P}| \sim \alpha n \frac{bd}{2a}$ , where  $\mathbf{P}$  is the total polarization per unit volume,  $n$  is the number of strands per unit volume, and we have assumed that the factors involving just  $r$   $q$  and  $\underline{\lambda}$  are of order unity. Substituting reasonable values ( $n \sim 10^{26}$ ,  $b/a \sim 0.1$ ,  $\alpha \sim 0.1$  and  $d \sim e \times 1\text{\AA}$ ) we get  $|\mathbf{P}| \sim 10^{-5}\text{Cm}^{-2}$ . This is of a similar magnitude to mechanically induced polarizations induced in quartz ( $|\mathbf{P}| \sim 10^{-4}\text{Cm}^{-2}$  at 0.2% strain) but at much higher strain ( $\sqrt{r} - 1$  vs. 0.2%) and much lower stress ( $10^5\text{Pa}$ . vs.  $10^8\text{Pa}$ .).

### 3.4 EXAMPLE OF A POLARIZATION-STRAIN CURVE

If a non-ideal nematic elastomer is prepared with its director oriented along the  $z$  axis, and is then stretched by a factor of  $\lambda$  along the  $x$  axis the elastomer passes through three regimes. Verwey & Warner [58] showed that there is a threshold deformation

$$\lambda_1 = \left( \frac{r - 1}{r - 1 - \alpha r} \right)^{1/3}, \quad (3.40)$$

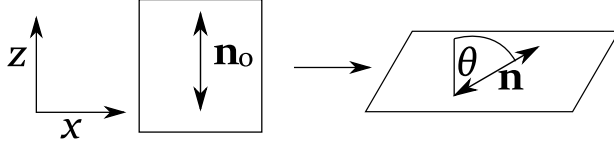


Figure 3.4: For intermediate stretches the energy of the elastomer is significantly reduced if it also undergoes  $x$ - $z$  shear and director rotation.

for extensions with  $\lambda \leq \lambda_1$  the deformation is simply that expected from a classical rubber,  $\underline{\underline{\lambda}} = \text{diag}[\lambda, 1/\sqrt{\lambda}, 1/\sqrt{\lambda}]$ , and the director does not rotate. However, in the second regime,  $\lambda_1 \leq \lambda \leq \sqrt{r}\lambda$ , the energy of the elastomer is significantly reduced if the deformation includes  $\lambda_{xz}$  shear and the director rotates to  $\theta$  with the  $z$  axis (see Fig. 3.4). More precisely,

$$\sin^2 \theta = \frac{r(\lambda^2 - \lambda_1^2)}{(r-1)\lambda^2} \text{ and } \underline{\underline{\lambda}} = \begin{pmatrix} \lambda & 0 & \lambda_{xz} \\ 0 & 1/\sqrt{\lambda_1} & 0 \\ 0 & 0 & \sqrt{\lambda_1}/\lambda \end{pmatrix}, \quad (3.41)$$

where the shear is given by

$$\lambda_{xz}^2 = \frac{(\lambda^2 - \lambda_1^2)(r\lambda_1^2 - \lambda^2)}{r\lambda^2\lambda_1^3}. \quad (3.42)$$

In the third regime,  $\lambda \geq \sqrt{r}\lambda_1$ , director rotation is complete so the director lies along the  $x$  axis and the elastomer again deforms classically,

$$\underline{\underline{\lambda}} = \text{diag}[\lambda, r^{1/4}/\sqrt{\lambda}, 1/(r^{1/4}\sqrt{\lambda})]. \quad (3.43)$$

These results were derived in [58] and are discussed in [64].

In the first and third region the vector part of the polarization gives zero. This is simply because the deformation is symmetric and

$\hat{\mathbf{n}}$  is along one of its eigen-directions, so

$$\mathbf{p} \propto \epsilon_{ijk} [\underline{\lambda} \underline{\lambda}^T \hat{\mathbf{n}} \hat{\mathbf{n}}]_{jk} \propto (\underline{\lambda} \underline{\lambda}^T \hat{\mathbf{n}}) \wedge \hat{\mathbf{n}} \propto \hat{\mathbf{n}} \wedge \hat{\mathbf{n}} = 0. \quad (3.44)$$

However in the second region  $\underline{\lambda}$  is not symmetric and the polarization is non-zero. Calculating the polarization is now a simple matter of substituting the expression for  $\underline{\lambda}$  into (3.10) to get

$$\mathbf{p} \propto \frac{r\lambda_1^3 - 1}{\sqrt{r}\lambda_1^3(r-1)} \sqrt{(\lambda^2 - \lambda_1^2)(r\lambda_1^2 - \lambda^2)} \mathbf{y}. \quad (3.45)$$

A plot of the polarization function is shown below in Fig. 3.5. The form of the polarization is rather unusual, with a very steep profile and non continuous changes of gradient at the onset and end of director rotation. Taking the derivative of eqn. 3.45 with respect to  $\lambda$ , we see that the slope is

$$\frac{d|\mathbf{p}|}{d\lambda} \propto \frac{r\lambda_1^3 - 1}{\sqrt{r}\lambda_1^3(r-1)} \lambda \left( \sqrt{\frac{r\lambda_1^2 - \lambda^2}{\lambda^2 - \lambda_1^2}} - \sqrt{\frac{\lambda^2 - \lambda_1^2}{r\lambda_1^2 - \lambda^2}} \right). \quad (3.46)$$

This diverges as  $1/\sqrt{\lambda - \lambda_1}$  near  $\lambda_1$ , and similarly near  $\sqrt{r}\lambda_1$  at the end of director rotation, so the slope is actually infinite. Since static polarizations tend to be screened out by atmospheric ions, it is generally changes in polarization that are important in experiments and applications, so the divergence of this derivative is significant.

In reality, if a sample is stretched in this manner without applying the energy-lowering shear with the clamps then the elastomer will split into stripes (see [25] for theory or [32] for experiment) each of which undergo opposite shear so that the average shear of the sample is zero. These stripes will have opposite polarization. This is shown in Fig. 3.6. This type of behavior can be eliminated by simultaneously imposing a stretch and a sympathetic shear. As discussed at the end

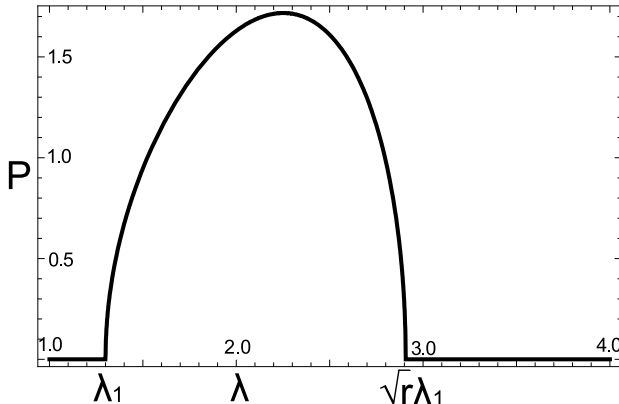


Figure 3.5: Polarization in the  $y$  direction as a function of strain for a elastomer with  $r = 5$  and  $\lambda_1 = 1.3$  The constant of proportionality in eqn. (3.10) has been set to one.

of the previous chapter, the modulus for shearing a stripe domain into a mono-domain is zero since the shear is accommodated by changing the volume fraction of the two types of stripe, so the energy density of the elastomer does not change. This means that a nematic stripe domain, which consists of stripes of alternating shear and polarization, can be sheared into a monodomain with a macroscopic polarization by an infinitesimal shear stress. and the sign of the polarization can be reversed by reversing the infinitesimal shear stress. This could make such a system an extremely sensitive shear stress sensor.

### 3.5 CONCLUSIONS

Semi-soft chiral nematic elastomers have low enough symmetry to exhibit strain-induced polarization. Such polarizations are expected to be caused by any deformation which causes incomplete director rotation, meaning more of the same deformation would lead to more director rotation and vice-versa. Rotation of the director through

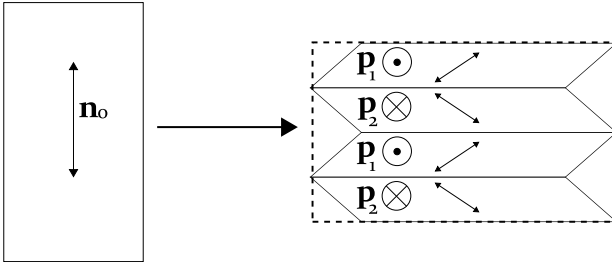


Figure 3.6: If an elastomer is subject to simple stretch with simple clamps then, to achieve the lower energy sheared and stretched state, it splits into stripes of opposite shear so that the total shear is zero. The two types of shear have opposite polarization.

the elastomer is at the root of the phenomena because, as the director rotates away from its preferred orientation, it can distinguish between rotation back to or further away from the preferred direction. The introduction of this rotational sense into the elastomer lowers the symmetry enough for a polarization to form.

On phenomenological grounds, the form of the polarization is expected to be  $\mathbf{p} \propto \epsilon_{ijk}[\underline{\underline{\lambda}} \cdot \underline{\underline{\lambda}}^T \hat{\mathbf{n}} \hat{\mathbf{n}}]_{jk}$ , where  $\underline{\underline{\lambda}}$  is the deformation tensor and  $\hat{\mathbf{n}}$  is the final state liquid crystal director. A microscopic minimal model using compositional fluctuations to model non-ideality and L-shaped liquid crystal mesogens to incorporate chirality also predicts a strain-induced polarization of this form. The microscopic model suggests that polarizations of the order of  $|\mathbf{P}| \sim 10^{-5} \text{ Cm}^{-2}$  could be achievable, which is comparable to the polarizations observed in quartz, but is predicted to occur at much higher strain and much lower stress.

### 3.6 APPENDIX: CONFORMATION DISTRIBUTION OF THE COPOLYMER

We need to calculate  $P(\mathbf{R}, \mathbf{V})$  given by eqn. (3.16). To complete the square in the exponent we substitute  $\mathbf{R}_2 = \mathbf{R}_1 - (\underline{\underline{\ell}}_1^{-1}/L_1 + \underline{\underline{\ell}}_2^{-1}/L_2)^{-1}(\underline{\underline{\ell}}_2^{-1}/L_2)\mathbf{R}$ . The result of this substitution can be simplified by noticing that,

$$\frac{\underline{\ell}_2^{-1}}{L_2} + \frac{\underline{\ell}_2^{-1}}{L_2} \left( \frac{\underline{\underline{\ell}}_1^{-1}}{L_1} + \frac{\underline{\underline{\ell}}_2^{-1}}{L_2} \right) \frac{\underline{\ell}_2^{-1}}{L_2} = \frac{\underline{\ell}}{L_1 + L_2} \quad (3.47)$$

where  $\underline{\ell}$  is the step length tensor with average anisotropy  $r$  given by

$$r = \frac{L_1 r_1 + r_2 L_2}{L_1 + L_2}. \quad (3.48)$$

This is easy to show by direct multiplication of the tensors since  $\underline{\underline{\ell}}_1$  and  $\underline{\underline{\ell}}_2$  are co-diagonal. The substitution gives the new exponent

$$-\frac{3}{2} \left( \mathbf{R}_2^T \left( \frac{\underline{\underline{\ell}}_1^{-1}}{L_1} + \frac{\underline{\underline{\ell}}_2^{-1}}{L_2} \right)^{-1} \mathbf{R}_2 + \mathbf{R}^T \frac{\underline{\ell}^{-1}}{L_1 + L_2} \mathbf{R} \right) - \frac{1}{N_2} \mathbf{V}^T \underline{\underline{M}}^{-1} \mathbf{V}. \quad (3.49)$$

Having completed the square, we can now treat  $\mathbf{R}_2$  as a gaussian distributed variable with second moment proportional to  $\underline{\underline{\ell}}_1^{-1}/L_1 + \underline{\underline{\ell}}_2^{-1}/L_2$  so that the integral can be written as an expectation,

$$P(\mathbf{R}, \mathbf{V}) \propto \exp \left( -\frac{3}{2(L_1 + L_2)} \mathbf{R}^T \underline{\ell}^{-1} \mathbf{R} - \frac{1}{N_2} \mathbf{V}^T \underline{\underline{M}}^{-1} \mathbf{V} \right) \quad (3.50)$$

$$\times \left( 1 + \frac{3b}{L_2^2} \langle (\mathbf{R} - \mathbf{R}_1) \wedge \underline{\underline{\ell}}_2^{-1} (\mathbf{R} - \mathbf{R}_1) \rangle_{\mathbf{R}_2} \cdot \underline{\underline{M}}^{-1} \mathbf{V} \right).$$

Substituting for  $\mathbf{R}_2$  into the expectation part of this expression using

$$\mathbf{R} - \mathbf{R}_1 = \frac{L_2}{L_1 + L_2} \underline{\ell}_2 \underline{\ell}^{-1} \mathbf{R} - \mathbf{R}_2, \quad (3.51)$$

we see that it contains terms of zeroth, linear and quadratic order in  $\mathbf{R}_2$ . The linear terms give zero because the first moment of a Gaussian is zero. The quadratic terms are also zero because the second moment tensor is co-axial with  $\underline{\ell}^{-1}$  so their product is symmetric and gives zero when contracted with  $\epsilon_{ijk}$ . This only leaves the zero order term which, just taking the part inside the expectation, is

$$\left( \frac{L_2}{L_1 + L_2} \right)^2 (\underline{\ell}_2 \underline{\ell}^{-1} \mathbf{R}) \times (\underline{\ell}^{-1} \mathbf{R}). \quad (3.52)$$

Again, because the  $\underline{\ell}$  matrices are co-diagonal, this can be multiplied out in a diagonal frame to show it is equal to

$$\left( \frac{L_2}{L_1 + L_2} \right)^2 \frac{r_2 - 1}{r - 1} \mathbf{R} \times (\underline{\ell}^{-1} \mathbf{R}). \quad (3.53)$$

Substituting this for the expectation in eqn. (3.50) we get the probability distribution stated in eqn. (3.17).

# Chapter 4

## CONVEXITY AND TEXTURED DEFORMATIONS

TEXTURED DEFORMATIONS are without doubt one of the richest behaviors exhibited by liquid crystal elastomers. The stripe domains discussed in the previous chapters are the original and best known textured deformations in liquid crystal elastomers, but many more have been predicted, some of which have been observed. Textured deformations also connect the relatively young field of liquid crystal elastomers to the more developed field of martensitic metals. The results on polydomain elastomers developed in the next chapter rest on several existing results originating in the study of textured deformations which are sufficiently subtle to necessitate introducing them first. Although this chapter is mostly a review of other authors work, the results about the morphology of stripe domains in nematic and smectic elastomers — sections 4.5.1 and 4.10.2 — are original. The latter was the subject of a detailed publication [13], but here only a brief overview will be given. The other parts of this chapter draw on a commissioned review published in the de Gennes memorial edition of the Journal of Liquid Crystals [12], and although the results are not original, they have not previously been assembled into a single coherent and physically reasoned exposition.

## 4.1 FORMULATING TEXTURE PROBLEMS

When a deformation is applied to a body we actually specify the configuration of the surface of the body, while the interior can relax to whatever configuration (consistent with the imposed surface configuration) has the lowest energy. Our intuition suggests that, if we have deformed the boundary homogeneously, we expect the interior to also undergo the same homogenous deformation. However, in textured deformations this is not the case. In these cases the energy of the interior is minimized by the body adopting a fine mixture of different deformations that are consistent with the deformed boundary. Our approach to understanding this type of problem is therefore one of energy minimization. We expect textures to occur if they are energetically favoured. If we know the materials energy function,  $W(\underline{\lambda})$ , which tells us the energy cost of imposing a homogenous deformation gradient  $\underline{\lambda}$ , then we wish to study the problem

$$W^r(\underline{\lambda}) = \min_{\mathbf{x}' = \underline{\lambda} \mathbf{x} \text{ on } \delta\Omega} \frac{1}{\text{Vol.}\Omega} \int W(\nabla \mathbf{x}'(\mathbf{x})) d\mathbf{x}. \quad (4.1)$$

By this definition, the relaxed energy function  $W^r(\underline{\lambda})$  is the average energy per unit volume of the body after the deformation gradient  $\underline{\lambda}$  has been imposed on the boundary of the body and the body has adopted the most favorable (in general non-homogenous/textured) deformation  $\mathbf{x}'(\mathbf{x})$  consistent with the imposed deformation of the boundary. A function is called quasiconvex if the formation of textured deformations does not lower the energy further. By definition, relaxed energy functions are quasiconvex. Although the above definition of  $W^r(\underline{\lambda})$  appears to be dependent on the shape of the body,  $\Omega$ , in fact it is not — some fairly simple rescaling arguments can be used to show that if  $W$  relaxes to  $W^r$  in  $\Omega$  it has the same relaxation for any shape of body [10].

## 4.2 GEOMETRIC BOUND ON THE DEFORMATIONS MADE SOFT BY TEXTURE

Since the ideal nematic energy, eq. (1.25), has a large set of relaxed states, there is scope for making states with other deformations with respect to the reference state relaxed if they can be made out of textures of relaxed states. We can place a simple (although, as we will show later, in practice perfect) bound on the set of deformations that can be made relaxed through the formation of texture.

Volume conservation requires that  $\det \underline{\lambda} = 1 = \lambda_1 \lambda_2 \lambda_3$  so we can substitute  $\lambda_2 = 1/(\lambda_1 \lambda_3)$  into eq. 1.25 giving

$$W(\underline{\lambda}) = \frac{1}{2}\mu \left( \lambda_1^2 + \frac{1}{\lambda_1^2 \lambda_3^2} + \frac{\lambda_3^2}{r} \right). \quad (4.2)$$

Simple differentiation shows that this is minimized at  $\frac{3}{2}\mu r^{-1/3}$  by  $\lambda_3 = r^{1/3}$ ,  $\lambda_1 = \lambda_2 = r^{-1/6}$ , which correspond to the ring of minima in Fig. 1.9. This means that any uniaxial stretch by a factor of  $r^{1/3}$  will turn the reference state into a low energy relaxed state, irrespective of the axis of the stretch. These are the spontaneous distortions of the system that are seen on cooling an isotropic sample to the nematic phase, seen, for example, in [21] and first predicted in [62]. If we define  $K^0$  as the set of minimizers of (4.2) then we can write<sup>1</sup>

$$K^0 = \{ \underline{\lambda} \in \mathbb{M}^{3 \times 3} : \lambda_1 = \lambda_2 = 1/r^{1/6}, \lambda_3 = r^{1/3} \}. \quad (4.3)$$

We can now put a simple bound on the set  $K^{qc}$ , the total set of deformations that, for ideal nematic elastomers, can be made relaxed by the formation of texture. If a texture is to be relaxed it must be

---

<sup>1</sup>This set notation will be familiar to mathematicians. The curly brackets denote a set,  $\in$  means “is a member of”,  $:$  means “such that” and  $\mathbb{M}^{3 \times 3}$  is the set of 3x3 matrices, so this expression reads “the set of 3x3 matrices  $\underline{\lambda}$  such that the principal values of  $\underline{\lambda}$  are  $\lambda_1 = \lambda_2 = 1/r^{1/6}$  and  $\lambda_3 = r^{1/3}$ .

made entirely out of deformations that are relaxed, i.e. members of  $K^0$ , so if  $\underline{\lambda}$  is a member of  $K^{qc}$ , it is built out of members of  $K^0$ . Therefore it is impossible for the largest principal value of  $\underline{\lambda}$  to exceed  $r^{1/3}$  as this would require  $\underline{\lambda}$  to be a larger deformation than any of the deformations that make it up. Similarly, the smallest principal value cannot be smaller than  $r^{-1/6}$ , so we can write

$$K^{qc} \subseteq \{\underline{\lambda} \in \mathbb{M}^{3 \times 3} : r^{-1/6} \leq \lambda_1 \leq \lambda_2 \leq \lambda_3 \leq r^{1/3}\}, \quad (4.4)$$

where  $\subseteq$  denotes that  $K^{qc}$  is either a subset of or equal to the set on the right. For example, in Fig. 1.12, the imposed stretch deformation is in  $K^{qc}$  because it can be made out of a texture of two sheared deformations that are in  $K^0$ .

### 4.3 CONTINUITY OF TEXTURED DEFORMATIONS

To establish that a deformation  $\underline{\lambda}$  actually is in  $K^{qc}$  we need to explicitly construct a texture of zero energy deformations that averages to  $\underline{\lambda}$ . To do this, it is not enough to find a set of deformation gradients in  $K^0$  that average to  $\underline{\lambda}$  and then apply them to small regions of the body in the appropriate volume fractions. This is because two deformation gradients cannot in general be applied in adjacent regions without the boundary between the regions fracturing. For example, it is impossible to rotate one part of a body and not an adjacent part without the boundary between the two ripping. Textured deformations require the deformation gradient to become a function of position in the material, so different parts of the material deform differently. However, when choosing spatially changing deformation gradients, we must remember that  $\underline{\lambda}(\mathbf{x}) = \frac{d\mathbf{x}'}{d\mathbf{x}}$  where  $\mathbf{x}'(\mathbf{x})$  gives the position vectors after deformation of points in the material originally at  $\mathbf{x}$ . If the body is not to fracture, then  $\mathbf{x}'(\mathbf{x})$  must be a smooth function which means

that  $\underline{\lambda}(\mathbf{x})$ , as the gradient of a smooth function, must have zero curl.

The zero curl condition is useful for situations where  $\underline{\lambda}(\mathbf{x})$  is a smoothly varying function. However, textured deformations are almost never smooth but rather consist of many small regions each with a constant deformation gradient, and therefore have sharp changes in the gradient across the boundaries. Applying the condition that  $\underline{\lambda}(\mathbf{x})$  has zero curl when it is piecewise constant is difficult. A simpler approach is to realize that two deformations,  $\underline{\lambda}_1$  and  $\underline{\lambda}_2$ , applied on either side of a plane boundary will not cause the material to rip provided that the boundary plane deforms into the same plane under both deformations. If  $\mathbf{m}$  is the boundary normal in the reference state, this requires that  $\underline{\lambda}_1 \mathbf{v} = \underline{\lambda}_2 \mathbf{v}$  for every vector  $\mathbf{v}$  perpendicular to  $\mathbf{m}$ , meaning every  $\mathbf{v}$  in the interfacial plane in the reference state. This will be true if the deformation gradients are rank-one connected, meaning

$$\underline{\lambda}_1 - \underline{\lambda}_2 = \mathbf{a} \otimes \mathbf{m} \quad (4.5)$$

where  $\mathbf{a}$  is any vector, we will show below that  $\mathbf{a}$  is actually always a vector in the interfacial plane in the final state. We can easily prove that this condition is sufficient to guarantee the material does not rip by contracting the equation with  $\mathbf{v}$  giving

$$\underline{\lambda}_1 \mathbf{v} - \underline{\lambda}_2 \mathbf{v} = 0, \quad (4.6)$$

which is precisely the condition required for continuity.

The condition of rank-one connectivity is equivalent to requiring that vector areas in the interfacial plane transform to the same vector areas under both deformations [10],

$$\underline{\lambda}_1^{-T} \mathbf{m} = \underline{\lambda}_2^{-T} \mathbf{m} \equiv \mathbf{m}', \quad (4.7)$$

where we have defined  $\mathbf{m}'$  as the final state boundary normal. Contracting the rank-one connectivity condition from the left with  $\mathbf{m}' = \underline{\lambda}_1^{-T} \mathbf{m} = \underline{\lambda}_2^{-T} \mathbf{m}$  we see that  $0 = (\mathbf{m}' \cdot \mathbf{a}) \otimes \mathbf{m}$ . This means that  $\mathbf{a}$  is perpendicular to the deformed state plane normal,  $\mathbf{m}'$ , and hence is a vector in the interfacial plane in the deformed state. The geometry of rank-one connected deformations is shown in Fig. 4.1.

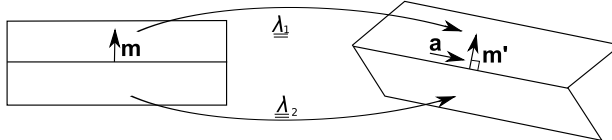


Figure 4.1: A body split into two regions by a plane with normal  $\mathbf{m}$  undergoes different deformations  $\underline{\lambda}_1$  and  $\underline{\lambda}_2$  on either side of the boundary. The two deformations are rank-one connected ( $\underline{\lambda}_1 - \underline{\lambda}_2 = \mathbf{a} \otimes \mathbf{m}$ ) so they do not cause the body to rip at the boundary.

Rather more insight into the nature of the rank-one connectivity constraint is yielded by writing it as

$$\underline{\lambda}_1 = (\underline{\delta} + \mathbf{a} \otimes \mathbf{m}') \underline{\lambda}_2, \quad (4.8)$$

where  $\underline{\delta}$  is the identity matrix and, since  $\mathbf{a}$  and  $\mathbf{m}'$  are orthogonal, the tensor preceding  $\underline{\lambda}_2$  on the right is a simple shear - see Fig. 4.2. This means that the deformation on one side of the boundary relative to the other side of the boundary is just a simple shear across the boundary. It is easy to see that a simple shear across a boundary does not cause the material to fracture, as shown in the stripes of opposite shear in Fig. 1.11. The rank-one connectivity condition places a very strong constraint on which deformation gradients can be applied next to each other. Most pairs of deformation gradients are not rank-one connected, and even if two deformation gradients are rank-one connected there will only be one plane (with normal  $\mathbf{m}$  in the

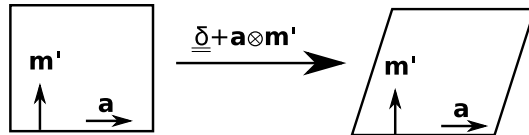


Figure 4.2: Two deformations that are rank-one compatible differ only by a final state simple shear across the final state boundary. The final state boundary normal is  $\mathbf{m}'$ .

reference state) across which they can join. This rules out most more complicated texture geometries such as those with curved boundaries.

#### 4.4 LAMINATE TEXTURES

There is a simple way for a material to form a fine texture out of two deformation gradients that are rank-one connected — it can form a laminate. All the planes that separate regions of different deformation must have the same layer normal ( $\mathbf{m}$  in the reference configuration), and hence be parallel so by splitting into a stack of layers separated by such parallel planes the material can oscillate between the two deformation gradients on a fine scale, achieving their average macroscopically. The Kundler and Finkelman stripe domain, Figs. 1.11 and 1.12, is an example of a laminate texture.

All the textures that have been explicitly considered in the field of liquid crystal elastomers are laminates. The reason for this is that the number of different types of boundary increases rapidly with number of deformation gradients in a texture, so with two gradients there is only one type of boundary, but with three there are three types and with four there are six. Each type of boundary needs to be rank-one connected, so the number of continuity relations that must be satisfied also increases rapidly. Furthermore, the different types of

boundaries will not be parallel so intersections between boundaries will need to be considered which have further continuity constraints, [10]. However, one trick which has been used to construct textures that involve more than two deformations in both SmC [3] and nematic [27] elastomers is higher order lamination. This entails lamination between two deformation gradients that are rank-one connected and are themselves made relaxed by the formation of laminates, making a second order lamination between two laminated deformations. This allows four deformation gradients to make up the final texture while only having three continuity equations (one for each simple lamination and one for the second order lamination) and, by separation of length scales, being able to neglect the intersections between the different laminate interfaces.

## 4.5 LAMINATES IN IDEAL NEMATIC ELASTOMERS

### 4.5.1 MORPHOLOGY OF NEMATIC STRIPE-DOMAINS

The minimizers of eq. (4.2) are any deformations with principal values  $\lambda_1 = \lambda_2 = r^{-1/6}$  and  $\lambda_3 = r^{1/3}$ , meaning any uniaxial stretch of magnitude  $r^{1/3}$ . Fig. 4.3 shows two such stretches applied on either side of a plane boundary. It is clear that only if the boundary bisects the axes of the two stretches will it be stretched to the same degree along the boundary by both deformations. However, if the deformations are simple stretches then, although the boundary will be stretched to the same degree by both, it will be rotated differently and the body will still fracture. For the deformations to be rank-one continuous the stretches must be followed by body rotations that restore the continuity of the boundary. This simple construction shows that the nematic director, which aligns with the long axis of the stretch, must always form equal and opposite angles with the boundary normal on either

side of the boundary, as was observed in the Kundler and Finkelman experiment, Fig. 1.12. This simple result does not seem to have previously appeared in the liquid crystal elastomer literature. The results of the Kundler and Finkelman experiment can be neatly explained by considering the successive states given by this construction as  $\theta$  moves from  $\pi/2$  (the start of the experiment) to 0 (the end of the experiment).

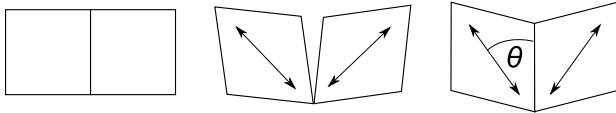


Figure 4.3: Left: A body in the reference configuration is split into two regions by a plane. Middle: Uniaxial stretches are applied to the two regions. They are not compatible so the sample rips along the boundary. The arrows indicate the axis of the stretch, and consequently the nematic director. Right: If the two regions are now rotated the boundary between them becomes continuous again. Many repetitions of this structure makes a stripe-domain.

This construction can be put on a more rigorous footing using two theorems originating in the study of solids showing martensitic transitions. These theorems are useful for establishing the morphology of textures. The first states that if  $\underline{\underline{Q}}$  is a rotation matrix the equation

$$\underline{\underline{\lambda}}_1 - \underline{\underline{Q}} \cdot \underline{\underline{\lambda}}_2 = \mathbf{a} \otimes \mathbf{m} \quad (4.9)$$

has, for fixed  $\underline{\underline{\lambda}}_1$  and  $\underline{\underline{\lambda}}_2$ , either two or zero solutions, which in general will have different  $\underline{\underline{Q}}$ ,  $\mathbf{a}$  and  $\mathbf{m}$ , [8]. The second, known as Mallard's law, states that if

$$\underline{\underline{\lambda}}_1^T \cdot \underline{\underline{\lambda}}_1 = \underline{\underline{R}} \cdot \underline{\underline{\lambda}}_2^T \cdot \underline{\underline{\lambda}}_2 \cdot \underline{\underline{R}} \quad (4.10)$$

for some  $\pi$  rotation  $\underline{\underline{R}}$  there are certainly two solutions, one of which has  $\mathbf{m}$  along the axis of  $\underline{\underline{R}}$  [30]. There are simple forms for  $\mathbf{m}$  and  $\mathbf{a}$

for both solutions [10], if  $\mathbf{s}$  is the axis of  $\underline{\underline{R}}$  then the two solutions are

$$I. \quad \mathbf{a} = 2 \left( \underline{\underline{\lambda}}_1 \mathbf{s} - \frac{\underline{\underline{\lambda}}_1^{-T} \mathbf{s}}{|\underline{\underline{\lambda}}_1^{-T} \mathbf{s}|^2} \right), \quad \mathbf{m} = \mathbf{s} \quad (4.11)$$

$$II. \quad \mathbf{a} = \tilde{\rho} \underline{\underline{\lambda}}_1 \mathbf{s}, \quad \mathbf{m} = \frac{2}{\tilde{\rho}} \left( \frac{\underline{\underline{\lambda}}_1^T \cdot \underline{\underline{\lambda}}_1 \mathbf{s}}{|\underline{\underline{\lambda}}_1 \mathbf{s}|^2} - \mathbf{s} \right) \quad (4.12)$$

where  $\tilde{\rho}$  is chosen to make  $\mathbf{m}$  a unit vector. Taking  $\underline{\underline{\lambda}}_1$  and  $\underline{\underline{\lambda}}_2$  as two uniaxial stretches that minimize eq. 4.2 with axes  $\mathbf{n}_1$  and  $\mathbf{n}_2$  (so  $\underline{\underline{\lambda}}_1 = r^{-1/6}(\underline{\underline{\delta}} + (\sqrt{r}-1)\mathbf{n}_1 \otimes \mathbf{n}_1)$  and likewise for  $\underline{\underline{\lambda}}_2$ ) we see that Mallard's law is satisfied if the axis of  $\underline{\underline{R}}$  is taken as either  $\mathbf{n}_1 + \mathbf{n}_2$  or  $\mathbf{n}_1 - \mathbf{n}_2$  so that  $\underline{\underline{R}}\mathbf{n}_2 = \pm \mathbf{n}_1$ . This means there are certainly two solutions to the continuity equation, one with  $\mathbf{m} \propto \mathbf{n}_1 - \mathbf{n}_2$  and one with  $\mathbf{m} \propto \mathbf{n}_1 + \mathbf{n}_2$ . Therefore any two minimizers of eq. (4.2) can, after an appropriate body rotation, form a laminate texture, and that the boundary normal of the stripe-domain must always bisect the nematic directors (which align with the stretch axes) on either side of the boundary. The first theorem then tells us that these are no more solutions to eq. (4.9) with minimizers of eq. 4.2 so there are no stripe-domains between relaxed states that do not have this property.

#### 4.5.2 THE FULL SET OF LOW ENERGY TEXTURED DEFORMATIONS

We can use the idea of laminate textures to find the full set of deformations that can be achieved with the same energy as a relaxed monodomain by the formation of texture,  $K^{qc}$ . In the following section we will explicitly construct textures (double and single laminates) that allow any deformation in the upper bound on  $K^{qc}$  in eq. (4.4) to be achieved with this energy density. This is necessarily quite abstract, so less mathematically inclined readers may prefer to skip to

section 4.6 where the full relaxation result is stated and discussed. This construction was first given in [27].

Let  $K^1$  be the set of deformations that can be made soft by forming laminate textures between two members of  $K^0$ . This means that if a deformation  $\underline{\lambda}$  is in  $K^1$  the elastomer can realize this deformation by splitting into a stack of layers with layer normal  $\mathbf{m}$  and undergoing alternating soft deformations  $\underline{\lambda}^+$  and  $\underline{\lambda}^-$  (both in  $K^0$ ). For this to work  $\underline{\lambda}^+$  and  $\underline{\lambda}^-$  must be compatible (rank-one connected), meaning that for some  $\mathbf{a}$ ,

$$\underline{\lambda}^+ - \underline{\lambda}^- = \mathbf{a} \otimes \mathbf{m}, \quad (4.13)$$

and the average deformation must be  $\underline{\lambda}$ , so, if the volume fractions of  $\underline{\lambda}^+$  and  $\underline{\lambda}^-$  are  $\alpha$  and  $1 - \alpha$  respectively,  $\alpha\underline{\lambda}^+ + (1 - \alpha)\underline{\lambda}^- = \underline{\lambda}$ . We can write this more compactly as

$$K^1 = \{\underline{\lambda} = \alpha\underline{\lambda}^+ + (1 - \alpha)\underline{\lambda}^- : \underline{\lambda}^+, \underline{\lambda}^- \in K^0, \underline{\lambda}^+ - \underline{\lambda}^- = \mathbf{a} \otimes \mathbf{m}\}. \quad (4.14)$$

If  $\underline{\lambda}$  is in  $K^1$  and is made soft by lamination between  $\underline{\lambda}^+$  and  $\underline{\lambda}^-$  with texture normal  $\mathbf{m}$ , we know that, since two of the principal values of  $\underline{\lambda}^+$  are  $r^{-1/6}$ , there is a whole plane of unit vectors such that  $|\underline{\lambda}^+ \hat{\mathbf{e}}| = r^{-1/6}$ . This plane must intersect with the plane perpendicular to  $\mathbf{m}$  with at least a line, let the vector  $\mathbf{v}$  be a unit vector on this common line. Dotting the continuity equation (4.13) onto  $\mathbf{v}$  we see that

$$\underline{\lambda}^+ \mathbf{v} = \underline{\lambda}^- \mathbf{v}. \quad (4.15)$$

Therefore  $\underline{\lambda} \mathbf{v} = \underline{\lambda}^+ \mathbf{v}$  and  $|\underline{\lambda} \mathbf{v}| = r^{-1/6}$ , so lamination between two soft deformations must produce an overall deformation  $\underline{\lambda}$  with  $\lambda_1 = r^{-1/6}$ , so,

$$K^1 \subseteq \{\underline{\lambda} \in \mathbb{M}^{3 \times 3} : r^{-1/6} = \lambda_1, \det(\underline{\lambda}) = 1\}. \quad (4.16)$$

Physically this simply means that in the direction perpendicular to both long stretches (into the page in Fig. 4.3) the total stretch must be  $r^{-1/6}$ . We now construct single laminates to show that all deformations with this property can be constructed by lamination of members of  $K^0$ .

The polar decomposition theorem tells us that any deformation can be fully characterized by three simple stretches in three orthogonal directions (by the three principal values of the deformation) followed by a body rotation. The latter cannot change the energy of the deformation, and since the reference state is isotropic (see eq. (4.2)), nor can the choice of directions to impose the three perpendicular stretches. Therefore we expect the energy of the deformation to be only a function of the principal values of the deformation.

According to eq. (4.16) the most general set of principal values that might be compatible with being in  $K^1$  are  $\lambda_1 = r^{-1/6}$ ,  $\lambda_2 = \mu_2$  and  $\lambda_3 = \mu_3$  where  $r^{-1/6} \leq \mu_2 \leq \mu_3$  and  $\mu_2\mu_3r^{-1/6} = 1$  but  $\mu_2$  and  $\mu_3$  are otherwise unconstrained. The simplest deformation with these principal values is the symmetric matrix with the principal values as its eigenvalues. If  $\underline{\underline{\lambda}}$  is this matrix then in some frame it is diagonal giving  $\underline{\underline{\lambda}} = \text{diag}(r^{-1/6}, \mu_2, \mu_3)$ . If we take

$$\underline{\underline{\lambda}}^\pm = \begin{pmatrix} r^{-1/6} & 0 & 0 \\ 0 & \mu_2 & \pm\delta \\ 0 & 0 & \mu_3 \end{pmatrix} \quad (4.17)$$

we see that  $\underline{\underline{\lambda}} = \frac{1}{2}\underline{\underline{\lambda}}^+ + \frac{1}{2}\underline{\underline{\lambda}}^-$  and

$$\underline{\underline{\lambda}}^+ - \underline{\underline{\lambda}}^- = 2\delta \mathbf{e}_2 \otimes \mathbf{e}_3, \quad (4.18)$$

so  $\underline{\underline{\lambda}}^+$  and  $\underline{\underline{\lambda}}^-$  are compatible and can form a laminate structure that averages to  $\underline{\underline{\lambda}}$ . Therefore, if  $\underline{\underline{\lambda}}^+$  and  $\underline{\underline{\lambda}}^-$  are in  $K^0$  (are soft deforma-

tions) then  $\underline{\lambda}$  can be made into a soft deformation by adopting this texture, and is in  $K^1$ . One principal value of both  $\underline{\lambda}^+$  and  $\underline{\lambda}^-$  is  $r^{-1/6}$  (by construction), the other two principal values are given by the square roots of the solutions of

$$\det \left[ \begin{pmatrix} \mu_2 & \pm\delta \\ 0 & \mu_3 \end{pmatrix} \begin{pmatrix} \mu_2 & \pm\delta \\ 0 & \mu_3 \end{pmatrix}^T - t \begin{pmatrix} 1 & 0 \\ 0 & 1 \end{pmatrix} \right] = 0. \quad (4.19)$$

The solutions of this characteristic equation, which are the same for both  $\underline{\lambda}^+$  and  $\underline{\lambda}^-$ , are given by

$$t = \frac{1}{2}(\mu_2^2 + \mu_3^2 + \delta^2) \pm \sqrt{\frac{1}{2}(\mu_2^2 + \mu_3^2 + \delta^2)^2 - \mu_2^2\mu_3^2}. \quad (4.20)$$

This solution explains the placement of  $\delta$  in eq. (4.17) — we can now tune its value to adjust the principal values of  $\underline{\lambda}^\pm$  to ensure they are in  $K^0$ . It could not have been placed in either the top row or left-hand column without disrupting the smallest principal value, which we need to be  $r^{-1/6}$ , but it could equivalently have been placed in the diagonally opposite slot. For  $\underline{\lambda}^+$  and  $\underline{\lambda}^-$  to be soft deformations, their principal values must be  $r^{-1/6}$ ,  $r^{-1/6}$  and  $r^{1/3}$ , so the solutions of this equation must be  $r^{-1/3}$  and  $r^{2/3}$ . These values for the solutions are obtained by taking

$$\delta = \frac{1}{r^{1/3}} \sqrt{r^{2/3} - \mu_2^2} \sqrt{r^{2/3} - \mu_3^2}. \quad (4.21)$$

Furthermore, we see that our existing conditions on  $\mu_2$  and  $\mu_3$  ( $r^{-1/6} \leq \mu_2 \leq \mu_3$ ,  $\mu_2\mu_3 r^{-1/6} = 1$ ) ensure that these square roots are always real, so for any  $\mu_2$  and  $\mu_3$  consistent with  $\det(\underline{\lambda}) = 1$  and the smallest principal value of  $\underline{\lambda}$  being  $r^{-1/6}$  we can find a  $\delta$  such that  $\underline{\lambda}^+$  and  $\underline{\lambda}^-$  are both soft deformations that can form a laminate structure averaging to  $\underline{\lambda}$ . Therefore we have shown that every element in the set

given in (4.16) is in  $K^1$ , so this upper bound on the set is in fact the exact result,

$$K^1 = \{\underline{\lambda} \in \mathbb{M}^{3 \times 3} : r^{-1/6} = \lambda_1, \det(\underline{\lambda}) = 1\}. \quad (4.22)$$

The physical description of these single laminates is straightforward — they are just a general presentation of the “stripe-domains” that have already been predicted [60] and observed [32]. They are simply stripes of alternating shear and director rotation with the directors and plane normal all being in a common plane, as sketched in Fig. 1.11. All the textures that have been constructed here have equal volume fractions of two deformations in  $K^0$ . Clearly laminate structures with different volume fractions can be made, but this cannot include any more deformations in  $K^1$  only provide alternate laminate textures for deformations that are already in  $K^1$ .

#### 4.5.2.1 Second Order Laminates

We have found the set of all deformations that can be made soft by simple laminate textures,  $K^1$ , but this is somewhat smaller than the upper bound for the full set of soft deformations given in (4.4). This suggests we should look at laminates within laminates, meaning laminates formed by alternating layers each of which have undergone a deformation in  $K^1$  that is itself soft by virtue of lamination. Let the set of all soft deformations that require second rank lamination be called  $K^2$ ,

$$\begin{aligned} K^2 = \{ & \underline{\lambda} = \alpha \underline{\lambda}^+ + (1 - \alpha) \underline{\lambda}^- \\ & : \underline{\lambda}^+, \underline{\lambda}^- \in K^1, \underline{\lambda}^+ - \underline{\lambda}^- = \mathbf{a} \otimes \mathbf{m} \}. \end{aligned} \quad (4.23)$$

As in the single laminate case, we expect membership of  $K^2$  to only depend on a deformations principal values. Taking the simplest pos-

sible matrix with principal values  $\mu_1 \leq \mu_2 \leq \mu_3$  (where  $\mu_1\mu_2\mu_3 = 1$ ),  $\underline{\lambda} = \text{diag}(\mu_1, \mu_2, \mu_3)$ , we see that

$$\underline{\lambda}^\pm = \begin{pmatrix} \mu_1 & 0 & \pm\delta \\ 0 & \mu_2 & 0 \\ 0 & 0 & \mu_3 \end{pmatrix} \quad (4.24)$$

are again compatible deformations that average to  $\underline{\lambda}$ , so if we can find a  $\delta$  such that  $\underline{\lambda}^\pm$  are in  $K^1$ ,  $\underline{\lambda}$  is indeed in  $K^2$ . One principal value of  $\underline{\lambda}^\pm$  is clearly  $\mu_2$ , the other two are given by the square roots of the solutions to the equation

$$\det \left[ \begin{pmatrix} \mu_1 & \pm\delta \\ 0 & \mu_3 \end{pmatrix} \begin{pmatrix} \mu_1 & \pm\delta \\ 0 & \mu_3 \end{pmatrix}^T - t \begin{pmatrix} 1 & 0 \\ 0 & 1 \end{pmatrix} \right] = 0. \quad (4.25)$$

which is familiar from the previous section. Its solutions are

$$t = \frac{1}{2}(\mu_1^2 + \mu_3^2 + \delta^2) \pm \sqrt{\frac{1}{2}(\mu_1^2 + \mu_3^2 + \delta^2)^2 - \mu_1^2\mu_3^2}. \quad (4.26)$$

For  $\underline{\lambda}^\pm$  to be in  $K^1$ , we require that their smallest principal value be  $r^{-1/6}$ , so the smaller root of this equation must be  $r^{-1/3}$ . This is true if we choose

$$\delta = r^{1/6} \sqrt{\mu_1^2 - r^{-1/3}} \sqrt{\mu_3^2 - r^{-1/3}}. \quad (4.27)$$

Since, by definition,  $\mu_1 \leq \mu_2 \leq \mu_3$  this choice of  $\delta$  is real provided that  $\mu_1 \geq r^{-1/6}$ . Clearly any  $\underline{\lambda}$  with  $r^{-1/6} \leq \mu_1 \leq \mu_3 \leq r^{1/3}$  satisfies this condition, moreover, since the requirement  $\det(\underline{\lambda}) = 1$  implies  $\mu_1\mu_2\mu_3 = 1$ , we cannot find any  $\underline{\lambda}$  with  $r^{-1/6} \leq \mu_1$  but  $\mu_3 \geq r^{1/3}$ . The principal values of  $\underline{\lambda}$  are simply  $\mu_1, \mu_2$  and  $\mu_3$  so we see that

$$K^2 \supseteq \{\underline{\lambda} \in \mathbb{M}^{3 \times 3} : r^{-1/6} \leq \lambda_1 \leq \lambda_3 \leq r^{1/3}\}. \quad (4.28)$$

However, this is precisely the same set as the upper bound on  $K^{qc}$  given in (4.4). Since  $K^{qc}$  is the set of all deformations that can be made soft by adopting microstructure, it must be bigger than or equal to  $K^2$ . Therefore the only possibility is that both sets and the bound are all equal, that is

$$K^2 = K^{qc} = \{\underline{\lambda} \in \mathbb{M}^{3 \times 3} : r^{-1/6} \leq \lambda_1 \leq \lambda_3 \leq r^{1/3}\}. \quad (4.29)$$

From this we conclude that the set of all fully relaxed deformations can be made relaxed by first or second order lamination, so there is no need to consider higher order laminates.

The physical interpretation of double laminates is a little harder than the single laminates. They can be thought of as the result of taking a single laminate structure and trying to stretch it perpendicular to the laminate normal and the liquid crystal directors (which are all in a plane). Deformations of this type clearly have the potential to be soft because the director starts perpendicular to the stretch direction so it can rotate towards it. However, as the director rotates, as well as stretching the sample in the required direction, shear also builds up. It is this shear that is eliminated by the second order lamination, which is between regions of opposite director rotation and opposite shear.

#### 4.5.3 LAMINATES THAT COST ENERGY

By inspecting  $K^{qc}$  we see that if a deformation  $\underline{\lambda}$  is not soft, it must have its smallest principal value  $\lambda_1 < r^{-1/6}$  (despite  $\det \underline{\lambda} = 1$  this does not require  $\lambda_3 > r^{1/3}$ , for example  $\lambda_1 = r^{-2/3}, \lambda_2 = \lambda_3 = r^{1/3}$  is not in  $K^{qc}$ ). This means that if it is built out of a texture, at least some of the deformations that make up the texture must also have smallest principal values less than  $r^{-1/6}$ . The energy of a monodomain that

has deformed without texture is

$$W = \frac{1}{2}\mu \left( \lambda_1^2 + \frac{1}{\lambda_1^2 \lambda_3^2} + \frac{\lambda_3^2}{r} \right). \quad (4.30)$$

If we fix  $\lambda_1$  and minimize over  $\lambda_3$  we see that the lowest energy deformation consistent with this choice of  $\lambda_1$  is given by

$$\lambda_3 = \frac{r^{1/4}}{\sqrt{\lambda_1}}, \quad (4.31)$$

which implies

$$\lambda_2 = \frac{1}{\lambda_1 \lambda_3} = \frac{1}{r^{1/4} \sqrt{\lambda_1}}. \quad (4.32)$$

This is a highly anisotropic deformation with  $\lambda_3/\lambda_2 = \sqrt{r}$ , which is that same high anisotropy as deformations in  $K^0$ . If we apply a deformation with this  $\lambda_1$  that is more anisotropic in  $\lambda_2$  and  $\lambda_3$  there is no scope for using textures to lower the energy, so the sample will just deform as a monodomain with the energy given by (4.30). Let the set of such deformations be  $S$ , where

$$S = \{ \underline{\lambda} \in \mathbb{M}^{3 \times 3} : \frac{\lambda_3}{\lambda_2} \geq \sqrt{r}, \det \underline{\lambda} = 1 \}. \quad (4.33)$$

This leaves the set

$$I = \{ \underline{\lambda} \in \mathbb{M}^{3 \times 3} : \frac{\lambda_3}{\lambda_2} < \sqrt{r}, \lambda_1 < \frac{1}{r^{1/6}} \det \underline{\lambda} = 1 \} \quad (4.34)$$

unaccounted for. These are deformations with  $\lambda_2$  and  $\lambda_3$  less anisotropic than is energetically desirable, so they can lower their energy by splitting into textures where each region is made out of more anisotropic (and hence lower energy) deformations. This sounds like it could get very complicated, but in fact the result is fairly simple — if you fix  $\lambda_1$ , any deformation with  $\frac{\lambda_3}{\lambda_2} < \sqrt{r}$  can be achieved by a single laminate

## TEXTURED DEFORMATIONS

structure built out of deformations which have the same value for  $\lambda_1$  but with the optimal values for  $\lambda_2$  and  $\lambda_3$ , namely  $\lambda_3/\lambda_2 = \sqrt{r}$ . Such a structure has energy

$$W = \lambda_1^2 + \frac{1}{\lambda_1^2 \lambda_3^2} + \frac{\lambda_3^2}{r} \quad (4.35)$$

$$= \frac{2}{\sqrt{r} \lambda_1} + \lambda_1^2. \quad (4.36)$$

Showing that this optimal energy can be achieved could be done straightforwardly by again using the constructions in the preceding sections to find the laminates that can form between domains with fixed  $\lambda_1$  and  $\frac{\lambda_3}{\lambda_2} < \sqrt{r}$ . However, it is more instructive to consider these deformations as derived from compressions of  $K^1$ . Deformations in  $K^1$  also have  $\lambda_3/\lambda_2 < \sqrt{r}$  because this is enforced by the condition  $\lambda_1 = r^{-1/6}$ . Therefore every deformation in  $I$  can be thought of as a deformation in  $K^1$  with principal values  $\lambda_1 = r^{-1/6}$ ,  $\lambda_2$  and  $\lambda_3$  that has been followed by a uniaxial compression along the direction of  $\lambda_1$  by  $\gamma$  to give a new deformation with principal values  $r^{-1/6}/\gamma$ ,  $\sqrt{\gamma}\lambda_2$  and  $\sqrt{\gamma}\lambda_3$ . Any deformation in  $I$  can be constructed in this way. However, the deformations in  $K^1$  were constructed out of laminates of deformations with principal values  $r^{-1/6}$ ,  $r^{-1/6}$  and  $r^{1/3}$ , so when we compress the structure to get the deformation in  $I$  it is still a laminate structure but built out of deformations with principal values  $r^{-1/6}/\gamma$ ,  $\sqrt{\gamma}r^{-1/6}$  and  $\sqrt{\gamma}r^{1/3}$ . These still have  $\lambda_3/\lambda_2 = \sqrt{r}$  so they are precisely the optimal laminate structures that were claimed to exist in the previous paragraph.

## 4.6 RELAXED ENERGY FUNCTIONS

We are now in a position to write out the full relaxed energy function for ideal nematic elastomers,

$$\frac{W^{qc}(\underline{\lambda})}{\frac{1}{2}\mu} = \begin{cases} 3r^{-1/3} & \text{if } \underline{\lambda} \in K^{qc} \\ 2/(r^{1/2}\lambda_1) + \lambda_1^2 & \text{if } \underline{\lambda} \in I \\ \lambda_1^2 + \lambda_2^2 + \lambda_3^2/r & \text{if } \underline{\lambda} \in S \\ \infty & \text{else} \end{cases} \quad (4.37)$$

where

$$\begin{aligned} I &= \{\underline{\lambda} \in \mathbb{M}^{3 \times 3} : \frac{\lambda_3}{\lambda_2} < \sqrt{r}, \lambda_1 < \frac{1}{r^{1/6}}, \det \underline{\lambda} = 1\} \\ S &= \{\underline{\lambda} \in \mathbb{M}^{3 \times 3} : \frac{\lambda_3}{\lambda_2} \geq \sqrt{r}, \det \underline{\lambda} = 1\} \\ K^{qc} &= \{\underline{\lambda} \in \mathbb{M}^{3 \times 3} : r^{-1/6} \leq \lambda_1 \leq \lambda_3 \leq r^{1/3}, \det \underline{\lambda} = 1\}. \end{aligned}$$

The “else” case only contains deformations with  $\det \underline{\lambda} \neq 1$  that do not conserve volume.

However, whilst the arguments in the preceding sections demonstrate that textures exist that allow the elastomer to relax to this energy, the arguments that this is the furthest it can relax have not been at all rigorous. This poses a general question — how do we know when an energy function is relaxed and no longer susceptible to the formation of further textures?

When a material is deformed, it will respond with a textured deformation if there is a texture of deformations such that the average of the energy of the deformations is lower than the energy of the average of the deformations. This suggests the underlying cause of the formation of textures is a lack of convexity in the energy function. This suggestion is backed up by the plots of the energy functions for

nematic and conventional elastomers (Fig. 1.9) which show that the nematic energy is much less convex than the conventional energy. Reassuringly if we plot the same graph for our relaxed nematic energy function it is now convex, Fig. 4.4.

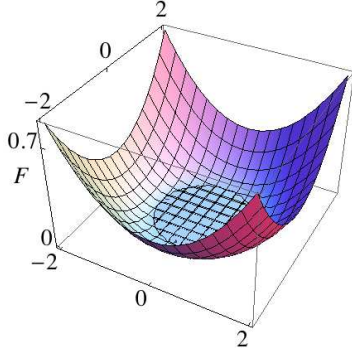


Figure 4.4: Energetic cost of imposing a uniaxial stretch on a nematic elastomer in the reference state after formation of the optimal texture — compare with Fig. 1.9. The flat disk at the middle of the plot is a set of deformations made completely relaxed by texture formation.

In one dimension lack of simple convexity is indeed the cause of textured deformations. Consider a long rod that is stretched (affinely) by a factor of  $\lambda$  at an energetic cost of  $W(\lambda)$ . It will be energetically favorable for the rod to disproportionate by splitting into length fractions  $f$  and  $(1-f)$  which undergo stretches  $\lambda_1$  and  $\lambda_2$  respectively if  $f\lambda_1 + (1-f)\lambda_2 = \lambda$ , so the average stretch matches that imposed, and  $fW(\lambda_1) + (1-f)W(\lambda_2) \leq W(\lambda)$  which is precisely the condition that  $W$  be a non-convex function. If we plot  $W(\lambda)$  and draw a straight line between  $W(\lambda_1)$  and  $W(\lambda_2)$ , a point on the line a fraction  $f$  of the distance between the two points gives the average energy and stretch of a texture consisting of a fraction  $f$  of the material undergoing  $\lambda_1$  and a fraction  $(1-f)$  of the material undergoing  $\lambda_2$ . If the point lies

above the curve, the texture does not save energy, but if it lies below it does. The relaxed energy function is thus simply the convex envelope of  $W(\lambda)$ , meaning the highest valued convex function that is nowhere larger than  $W(\lambda)$ . An example of this construction is shown in Fig. 4.5. This can be constructed using the “common tangent” construction where regions of non-convexity are replaced by the straight line which is tangent to the curve on both sides of the region.

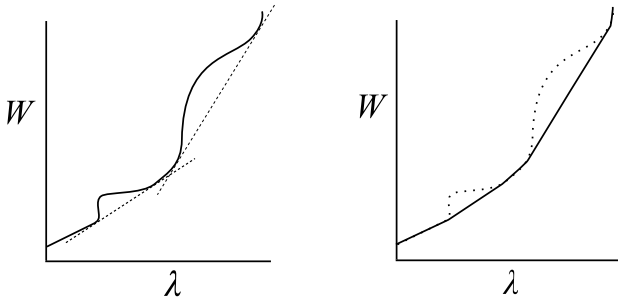


Figure 4.5: Left: A non convex 1D energy function  $W(\lambda)$ , the dotted lines are tangent to points on the curve on either side of the regions of non-convexity . Right: Texture formation allows the energy function to relax to its convex envelope, which falls on the common tangents sketched on the left over intervals in which the original function was non-convex.

In higher dimensions the notion of convexity is not as helpful in making progress because  $W$  is a function of the deformation gradient  $\underline{\underline{\lambda}}$  not the scalar stretch  $\lambda$ . The problem is that convexity is not compatible with the principle of frame-indifference, which states that simply rotating the final state after deformation should not cost any energy. Consider the deformation gradients  $\underline{\underline{\lambda}}_1 = \text{diag}(1, 1, 1)$  and  $\underline{\underline{\lambda}}_2 = \text{diag}(1, -1, -1)$ . The first is simply identity, which is to say it does not deform at all, while the second is a  $\pi$  rotation about some axis. The principle of frame-indifference dictates that both these deformations must cost the same amount of energy since they are only

different by a final state body rotation. If  $W(\underline{\lambda})$  was genuinely convex then  $\underline{\lambda}_3 = \frac{1}{2}\underline{\lambda}_1 + \frac{1}{2}\underline{\lambda}_2 = \text{diag}(1, 0, 0)$  would have to also cost the same energy, despite the fact that it has a determinant of zero and collapses a three-dimensional solid body onto a line. This does not matter because it is impossible to build a texture out of  $\underline{\lambda}_1$  and  $\underline{\lambda}_2$  without ripping the body, so although the energy function is not convex between  $\underline{\lambda}_1$  and  $\underline{\lambda}_2$  we cannot build textures that exploit this lack of convexity. However, if  $\underline{\lambda}_1$  and  $\underline{\lambda}_2$  had been rank-one connected and hence able to form laminate textures, we would be able to form textures that exploited the lack of convexity. This means that relaxed energy functions need to be rank-one convex [24], meaning that  $W^r(\underline{\lambda} + \gamma \mathbf{a} \otimes \mathbf{n})$  is a convex function of  $\gamma$  for any  $\underline{\lambda}$ ,  $\mathbf{a}$  and  $\mathbf{n}$ .

A rank-one convex energy function is not susceptible to the formation of laminate textures. However, such a function may be subject to the formation of other more exotic textures. The true defining feature of a relaxed function is that it is quasi-convex, meaning

$$W^{qc}(\underline{\lambda}) = \min_{\mathbf{x}' = \underline{\lambda} \mathbf{x} \text{ on } \delta\Omega} \frac{1}{\text{Vol.}\Omega} \int W^{qc}(\nabla \mathbf{x}'(\mathbf{x})) d\mathbf{x}, \quad (4.38)$$

which simply states that a function is quasiconvex if its energy cannot be lowered by texture formation, so the minimum over all possible textured deformations consistent with imposing  $\underline{\lambda}$  on the boundary (right hand side) is simply the same as the energetic cost of imposing  $\underline{\lambda}$  homogeneously throughout the body (left hand side). However, proving quasiconvexity directly is usually very difficult. In the case of ideal nematic elastomers we can proceed using an important theorem proved by Ball [7]. We say that a scalar function  $W^{pc}(\underline{\lambda})$  is polyconvex if there is another function  $g$  with two matrix arguments  $\underline{A}$  and  $\underline{B}$  and a scalar argument  $c$  such that  $g(\underline{A}, \underline{B}, c)$  is convex in  $\underline{A}$ ,  $\underline{B}$  and  $c$  and has the property that if you replace  $\underline{A}$  with  $\underline{\lambda}$ ,  $\underline{B}$

with  $\underline{\lambda}^{-T}$  and  $c$  with  $\det \underline{\lambda}$  you get  $W^{pc}(\underline{\lambda})$ . Ball's theorem says that a polyconvex function is quasiconvex and hence fully relaxed and not susceptible to further formation of texture [7], although the reverse is not true, and the physical meaning of polyconvexity is unknown.

To show that the proposed form, eq. 4.37, is polyconvex, we write it as a function of  $\alpha = 1/\lambda_1$  and  $\beta = \lambda_3$  (using  $\det \underline{\lambda} = 1$ ) and then differentiate each part of the result,  $\psi(\alpha, \beta)$ , twice to show that it is a continuous, non-decreasing and convex function of both variables. This is a tedious exercise so it is not reproduced here. We then write  $\alpha = \max_{\hat{\mathbf{e}}} |\underline{A}\hat{\mathbf{e}}|$  and  $\beta = \max_{\hat{\mathbf{e}}} |\underline{B}\hat{\mathbf{e}}|$ . These are convex functions of  $\underline{A}$  and  $\underline{B}$  respectively because the maximum of a sum is always less than or equal to the sum of the maxima. The function  $g(\underline{A}, \underline{B}) = \psi(\max_{\hat{\mathbf{e}}} |\underline{A}\hat{\mathbf{e}}|, \max_{\hat{\mathbf{e}}} |\underline{B}\hat{\mathbf{e}}|)$  is therefore a convex function of  $\underline{A}$  and  $\underline{B}$  because a convex non-decreasing function of a convex function is always a convex function. Finally, since  $g(\underline{\lambda}, \underline{\lambda}^{-T}) = W^{qc}(\underline{\lambda})$ , we conclude that  $W^{qc}$  is polyconvex and hence relaxed.

## 4.7 PHYSICAL INTERPRETATION OF $W^{qc}$

The physical interpretation of  $W^{qc}$  is clouded by the fact that it is written in terms of deformations from a high energy reference state whereas in practice one normally thinks of deformations from a well aligned relaxed state. However, to reach the four different regimes from an aligned state is straightforward. If you stretch perpendicular to the director we enter  $K^1$  and the elastomer forms zero-energy, planar single laminates. This is the Kundler and Finkelmann geometry, [32]. If you take such a sample already showing laminates and stretch it in the third direction (i.e. perpendicular to the original director and the original stretch) it enters  $K^2$  and forms zero energy double laminate textures. If instead of stretching a laminate sample

you compress it in this third direction it will enter the  $I$  regime of energy-costing single laminates. Finally if you take an aligned monodomain and stretch it along its director you will enter  $S$ , the regime of hard elasticity without texture or director rotation.

If the result for  $W^{qc}$  is taken literally, the elastomer can be regarded as being liquid like when it is in  $K^{qc}$  since, at the set's interior, which is  $K^2$ , all deformations in the vicinity of the current deformation are soft so the elastomer should be able to flow. In contrast in the  $S$  regime the elastomer is definitely behaving as a conventional elastic solid, with greater deformations costing more energy. In the  $I$  regime, behavior is intermediate since the deformations do cost energy but the energy only depends on the smallest principal value of the deformation. In the plane perpendicular to this direction the elastomer is still behaving like a fluid. However, these classifications neglect both the semi-soft nature of real elastomers and the interfacial energies of texture planes which, in particular, will mean the zero energy set of deformations is not actually zero energy, so the elastomer will not truly flow.

#### 4.8 LENGTH-SCALE OF TEXTURES

In all the above work, we have implicitly assumed that the laminate textures are formed on an infinitely small length scale. In practice, in the Kundler and Finkelmann experiment the laminates formed with widths between one and 100 microns. This length scale can be understood as the result of a competition between the interfacial energy of the laminate boundaries and the energy cost to the material of not quite meeting the imposed deformation at the boundary. A full analysis of this competition can be found in [32], here we simply give an overview of the source of the interfacial energy.

To model the interfacial energy we need two new physical ideas. The first is Frank-energy, familiar from conventional liquid crystals, which is an energy penalty for gradients (curves) in the nematic director. Secondly, the energy function, eq. (4.2), was developed under the assumption that the nematic director always aligns with axis of most stretch from the isotropic state. This is certainly the conformation that minimizes the elastic energy, but in situations where there are other processes that couple to the director (such as Frank-energy) it is possible for the nematic director to rotate away from this direction. The full model, eq. 1.21, includes this possibility and predicts a large elastic cost for this type of director rotation. At the boundary between laminates these two ideas conflict because the nematic director must bend sharply at the boundary. If the bend is very sharp it carries a high Frank-energy, but if it is not sharp there is a large region in the middle of the boundary where the nematic director is rotated away from its preferred orientation. The competition between these two effects determines both the width and the interfacial cost of the boundary. A dimensional analysis suggests (correctly) that the appropriate characteristic width is  $\sqrt{K/\mu} \sim 10^{-8}\text{m}$ , where  $K$  is the Frank coefficient (in the one constant approximation) and  $\mu = k_b T n$ , where  $n$  is the number density of cross-links, is the shear modulus of the nematic elastomer. This is much less than the characteristic stripe width of  $\sim 10^{-5}\text{m}$ , so the picture of stripes of completely homogenous deformations with very thin interfaces between them is accurate.

#### 4.9 THE EFFECT OF NON-IDEALITY

As discussed at length in the first two chapters, in reality nematic elastomers are not ideal, rather the nematic director has a slight preference to align in a certain direction and deformations that cause the

director to rotate away from this preferred direction are not truly soft but rather cost a little energy, so we would like to discuss the relaxation of the generic compositional fluctuations energy, eq. (2.3). Unfortunately, the full relaxed form of this energy has not been found, although it has been solved for thin films in extension, [25]. From the perspective of texture, the addition of non-ideality has two consequences. First, it breaks the large degeneracy of the ideal system — it assigns slightly different energies to different textures that previously produced the same macroscopic deformation at the same energy cost. For example, all the textures that have been explicitly constructed in the ideal nematic case are laminates involving equal volume fractions of two different energy gradients, however once two deformation gradients have been found to be rank-one compatible, and hence can laminate, they can do so with any volume fraction, meaning that the laminate textures in  $K^1$  can in fact be realized in many different ways. The construction shows that all deformations in  $K^1$  can be achieved by simple lamination of two soft deformation gradients, and that no other deformation gradients can be made soft in this way, but it does not help to determine which lamination will take place. Non-ideality breaks this degeneracy and helps determine which textures will actually occur. In particular, one of the main results of [25] is that laminations which have their layer normal along  $\mathbf{n}_0$  (in the reference configuration) are preferred, and often will not have equal volume fractions.

The second important consequence of non-ideality is that deformations in the neighborhood of the relaxed (nematic and aligned) state do not texture until they reach a (small) threshold magnitude. This was observed in the original Kundler and Finkelmann experiment and analysed in [32]. The nature of the onset of rotation was analyzed in chapter 2. This second effect can be understood qualitatively as a

consequence of the energy now having a unique global minimum at the relaxed state of the elastomer. Around this minimum the form of the energy is the same as that of a simple uniaxial solid, which is to say it is locally convex enough to stop textures forming between different deformations in the neighborhood, and there is no incentive to form textures with deformations that lie outside the neighborhood because they are far from the global minimum and hence higher in energy. Textures only form for deformations that are far enough away from the global minimum that there are other deformations even further away that are lower in energy.

#### 4.10 SMECTIC ELASTOMERS

In addition to the nematic phase that has been the focus of the previous chapters, there are several lower symmetry liquid crystal phases that supplement the nematic orientational order with varying amounts of positional order. Two layered (smectic) phases are particularly common — SmA phases in which as well as an average orientation the rods are also confined to layers, and the average alignment is along the layer normal, and SmC phases in which the average alignment makes an angle with layer normal. These two possibilities are illustrated in Fig. 4.6. If the liquid crystal rods are chiral then they can form the technologically important SmC\* phase which exhibits an electrical polarization along the direction  $\hat{\mathbf{n}} \times \mathbf{k}$  where  $\hat{\mathbf{n}}$  is the smectic director and  $\mathbf{k}$  is the layer normal. This is because, although both  $\hat{\mathbf{n}}$  and  $\mathbf{k}$  are quadrapolar vectors, the addition of a handedness into the system allows us to form the vector  $(\hat{\mathbf{n}} \cdot \mathbf{k})(\hat{\mathbf{n}} \times \mathbf{k})$  which is a true single headed vector. Elastomers can be prepared in SmA, SmC and SmC\* phases. The effect of the cross-linking is to embed the smectic layers into the elastomer matrix, so the layers deform affinely under

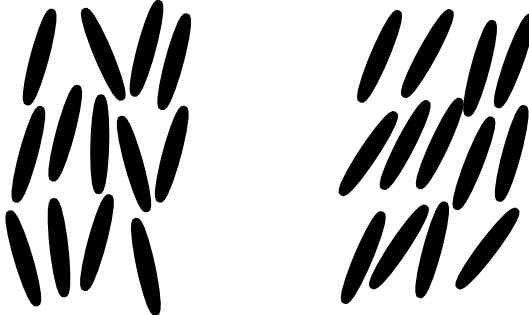


Figure 4.6: The rods in SmA liquid crystals (left) are confined to layers and have an average alignment along the layer normal. Those in SmC elastomers (right) are aligned at an angle to the layer normal.

subsequent deformations. However, the liquid crystal free energy is still dominant over the elastic free energy, so we model smectic elastomers by adding terms to the nematic energy that heavily penalize deformations that change the interlayer spacing or cause the director to rotate away from its preferred angle with the layer normal [5]. This prevents SmA elastomers from having any soft elastic modes, since any deformation can only be made soft by director rotation, but this would require rotation away from the layer normal which costs energy. SmC elastomers however do have a residual soft mode of deformation associated with rotation of the director in a cone around the layer normal.

#### 4.10.1 SMA ELASTOMERS

Despite not having any soft modes, SmA elastomers are still susceptible to the formation of texture [4, 5, 51]. In this case the lack of convexity underlying the texture formation is caused by the large discrepancy between the high energetic cost of deformations that change

the layer spacing and the much lower cost of those that do not. Fig. 4.7 shows an example in which an average deformation of stretch along the layer normal is constructed out of two low energy in-plane shears. This is completely analogous to the “Helfrich-Hurault” effect in liquid SmA systems first described in [20].

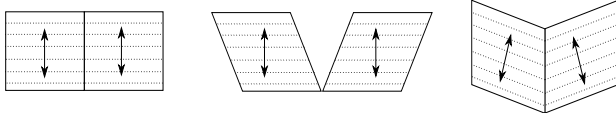


Figure 4.7: Texture formation in a SmA elastomer. The smectic layers are shown as dotted lines, and the director, which is always perpendicular to the layers, is shown as a double headed arrow. By splitting into two regions that first shear then body rotate the average deformation is a simple stretch along the layer normal, but the inter-layer spacing has not changed.

The full form of the relaxed energy for a simplified SmA type energy function is presented in [4], the proof proceeds in an analogous way to the analysis of the ideal nematic system and depends on the construction of double laminate structures. Stretching experiments have been conducted on SmA elastomers, including along their layer normal [46,47]. In these experiment the elastomer deformed affinely at small stretches but with a complex texture at large stretches, which is the behavior predicted by the model in [4]. The instability to texture formation in this geometry was first analyzed in [5].

#### 4.10.2 SmC ELASTOMERS

As discussed above, SmC elastomers retain a soft mode of deformation associated with rotation of the liquid crystal director in a cone around the layer normal. These modes are soft because they do not change the angle between the director and the normal or change the spacing between the layers, both of which would be penalized by the

liquid crystal energy, and are associated with deformations because the director rotation changes the preferred polymer conformation distribution. We recall that we can write the soft modes of deformation of a nematic elastomer as

$$\underline{\lambda} = \underline{\ell}^{1/2} \cdot \underline{\underline{R}} \cdot \underline{\ell}_0^{-1/2}, \quad (4.39)$$

where  $\underline{\underline{R}}$  is any rotation matrix. This form has a simple interpretation — the deformation  $\underline{\ell}_0^{-1/2}$  compresses the nematic elastomer along its director back into a state with an isotropic polymer conformation distribution, then the rotation matrix is rotating an isotropic state so it does not change the energy of the system, then finally the deformation  $\underline{\ell}^{1/2}$  is a spontaneous stretch along a new nematic director, taking the elastomer back to a low energy relaxed state. A similar argument yields the set of soft deformations of SmC elastomers, but in this case having compressed the polymers into an isotropic conformation distribution, the system is still layered, so the deformation will only be soft if the rotation is around the layer normal and the director chosen in  $\underline{\ell}$  makes the preferred angle with the layer normal. We write this as

$$\underline{\lambda} = \underline{\ell}^{1/2} \cdot \underline{\underline{R}_{\mathbf{b}}} \cdot \underline{\ell}_0^{-1/2} \quad (4.40)$$

where  $\underline{\underline{R}_{\mathbf{b}}}$  is any rotation about the vector  $\mathbf{b}$ , defined as the layer normal in the state with isotropic polymer conformation distribution. Evidently this is a subset of the soft modes in the nematic elastomer case. The full set of deformations made relaxed by textures of these soft deformations has been found [3] in a manner analogous to the ideal nematic case reviewed previously, although in this case not only double but triple laminates were required to complete the construction.

The description of simple laminates in SmC elastomers is more subtle than in nematics because the layers also form part of the mor-

phology. The following results relating to SmC laminate morphology are original research which I published in [13]. However, since the topic is somewhat tangential to the main body of this thesis, the results will simply be described and heuristically motivated<sup>2</sup>.

Since the relaxed states of SmC elastomers are simply a sub-set of those of nematic elastomers the stripe domains all have the same essential character as the nematic ones (discussed in section 4.5.1, and also original research), namely that the laminate boundary normal bisects the two directors. However, in addition to this basic property, the types of laminates that can form fall into two categories, one in which the smectic layers pass through the texture boundary apparently undeformed [2, 13] and one in which the smectic layers are bent at the laminate boundary and the laminate boundary bisects the layer planes on either side of it [13]. As in the nematic case the laminates are all of a Mallard's law type and the pair of morphologies arrises because each  $\underline{R}$  that satisfies Mallard's law (see eqn. 4.10) generates two solutions to the twinning equation and hence to distinct laminates. We can use the simple bisection rule to see that the two types of twin have different morphologies in the SmC case. If we consider a relaxed elastomer with the layer normal in the  $(0, 0, 1)$  direction and initial relaxed director  $(\sin \theta, 0, \cos \theta)$  (so  $\theta$  is the relaxed director tilt angle) then, after some soft deformation causing the director to rotate by  $\pm \phi$ , the two rotated directors will be  $(\sin \theta \cos \phi, \pm \sin \theta \sin \phi, \cos \theta)$ . Using the rule that the laminate normals must bisect the directors, this means the laminate normal must either be  $(\sin \theta \cos \phi, 0, \cos \theta)$  or  $(0, 1, 0)$ , the first of these evolves with  $\phi$  while the second does not,

---

<sup>2</sup>Some of this work was also previously submitted as a part III undergraduate research project. The project contained the essential result that there are two types of domain with different morphologies and the general argument about polarization, however the geometric construction, the diagrams and the description of the shear across the stripe boundaries are new

## TEXTURED DEFORMATIONS

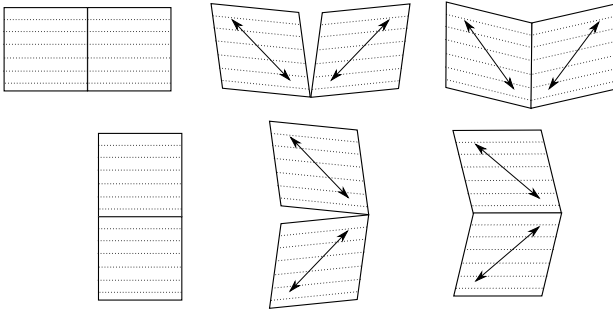


Figure 4.8: A construction analogous to Fig. 4.3 but for SmC elastomers. As in the nematic case, the boundary normal must bisect the liquid crystal director for the deformations to be compatible. The smectic layers are shown as dotted lines, importantly the smectic layer normal may have a component out of the page although the boundary normal does not. The liquid crystal directors must also form equal angles with the dotted lines so that both the directors form the same angle with the smectic layer normal. For the elastomer to be in a relaxed state this must be the preferred tilt angle. These constraints permit two different morphologies, the first, shown on top, in which the smectic layers are bent at the boundary, and the second, shown below where they are not.

giving two different morphologies. A construction illustrating these two basic types of interface is shown in Fig. 4.8.

A straightforward but lengthy calculation permits all the details of the morphology of these two types of laminates to be worked out. Since chiral SmC elastomers can also have an electrical polarization along  $\mathbf{c} = (\hat{\mathbf{n}} \cdot \mathbf{k})(\hat{\mathbf{n}} \times \mathbf{k})$ , where  $\mathbf{k}$  is the layer normal and  $\mathbf{n}$  is the director, a full description of the morphology should also include the patterns formed by the  $\mathbf{c}$  vector at the interface. In particular, since both  $\hat{\mathbf{n}}$  and  $\mathbf{k}$  are discontinuous at the laminate boundaries,  $\mathbf{c}$  will also be discontinuous, which means it may have a finite divergence on the boundary. Since  $\mathbf{c}$  is an electrical polarization, this would correspond to the laminate boundary being charged. I detailed these calculations

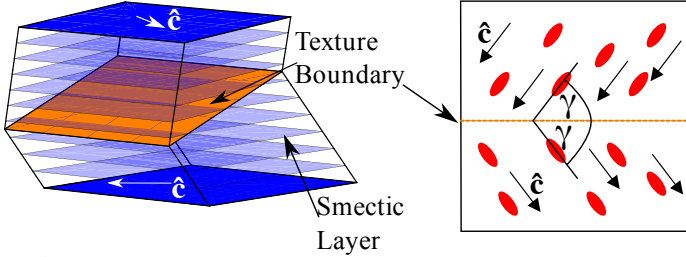


Figure 4.9: Top: A small region of a SmC elastomer after the formation of the first category of stripe-domain. The region was cuboidal before deformation and has undergone different soft-deformations on either side of the orange boundary plane. The smectic layers, which deform affinely, pass through the boundary without being bent. This figure was drawn with the material parameters  $r = 25$  and  $\theta = 0.6$ . Bottom: A top-view of a square region of a smectic layer that passes through the boundary, which is shown as an orange dashed line. The ovals represent the projection of the liquid-crystal rods in the plane and the arrows show the projection of the liquid-crystal director in the plane. The component of the LC director in the smectic plane, which we call  $\hat{c}$ , is also shown in red on the top figure.

in [13], but here I simply state the results. In the first category of laminate, described in Fig. 4.9 the layers are not bent at the interface, the boundary is charged and, using the angles described in the figure,

$$\tan(\chi) = \tan(\theta) \sin(\gamma). \quad (4.41)$$

In the second class of laminates, described in Fig. 4.10, the layers are bent at the interface but the interface is not charged, and, once again using the angles in the figure,

$$\sin(\gamma) = \frac{(r - 1) \cos^2(\theta) + 1}{(1 - r) \sin(\theta) \cos(\theta)} \cot(\chi). \quad (4.42)$$

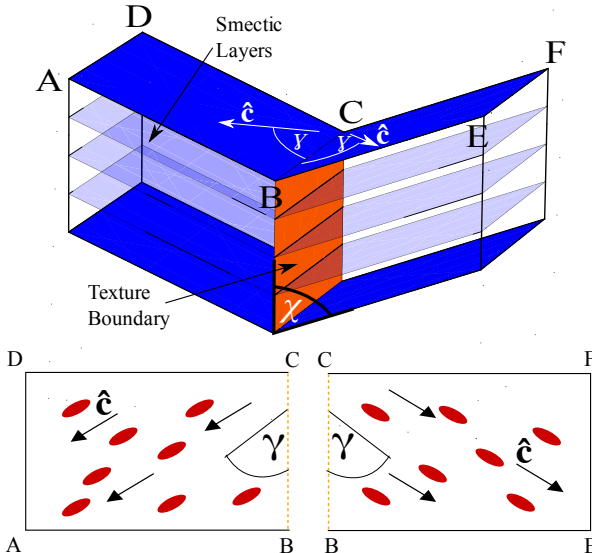


Figure 4.10: Top: A small region of a sample of SmC elastomer after the formation of the second type of stripe-domain. Before deformation the sample was cuboidal. In this type of stripe-domain the smectic layers are bent at the boundary. This figure was drawn with the material parameters  $r = 25$  and  $\theta = 0.6$ . Bottom: The two halves of the region on top each viewed down its smectic layer normal. The red ovals are the components of the LC rods in the LC layer plane and the black arrows are the components of the LC director in the LC layer plane. The component of the LC director in the smectic plane, which we call  $\hat{c}$ , is also shown in red on the top figure.

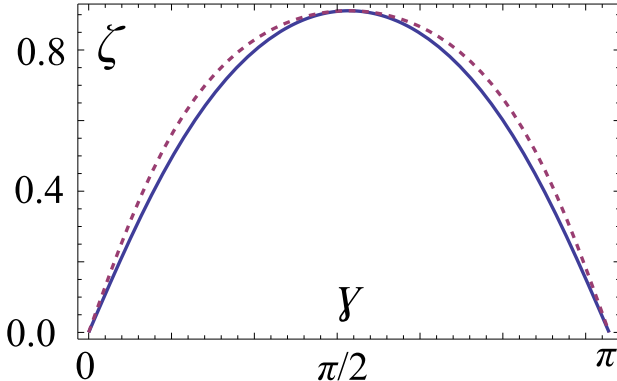


Figure 4.11: Shear angle  $\zeta$  against  $\gamma$  for the Class I (blue) and Class II (dashed, pink) stripe domains, plotted using  $r = 25$  and  $\theta = 0.6$ . The maximum in both cases is at  $\gamma = \pi/2$  and is given by  $\tan(\zeta) = \frac{2(r-1)\cos(\theta)\sin(\theta)}{1+(r-1)\cos^2(\theta)}$ .

Another important aspect of the morphology of a stripe-domain is the amount of shear across the twin boundary. As observed in eqn. (4.8) the two deformations in a stripe domain can always be related by a simple shear across the boundary. We characterize the magnitude of this shear by introducing the angle  $\zeta$ , defined as

$$\tan(\zeta) = |\mathbf{a}||\mathbf{m}'| = |\mathbf{a}||\underline{\lambda}_1^{-T}\mathbf{m}| = |\mathbf{a}||\underline{\lambda}_2^{-T}\mathbf{m}|. \quad (4.43)$$

If a straight line is embedded in the sample in the reference state it will kink at the boundary after deformation. Physically this shear angle is the amount such a line kinks if after deformation it is normal to the boundary on one side of the boundary [10]. This angle can be calculated straightforwardly once the two deformations that are making a stripe domain are fully described. A graph of shear angle against  $\gamma$  is shown for both types of stripe domain in Fig. 4.11.

Although the full morphology calculations are not reproduced here, one result relating to the charge structure of Mallard's law type lami-

nates which may be of more general applicability than SmC elastomers is worth discussing. Consider two deformations  $\underline{\underline{Q}}_1 \cdot \underline{\underline{\lambda}}_1$  and  $\underline{\underline{\lambda}}_2$  that act on two regions separated by a plane boundary with normal  $\mathbf{m}$  in the reference configuration. Let the boundary normal be  $\mathbf{m}'$  in the final state. The continuity condition gives

$$\underline{\underline{Q}}_1 \cdot \underline{\underline{\lambda}}_1 - \underline{\underline{\lambda}}_2 = \mathbf{a}' \otimes \mathbf{m}.$$

If the deformation  $\underline{\underline{\lambda}}_1$  results in a polarisation  $\mathbf{p}_1$  and the deformation  $\underline{\underline{\lambda}}_2$  results in a polarisation  $\mathbf{p}_2$  (which subsequently transform as line elements) then the condition that the texture boundary is not charged is that the component of the polarisation normal to the boundary is continuous across the boundary,

$$(\underline{\underline{Q}}_1 \cdot \mathbf{p}_1 - \mathbf{p}_2) \cdot \mathbf{m}' = 0.$$

If the stripe-domain obeys Mallard's law then

$$\underline{\underline{\lambda}}_1 = \underline{\underline{Q}}_2 \cdot \underline{\underline{\Lambda}}_2 \cdot \underline{\underline{R}}, \quad (4.44)$$

and if

$$\mathbf{p}_1 = \underline{\underline{Q}}_2 \cdot \mathbf{p}_2 \quad (4.45)$$

the first Mallard's law solution will not be charged and the second will be. The proof is simple. First we make the following rearrangement:

$$\begin{aligned} \mathbf{p}_1 &= \underline{\underline{Q}}_2 \cdot \mathbf{p}_2 \\ \underline{\underline{\lambda}}_1^{-1} \cdot \mathbf{p}_1 &= (\underline{\underline{Q}}_2 \cdot \underline{\underline{\Lambda}}_2 \cdot \underline{\underline{R}})^{-1} \cdot \underline{\underline{Q}}_2 \cdot \mathbf{p}_2 \\ \underline{\underline{\lambda}}_1^{-1} \cdot \mathbf{p}_1 &= \underline{\underline{R}} \cdot \underline{\underline{\lambda}}_2^{-1} \cdot \mathbf{p}_2 \\ (\underline{\underline{\lambda}}_1^{-1} \cdot \mathbf{p}_1) \cdot \mathbf{m} &= (\underline{\underline{R}} \cdot \underline{\underline{\lambda}}_2^{-1} \cdot \mathbf{p}_2) \cdot \mathbf{m}. \end{aligned}$$

Second, we use the fact that we know  $\mathbf{m}$  for a general Mallard's law stripe-domain — for the first Mallard's Law solution  $\mathbf{m}$  is along the axis of  $\underline{\underline{R}}$  so  $(\underline{\underline{R}} \cdot \underline{\underline{\lambda}_2}^{-1} \cdot \mathbf{p}_2) \cdot \mathbf{m} = (\underline{\underline{\lambda}_2}^{-1} \cdot \mathbf{p}_2) \cdot \mathbf{m}$ . For the second solution  $\mathbf{m}$  is perpendicular to the axis of  $\underline{\underline{R}}$  so  $(\underline{\underline{R}} \cdot \underline{\underline{\lambda}_2}^{-1} \cdot \mathbf{p}_2) \cdot \mathbf{m} = -(\underline{\underline{\lambda}_2}^{-1} \cdot \mathbf{p}_2) \cdot \mathbf{m}$ . These results can be written as

$$(\underline{\underline{\lambda}_1}^{-1} \cdot \mathbf{p}_1) \cdot \mathbf{m} = \pm (\underline{\underline{\lambda}_2}^{-1} \cdot \mathbf{p}_2) \cdot \mathbf{m},$$

which can be rewritten as

$$\underline{\underline{Q}_1} \cdot \mathbf{p}_1 \cdot (\underline{\underline{Q}_1} \cdot \underline{\underline{\lambda}_1})^{-T} \mathbf{m} = \pm \mathbf{p}_2 \cdot \underline{\underline{\lambda}_2}^{-T} \mathbf{m}.$$

However,  $\mathbf{m}$  transforms to  $\mathbf{m}'$  under both  $\underline{\underline{Q}_1} \cdot \underline{\underline{\lambda}_1}$  and  $\underline{\underline{\lambda}_2}$  so

$$(\underline{\underline{Q}_1} \cdot \mathbf{p}_1 \mp \mathbf{p}_2) \cdot \mathbf{m}' = 0.$$

Therefore the first Mallard's law solution is uncharged and the second is charged. This result suggests that a structure of two classes of stripe-domains, one of which is charged and one of which is neutral, may be quite widespread in ferroelectric systems. We note that in occasional degenerate cases (if  $\underline{\underline{Q}_1} \cdot \mathbf{p}_1$  and  $\mathbf{p}_2$  are parallel) the above condition is consistent with both classes being uncharged. The disproportionation stripe domain discussed in [2] is such an example.

# Chapter 5

## ELASTICITY OF POLYDOMAIN LIQUID CRYSTAL ELASTOMERS

**M**ONODOMAIN ELASTOMERS are, as we have discussed in the preceding chapters, necessarily semi-soft. Fundamentally, this is because to make a monodomain one must imprint on the elastomer a single orientation for the liquid crystal rods to align in, removing the isotropic reference state that generates the completely soft elastic modes. Elastomers cross-linked without such an aligning field form as polydomains which have local orientational order but in which the liquid crystal director varies from point to point, making the elastomer macroscopically isotropic. In this chapter we will address the elasticity of these polydomain systems, focussing on whether it is hard, soft or semi-soft. We will conclude that both hard and soft polydomain elastomers can be synthesized, and that the key distinguishing point is whether the cross-linking state is isotropic or nematic. We will also analyze smectic polydomain elastomers and propose that polydomain SmC\* elastomers cross-linked in the SmA monodomain state are promising candidates for low field electrical actuation.

### 5.1 MODELS OF POLY- AND MONODOMAIN ELASTOMERS

A liquid crystal elastomer is a monodomain if the director is the same at every point in the relaxed elastomer and a polydomain if it points in

different directions at different points in the relaxed elastomer. Synthesizing monodomains is difficult because, in order to make the elastomer choose the same director at each point, this direction must be imprinted on the elastomer at cross-linking, normally by cross-linking under uniaxial stress [41]. If the elastomer is cross-linked without any such imprinting, in either the isotropic or the nematic state, then it forms a polydomain. Polydomains and monodomains are easily distinguished because monodomains are highly transparent and exhibit large spontaneous deformations at the isotropic-nematic transition while polydomains have no macroscopic spontaneous deformation, and are opaque in the nematic state (because the gradients in the director scatter light) but become transparent if they are stretched enough to align the director throughout the sample [22].

We extend the monodomain energies in the previous chapters to polydomain energies by allowing  $\hat{\mathbf{n}}$ ,  $\hat{\mathbf{n}}_0$  and  $\underline{\underline{\gamma}}$  to become spatially varying fields. We define  $\underline{\underline{\gamma}}(\mathbf{x}) = \nabla \mathbf{y}$  to be the deformation gradient from the cross-linking state<sup>1</sup>. This means that, ignoring non-ideal terms, the energy function for a polydomain cross-linked in the nematic state will be

$$F = \frac{1}{2}\mu \text{Tr} \left( \underline{\underline{\gamma}} \cdot \underline{\underline{\ell}}_0 \cdot \underline{\underline{\gamma}}^T \cdot \underline{\underline{\ell}}^{-1} \right) \quad (5.1)$$

where  $\underline{\underline{\ell}}_0$  is derived from  $\hat{\mathbf{n}}_0(\mathbf{x})$  which is the nematic director at cross-linking. In this case the form of this field will be the nematic disclination pattern present in the nematic-melt before cross-linking. This energy is very different to the monodomain energy from which it was derived because it has a very significant  $\mathbf{x}$  dependence in  $\hat{\mathbf{n}}_0(\mathbf{x})$ . However, the energy function for a polydomain cross-linked in the isotropic

---

<sup>1</sup>we use  $\underline{\underline{\gamma}}$  for deformations from the cross-linking state so we can reserve  $\underline{\underline{\lambda}}$  for the deformations imposed from the relaxed state

state is simply

$$F = \frac{1}{2}\mu\text{Tr}(\underline{\underline{\gamma}}^T \cdot \underline{\underline{\ell}}^{-1} \cdot \underline{\underline{\gamma}}) \quad (5.2)$$

which is exactly the same as the corresponding monodomain energy, eqn. (1.23). There is no intrinsic spatial variation in this function, which is not surprising since the cross-linking state is completely isotropic and homogeneous. However, monodomains and polydomains cross-linked in the isotropic state are manifestly different. We propose that this is because of the form of the non ideal terms that must be added to this energy. In the monodomain case the elastomer is cross-linked in the presence of a uniaxial stress which imprints a constant preferred direction  $\mathbf{n}_0$  (in effect a field) on the elastomer so that when it cools to the nematic state it adopts the same nematic director everywhere, leading us to a mono-domain energy

$$F = \frac{1}{2}\mu\text{Tr}(\underline{\underline{\gamma}} \cdot \underline{\underline{\gamma}}^T \cdot \underline{\underline{\ell}}^{-1} + \alpha r^{1/3} \underline{\underline{\gamma}} \cdot (\underline{\underline{\delta}} - \hat{\mathbf{n}}_0 \hat{\mathbf{n}}_0) \cdot \underline{\underline{\gamma}}^T \cdot \hat{\mathbf{n}} \hat{\mathbf{n}}). \quad (5.3)$$

This is simply the standard semi-soft compositional-fluctuations free-energy considered in the previous chapters (eqn (2.3)) but with the substitution  $\underline{\lambda} = \underline{\underline{\gamma}} \cdot \underline{\underline{\ell}}_0^{-1/2} / \det(\underline{\underline{\ell}}_0^{1/2})$  so that  $\underline{\underline{\gamma}}$  represents the deformations from the high temperature “isotropic” state, rather than the relaxed extended state. The factor of  $r^{1/3}$  multiplying the semi-soft term arises from this change of variables. It is important that although the elastic reference state is the high temperature state, the energy represents an elastomer in a low temperature nematic phase, and is therefore minimized by  $\underline{\underline{\gamma}}$  being a stretch of  $r^{1/3}$  along  $\hat{\mathbf{n}}_0$ , that is by  $\underline{\underline{\gamma}} \propto \underline{\underline{\ell}}_0^{1/2}$ . This is by no means the unique non-ideal theory one could consider — there could be terms which are not quadratic in  $\underline{\lambda}$ , biaxial semi-soft terms that introduce another reference state direc-

tions perpendicular to  $\hat{\mathbf{n}}_0$  and terms of the form  $\text{Tr} \left( \underline{\underline{\gamma}} \cdot \hat{\mathbf{n}}_0 \hat{\mathbf{n}}_0 \cdot \underline{\underline{\gamma}}^T \right)$ .<sup>2</sup> However, all these forms will have the generic property of having a large soft ideal term minimized by any stretch by  $r^{1/3}$  and a small non-ideal term that locally causes the director to favor a single alignment but is macroscopically isotropic, and will therefore have very similar macroscopic stress-strain behavior.

In the polydomain case there is no imprinting so there is very little to break the isotropy of the cross-linking state and introduce any non-ideal terms at all. However, weak mechanisms do exist such as cross-linking molecules having a rod like character which impose an additional direction locally on the network [59]. Consequently, in any finite region the cross-linking rods develop a slight average orientation [23, 34]. These mechanisms permit the inclusion of a very small non-ideal term with a spatially varying preferred direction  $\hat{\mathbf{n}}_0(\mathbf{x})$ . It is this distinction between the large homogeneous non-ideal term in the monodomain case and the small spatially varying term in the polydomain case that drives the distinction between the two systems.

### 5.1.1 POLYDOMAINS - MACROSCOPICALLY HARD OR SOFT?

In this chapter we argue that whether polydomain elastomers are macroscopically hard or soft depends on the relative symmetry of the cross-linking state and the final polydomain state. In this section we will give a qualitative overview of the cause of this behaviour, then in subsequent sections we will work through three examples of possible polydomain systems.

An ideal liquid crystal elastomer energy typically locally has a set of deformations that minimize the free-energy. These are generated by

---

<sup>2</sup>The result derived in the second chapter that this form of the free energy is the only admissible quadratic form does not apply here since the energy is not relaxed.

a symmetry breaking phase transition from a high temperature parent state that is accompanied by a deformation. Since the transition breaks a symmetry there are many ground states, each with a different deformation with respect to the parent state. We visualize this set of energy minimizing deformations as a ring with the parent state at the centre — Fig. 5.1. Such a system is vulnerable to the formation of textured deformations since, if a deformation on the interior of the ring is imposed this is not a low energy state, but it is possible that the energy of the deformation can be reduced to zero by the elastomer splitting into many small regions each of which undergoes one of the low energy deformations in such a way that the macroscopic deformation is what was imposed. The ability of LCE’s to form such textured deformations has been the subject of several studies — [3, 25, 27, 32]. We represent the set of all deformations that can minimize the energy after the formation of the most advantageous textured deformations, the quasi-convex hull (QCH) of the set of energy minimizing deformations, as the interior of the ring of energy minimizing deformations — Fig. 5.1.

A polydomain sample cross-linked in the high symmetry (high temperature) state is effectively cross-linked at the centre of the quasi-convex hull and, on cooling to the aligned state, forms the *same* quasi-convex hull at each point. Although at each point the elastomer has undergone a deformation that takes it to the boundary of the set, these deformations are put together in an elastically compatible way so that the elastomer as a whole is in a textured state at the centre of the set. Such an elastomer can be deformed macroscopically softly simply by moving the constituent domains around the quasi-convex hull, which will cause different soft textures to evolve as the elastomer as a whole moves across the quasi-convex hull.

In contrast, if the elastomer is cross-linked in the low temper-

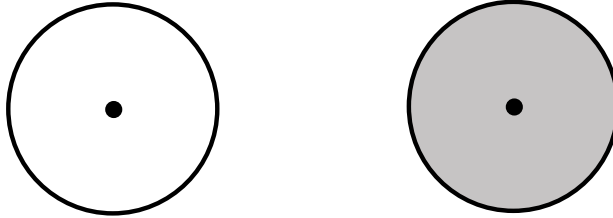


Figure 5.1: Left - the ring of deformations leading to low energy states for a liquid crystal elastomer. The dot in the center is the high symmetry parent state from which the broken-symmetry, low energy states on the ring are derived. Right - visualization of the quasi-convex hull of the set of low energy deformations. These deformations, inside the ring (shaded grey), can be imposed with minimal energy because they can be constructed out of textures of the soft deformations that each lie on different points of the ring.

ature, symmetry-broken state then, although each point still has a quasi-convex hull of the same form each domain sits on the edge of its quasi-convex hull and the deformation required to take each domain back to the center of its hull is different. This corresponds to a picture like fig. 5.2. Although each domain has a hull and soft modes, there are no deformations that are soft for all domains so the elastomer is macroscopically hard. As discussed in the previous section the distinction between a polydomain cross-linked in the high symmetry state and a monodomain is driven by the addition of different non ideal terms. This is easily visualized in terms of the above sets - the ideal monodomain and high symmetry cross-linking polydomain have the same quasi-convex hull at each point, but the addition of non-ideal terms breaks the degeneracy of the states in the quasi-convex hull, making one a unique global minimum. In the monodomain case this is a point on the boundary of the set with a uniform director throughout the sample. In the polydomain case, the non-ideal terms vary spatially such that a different low energy state on the boundary of

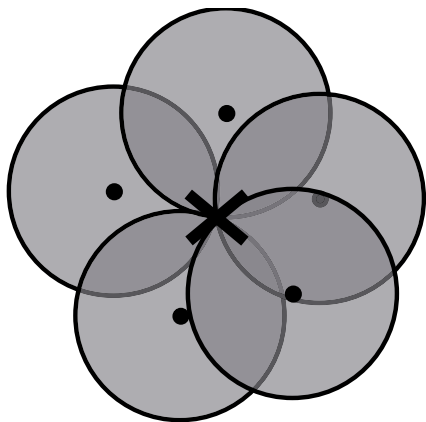


Figure 5.2: If the elastomer is cross-linked in the low symmetry polydomain state then, although every domain still has a quasi-convex hull of the same form, each domain is cross-linked at the boundary of its quasi-convex hull and requires a different deformation to get to the its centre. The quasi-convex hulls of a few domains are illustrated in the diagram, and the cross represents the cross-linking configuration. The cross is the only point in every quasi-convex hull so if the elastomer deforms away from this point some domains will leave their convex hull and the response will be hard.

the QCH is favoured for different points. The global minimum is the point at the centre of the set, no deformation, and is achieved by a complicated textured, low energy, deformation of the different regions of the polydomain.

The above analysis of soft polydomains has a very simple physical interpretation. If an elastomer is cross-linked in the high symmetry state then cooled to the low symmetry state there is no energetic penalty (except small deviations from ideality) to stop it breaking the symmetry in the same way at every point in the elastomer. Therefore the macroscopic deformations that take the polydomains into these well-aligned states must be soft. This will not be true if the crosslinking is in the low symmetry polydomain state. This looks remarkably like a simple restatement of the original result about symmetry breaking soft elasticity by Golubovic and Lubensky [36], and the softness of high symmetry genesis polydomains could certainly be seen as a straightforward consequence of their work. However, symmetry breaking soft elasticity is fundamentally a way of understanding which local deformations can be applied softly, and it is important to remember that both types of elastomer do have local soft modes caused by a high-symmetry reference state in precisely the manner introduced in [36]. This work studies the elastic compatibility of these soft modes, to establish the softness of the macroscopic elastomer, showing that in elastomers with high symmetry cross-linking states the local soft modes can all cooperate in an elastically compatible manner to make a set of macroscopic deformations soft that is far larger than the local symmetry-broken soft modes. In contrast, in elastomers cross-linked in the low symmetry state, the equivalently sized sets of local soft modes cannot cooperate in an elastically compatible way to make any macroscopic modes soft at all.

In the remainder of this chapter we will analyze nematic polydo-

mains cross-linked in the isotropic state and the nematic state and SmC polydomains cross-linked in the SmA monodomain state. The first and last of these are examples of soft polydomains, while the middle is a hard polydomain.

## 5.2 NEMATIC POLYDOMAINS

### 5.2.1 FORMULATING THE ELASTICITY PROBLEMS

We expect a profound difference between nematic polydomains cross-linked in the isotropic and nematic state, and we further distinguish between ideal and non-ideal polydomains. Ideal systems have no locally preferred director orientation and therefore locally completely soft modes. The addition of non-ideal terms slightly favours a particular local director orientation making the modes that were previously completely soft now cost a small amount of energy. This leads us to four types of nematic polydomain corresponding to four different free energies,

$$F = \begin{cases} \frac{1}{2}\mu\text{Tr}(\underline{\underline{\gamma}} \cdot \underline{\underline{\gamma}}^T \cdot \underline{\underline{\ell}}^{-1}) & \text{iI} \\ \frac{1}{2}\mu\text{Tr}(\underline{\underline{\gamma}} \cdot \underline{\underline{\gamma}}^T \cdot \underline{\underline{\ell}}^{-1} + \alpha r^{1/3} \underline{\underline{\gamma}} (\underline{\delta} - \hat{\mathbf{n}}_0 \hat{\mathbf{n}}_0) \underline{\underline{\gamma}}^T \hat{\mathbf{n}} \hat{\mathbf{n}}) & \text{nI} \\ \frac{1}{2}\mu\text{Tr}(\underline{\underline{\gamma}} \cdot \underline{\underline{\ell}}_0 \cdot \underline{\underline{\gamma}}^T \cdot \underline{\underline{\ell}}^{-1}) & \text{iN} \\ \frac{1}{2}\mu\text{Tr}(\underline{\underline{\gamma}} \cdot \underline{\underline{\ell}}_0 \cdot \underline{\underline{\gamma}}^T \cdot \underline{\underline{\ell}}^{-1} + \alpha \underline{\underline{\gamma}} (\underline{\delta} - \hat{\mathbf{n}}_0 \hat{\mathbf{n}}_0) \underline{\underline{\gamma}}^T \hat{\mathbf{n}} \hat{\mathbf{n}}) & \text{nN} \end{cases} \quad (5.4)$$

where iI/nI denote ideal/non-ideal elastomers crosslinked in the isotropic state, and iN/nN ideal/non-ideal elastomers crosslinked in the nematic state. The bulk modulus of elastomers is several orders of magnitude higher than the shear modulus, so all deformations are volume preserving, that is  $\text{Det}(\underline{\underline{\gamma}}) = 1$ . The preferred direction  $\hat{\mathbf{n}}_0$  is discussed below. These four energies are physically interpreted as follows: the iI energy is minimized by a stretch of  $r^{1/3}$  because it is written with re-

spect to the isotropic cross-linking state, but does not distinguish any preferred direction for this stretch because it is ideal. The nI energy is also minimized by a stretch of  $r^{1/3}$  because it is also written with respect to the isotropic cross-linking state, but has a weak energetic preference for this stretch to be along  $\hat{\mathbf{n}}_0$ , a local preferred direction caused by random fluctuations in the cross-linking state. The iI energy is in a relaxed state because it is written with respect to an already aligned nematic cross-linking state, but can locally accommodate deformations that rotate the nematic director completely softly because it is an ideally soft energy. The nN energy is also already relaxed because it is written with reference to an aligned nematic cross-linking state, but in this case the energy is non-ideal so even deformations associated with “soft” rotations of the director cost some energy.

Having identified four types of polydomain, ideal and non-ideal, with either a nematic or an isotropic crosslinking state (genesis), we wish to study the energetic cost of imposing macroscopically homogeneous stretches on large blocks of these different types of polydomains. By large, we mean large enough to contain very many domains and be macroscopically isotropic. In each case we take the cross-linking state of the elastomer as the reference configuration from which deformations will be measured, and define the displacement field from this state as  $\mathbf{y}(\mathbf{x})$ , so that the local deformation gradient is  $\underline{\gamma}(\mathbf{x}) = \nabla \mathbf{y}$ . We then wish to study the energy of a large sample occupying a domain  $\Omega$  (with boundary  $\delta\Omega$ ) in the reference configuration, that is subject to a macroscopic deformation  $\underline{\lambda}$  after it has adopted the most favourable internal deformation and director pattern. We define this relaxed energy function as

$$F^r(\underline{\lambda}, \hat{\mathbf{n}}_0(\mathbf{x})) = \min_{\substack{\mathbf{y}(\mathbf{x}) \text{ s.t. } \hat{\mathbf{n}}(\mathbf{x}) \\ \mathbf{y} = \underline{\lambda} \cdot \mathbf{x} \\ \text{on } \delta\Omega}} \frac{1}{\text{Vol } \Omega} \int F(\nabla \mathbf{y}, \mathbf{n}(\mathbf{x}), \mathbf{n}_0(\mathbf{x})) d\mathbf{x}, \quad (5.5)$$

and the four different types of polydomain correspond to four different choices for  $F(\nabla y, \mathbf{n}(\mathbf{x}), \mathbf{n}_0(\mathbf{x}))$ .

There is an important distinction between the two fields  $\hat{\mathbf{n}}_0(\mathbf{x})$ , which defines the local preferred nematic alignment, and  $\hat{\mathbf{n}}(\mathbf{x})$  which is the nematic field after deformation. The former is a fixed field for a given polydomain that encodes all its spatial heterogeneity, while the latter is a variable field which the elastomer will adjust to minimize its free energy as it evolves under the macroscopic  $\underline{\lambda}$ . Furthermore, in the nematic genesis case we expect the form of  $\hat{\mathbf{n}}_0(\mathbf{x})$  to be a disclination texture, while in the isotropic genesis case it will be a random field arising from the sources of disorder in the crosslinking state. In the latter case  $\mathbf{n}_0$  does not correspond to the equilibrium director pattern at zero stress, but rather locally it is the director that a domain would adopt if it were unconstrained by its neighbors (e.g. by cutting it out of the sample). These locally optimal strain fields  $\underline{\underline{\gamma}}(\mathbf{x})$  associated with this director pattern are extremely unlikely to be compatible deformations (be the gradient of a continuous displacement field) and thus would require the sample to fracture.

Our task is to find the lowest energy compatible strain fields – in general a difficult task. It is not clear whether they are subtle fields associated with a continuous director variation (but still compatible) or are compatible combinations (textures and laminates) of strains as are observed in the deformation of monodomains under boundary constraints at variance with soft deformations as discussed in chapter 4. We shall proceed to find bounds on the elastic energy. In the ideal case, we know that textures of deformations each on the boundary of the QCH can give zero energy cost for macroscopic deformations within the QCH and thus give an exact value for the energy (a continuous field could not do better than this choice of test field). In the non-ideal case we will use these exact minimizers of the ideal part of

the free energy and evaluate the extra, non-ideal cost associated with them, thus forming an upper bound. In reality an elastomer could, by adjusting the laminates, or by finding an unlikely continuous field, lower the energy by correlating distortion fields with the random field. We discuss that energy reduction strategy briefly later.

### 5.2.2 IDEAL ISOTROPIC GENESIS POLYDOMAINS

The only completely solvable system is that of ideal isotropic genesis (ii). The energy function has no  $\hat{\mathbf{n}}_0$  dependence so it is not really spatially heterogenous at all. This is unsurprising since the isotropic cross-linking state appears to be completely homogeneous. It is the same model as is used for ideal monodomain samples, so we can directly apply DeSimone and Dolzman's results about its relaxation [27] discussed in chapter 4, namely that, if the principal stretches of  $\underline{\lambda}$  are  $f_1 \leq f_2 \leq f_3$ , the fully relaxed energy function is

$$\frac{2F_{iI}^r(\underline{\lambda})}{\mu} = \begin{cases} 3 & \text{if } \underline{\lambda} \in K^{qc} \\ r^{1/3}(2/(r^{1/2}f_1) + f_1^2) & \text{if } \underline{\lambda} \in I \\ r^{1/3}(f_1^2 + f_2^2 + f_3^2/r) & \text{if } \underline{\lambda} \in S \\ \infty & \text{else} \end{cases} \quad (5.6)$$

where

$$\begin{aligned} I &= \{\underline{\lambda} \in \mathbb{M}^{3 \times 3} : \frac{f_3}{f_2} < \sqrt{r}, f_1 < \frac{1}{r^{1/6}}, \text{Det}(\underline{\lambda}) = 1\} \\ S &= \{\underline{\lambda} \in \mathbb{M}^{3 \times 3} : \frac{f_3}{f_2} \geq \sqrt{r}, \text{Det}(\underline{\lambda}) = 1\} \\ K^{qc} &= \{\underline{\lambda} \in \mathbb{M}^{3 \times 3} : r^{-1/6} \leq f_1 \leq f_3 \leq r^{1/3}, \text{Det}(\underline{\lambda}) = 1\}. \end{aligned}$$

The “else” case only contains deformations with  $\text{Det}(\underline{\lambda}) \neq 1$  that do not conserve volume. Textured deformations are required for macroscopic deformations in  $I$  and  $K^{qc}$  but not  $S$ . The set  $K^{qc}$  is an eight dimensional set of zero energy deformations, so if an elastomer is at a point in the interior of  $K^{qc}$  all small volume preserving deformations of the elastomer are also in  $K^{qc}$  and do not cost energy to impose – the energy is liquid-like. In  $S$  the energy depends on all three principal values of the deformation so the energy is solid-like while in  $I$  it depends on only the smallest principal value so the energy is intermediate between that of a solid and that of a liquid. Physically, the set  $S$  consists of stretches,  $f_3$ , sufficient that the director has completely aligned with this stretch direction, so the elastomer responds to further stretching in the same way as a conventional rubber, while the set  $K^{qc}$  consists of deformations that can be made soft by the formation of textured deformations of spontaneous deformations. The set  $I$  contains compression in one direction making the sample thinner than any spontaneous deformation would. The director lies perpendicular to the compression axis but still forms textures in that plane allowing any macroscopic in-plane shapes bounded by  $f_3/f_2 < \sqrt{r}$ . The energy however only depends on the degree of compression.

In this work we are concerned with uniaxially stretching polydomains to induce the polydomain-monodomain transition. This corresponds to macroscopic deformations of the form  $\underline{\lambda} = \text{diag}(\lambda, 1/\sqrt{\lambda}, 1/\sqrt{\lambda})$  for  $\lambda \geq 1$ . Applying the above relaxation result, these deformations will be achieved at the energies

$$F_{II}(\lambda) = \begin{cases} \frac{3\mu}{2} & \text{if } 1 \leq \lambda \leq r^{1/3} \\ \frac{\mu r^{1/3}}{2} \left( \frac{2}{\lambda} + \frac{\lambda^2}{r} \right) & \text{if } \lambda \geq r^{1/3}. \end{cases} \quad (5.7)$$

Differentiating this gives the engineering stress,

$$\sigma_{iI}(\lambda) = \frac{dF_{iI}}{d\lambda} = \begin{cases} 0 & \lambda \leq r^{1/3} \\ \mu r^{1/3}(\lambda/r - 1/\lambda^2) & \lambda \geq r^{1/3}. \end{cases} \quad (5.8)$$

This simply means that ideal isotropic genesis polydomains will deform at zero stress but with textured deformations until they have been stretched by  $r^{1/3}$ , at which point they are completely aligned monodomains and respond to further deformation as a neo-Hookean solid. This result is quantitatively wrong, real isotropic genesis polydomains do not deform at absolutely zero stress, and when stress is removed they (macroscopically) return to their original configuration. This motivates the consideration of non-ideal theories. However, since the cross-linking state is almost isotropic, non-ideality must be very small so we expect several key features of the ideal model to persist. Extension will not occur at zero stress, but extensions up to  $\lambda \leq r^{1/3}$  will occur at energies  $O(\alpha) \ll 1$ . Furthermore, the deformation patterns and director patterns in the non-ideal case must still be very close in energy to those in the ideal case, so the observed patterns will still be characterized as textured deformations driven by elastic compatibility – not disclination textures. Indeed, nematic disclinations never have zero-energy elastically compatible associated distortions [35], so cannot be observed in isotropic genesis systems.

### 5.2.3 NON-IDEAL ISOTROPIC GENESIS POLYDOMAINS

Finding the full relaxation of the non-ideal polydomain energy is probably intractable. At the moment the relaxation is not known for the easier monodomain case (except in a thin film limit [25]), and the polydomain result will depend to some extent on the exact form of  $\hat{\mathbf{n}}_0(\mathbf{x})$ . However, we can put upper and lower bounds on the energy-strain

curves. Developing an upper bound on the energy is straightforward. We simply use a textured test strain field from the ideal case and calculate its energy in the non ideal case. Since the relaxed energy function is a minimum over all strain fields, evaluating the energy at one example of a strain field is an upper bound on the energy. In a sense this is a Taylor-like bound of uniform strain, but our uniform macroscopic strain is in fact composed of textures that allow deformation anywhere in the QCH. We depart also from conventional Taylor bounds in that our bound is valid for large strains, up to  $r^{1/3}$  which can be 100s% for nematic elastomers.

If a point in the elastomer undergoes a uniaxial extension of magnitude  $\gamma$  from the crosslinking state, at an angle  $\theta$  to the preferred direction  $\hat{\mathbf{n}}_0$ , then the energy of the deformation is

$$\begin{aligned} F &= \min_{\hat{\mathbf{n}}} \frac{\mu}{2} \text{Tr} \left( \underline{\underline{\gamma}} \cdot \underline{\underline{\gamma}}^T \cdot \underline{\underline{\ell}}^{-1} + \alpha r^{1/3} \underline{\underline{\gamma}} (\underline{\underline{\delta}} - \hat{\mathbf{n}}_0 \hat{\mathbf{n}}_0) \underline{\underline{\gamma}}^T \hat{\mathbf{n}} \hat{\mathbf{n}} \right) \\ &= \frac{1}{2} \mu r^{1/3} \left( \frac{2}{\gamma} + \left( \frac{1}{r} + \alpha \right) \gamma^2 - \alpha \gamma^2 \cos^2 \theta \right), \end{aligned} \quad (5.9)$$

where the minimization over  $\hat{\mathbf{n}}$  is achieved by taking  $\hat{\mathbf{n}}$  along the axis of  $\underline{\underline{\gamma}}$ . If the region of constant deformation is much larger than the individual domain size (region of given  $\hat{\mathbf{n}}_0$ ) then averaging over  $\hat{\mathbf{n}}_0$  gives:

$$F = \frac{1}{2} \mu r^{1/3} \left( \frac{2}{\gamma} + \left( \frac{1}{r} + \alpha \right) \gamma^2 - \frac{\alpha \gamma^2}{3} \right), \quad (5.10)$$

which is minimized at  $\gamma_m^3 = r/(1 + 2\alpha r/3)$  with a value

$$F = \frac{3\mu}{2} \left( 1 + \frac{2\alpha r}{3} \right)^{1/3}. \quad (5.11)$$

This free energy density can be achieved if every point in the sam-

ple undergoes a uniaxial elongation of magnitude  $\gamma_m$  in any direction. This situation is completely analogous to the situation in ideal elastomers in the isotropic configuration where the same (in this case minimal) energy can be reached by applying an elongation of magnitude  $r^{1/3}$  in any direction. The DeSimone and Dolzmann texture result [27] shows that any uniaxial macroscopic deformation with magnitude less than  $\gamma_m$  can be achieved by a texture of deformations in which each deformation is a uniaxial deformation by  $\gamma_m$ . This allows us to place an upper bound on the total energy of the sample after it has undergone a macroscopic uniaxial elongation by  $\lambda$ ,

$$\frac{2F^r(\lambda)}{\mu} \leq \begin{cases} 3\left(1 + \frac{2\alpha r}{3}\right)^{1/3} & \lambda^3 \leq r/(1 + 2\alpha r/3) \\ r^{1/3} \left(\frac{2}{\lambda} + \left(\frac{1}{r} + \frac{2\alpha}{3}\right)\lambda^2\right) & \lambda^3 \geq r/(1 + 2\alpha r/3). \end{cases} \quad (5.12)$$

Although this upper bound has been calculated by using textures with regions of constant deformation that are very large compared to the length scales  $\hat{\mathbf{n}}_0$  varies on, the same result can be achieved with any size. This is because the averaging to 1/3 of the  $\cos^2 \theta$  in eq. (5.9) will still be true after averaging over many domains provided the axes of the domains are not correlated with the  $\hat{\mathbf{n}}_0$  field. Introducing such correlations would reduce the energy of the elastomer and would also determine length scales involved in the actual deformation and director fields. An Imry-Ma style attack on this problem, but not involving textured test fields as here, is due to Terentjev and Fridrikh [34]. Domain size would be selected to take advantage of fluctuations in the random ordering field from crosslinking. We return to this problem elsewhere.

The ideal system provides a very simple lower bound on the energy, eq. (5.7), since the non-ideal term is never negative. We can improve on this bound by using the Sachs limit of stress uniform through the

sample. This provides a lower bound because it neglects the requirement of compatibility of deformations ( $\underline{\underline{\gamma}} = \nabla \mathbf{y}$ ). We calculate this bound numerically by minimizing  $F_{nI}(\underline{\underline{\gamma}}, \hat{\mathbf{n}}, \hat{\mathbf{n}}_0) - \sigma \gamma_{xx}$  across all  $\underline{\underline{\gamma}}$  and  $\hat{\mathbf{n}}$  at fixed  $\sigma$  for a given domain ( $\hat{\mathbf{n}}_0$ ) to find the optimal deformation  $\underline{\underline{\gamma}}_m$  and director orientation  $\hat{\mathbf{n}}_m$  of the domain at the stress  $\sigma$ . The energy and extension of the whole sample are then found by averaging  $F_{nI}(\underline{\underline{\gamma}}_m, \hat{\mathbf{n}}_m, \hat{\mathbf{n}}_0)$  and  $(\underline{\underline{\gamma}}_m)_{xx}$  across all domain orientations.

Although we have calculated the full Sachs bound numerically, we can understand its behavior at small extension analytically. At zero stress every domain is free to undergo an energy minimizing spontaneous deformation - anything of the form  $\underline{\underline{\gamma}} = \underline{\underline{R}} \cdot \underline{\underline{\ell}_0}^{1/2}$ , where  $\underline{\underline{R}}$  is a rotation. The  $xx$  component of this is simply  $\mathbf{x} \cdot \underline{\underline{R}} \cdot \underline{\underline{\ell}_0}^{1/2} \cdot \mathbf{x}$ , which is to say it is the component of  $\underline{\underline{\gamma}} \cdot \mathbf{x}$  that is parallel to  $\mathbf{x}$ . For each domain a rotation  $\underline{\underline{R}}$  can be chosen such that  $\underline{\lambda}_{xx}$  lies anywhere between 0 and  $|\underline{\underline{\ell}_0}^{1/2} \cdot \mathbf{x}|$ . Since we are studying extension we are not concerned with  $\lambda_{xx} \leq 1$ , but this means that any  $\lambda_{xx}$  between 1 and  $\langle |\underline{\underline{\ell}_0}^{1/2} \cdot \mathbf{x}| \rangle$  can, in the Sach's limit, be achieved without stress. Therefore the Sach's limit on the energy is simply  $3\mu/2$  for  $1 \leq \lambda_{xx} \leq \langle |\underline{\underline{\ell}_0}^{1/2} \cdot \mathbf{x}| \rangle$ . It is straightforward to calculate this average giving

$$\langle |\underline{\underline{\ell}_0}^{1/2} \cdot \mathbf{x}| \rangle = \frac{r^{-1/6}}{2} \left( \sqrt{r} + \frac{\sinh^{-1} \sqrt{r-1}}{\sqrt{r-1}} \right). \quad (5.13)$$

This threshold tends to  $1+O(\epsilon^2)$  for  $r = 1+\epsilon$ , so for small anisotropies it is insignificant, but for large  $r$  it tends to  $r^{1/3}/2$ .

The energy plot, Fig. 5.3, shows that the bounds constrain the energy very tightly: the bounds reproduce the exact ideal result if  $\alpha = 0$ , and  $\alpha$  is expected to be very small for isotropic genesis. The Sachs free energy is in effect plotted parametrically since one sets the stress and obtains the free energy and strain by minimisation

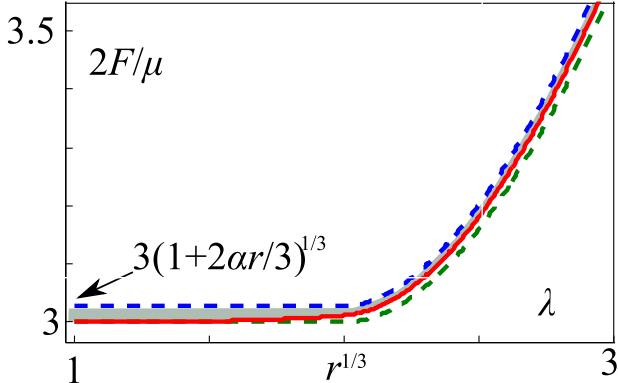


Figure 5.3: Bounds on the free energy density of an isotropic genesis polydomain nematic elastomer as a function of strain, plotted in units of  $\mu r^{1/3}/2$  with  $r = 8$  and  $\alpha = 0.005$ . Upper curve (dashed, blue): upper bound from a test strain field. Middle curve (smooth, red): Sachs lower bound. Lower curve (dashed, green): ideal result, lowest bound.

and averaging. The bounds show that stretching the elastomer by  $\sim r^{1/3}$  cannot require an increase in the energy density of more than  $3\mu/2((1 + 2\alpha r/3)^{1/3} - 1) \approx \mu\alpha r/3$ . This means that although the extensions up to  $r^{1/3}$  can take place at finite stress, the stress cannot be higher than  $\partial F/\partial\lambda \sim \mu\alpha r/[3(r^{1/3} - 1)]$ , which will be a very small number since  $\alpha$  is small. As in the ideal case, extensions larger than  $\sim r^{1/3}$  behave in a neo-Hookean manner.

We can calculate bounds on the stress-strain curve for these extensions by using the requirement, which applies to all one dimensional elastic energies, that the relaxed energy curve be convex, meaning the stress curve is monotonic for  $\lambda \geq 1$ . This means that at a given extension  $\lambda_{xx}$  not only must the energy function lie between the two bounds, but the gradient of the energy function must not be so great that, if extrapolated forwards as a straight line, the energy curve intersects the upper-bound (used above for estimating the approximate

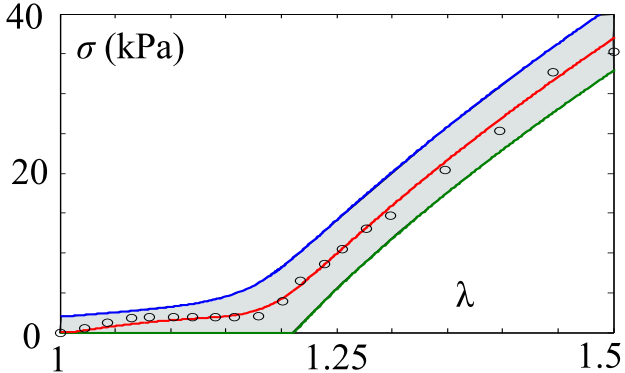


Figure 5.4: Upper and lower bounds on the stress-strain curve for a non-ideal isotropic genesis polydomain. Material parameters are  $r = 1.65$  and  $\alpha = 0.01$  and  $\mu = 33000$ . The middle curve is the derivative of the Sachs lower bound on the energy, which provides an estimate of the stress-strain curve, while the upper and lower curves are the bounds derived by requiring the energy function be convex. The circles are stress-strain data for a real sample. We thank K. Urayama for permission to reproduce this data.

maximal stress), or so little that if extrapolated backwards it does the same. This bounds the gradient of the energy and hence the stress at each extension.

A plot of the two bounds on the stress strain curve is shown in Fig. 5.4, which shows that the very soft stress plateau for  $\lambda \leq r^{1/3}$  does indeed survive the introduction of semi-softness. The experimental results of Urayama *et al* for isotropic genesis polydomain stress [56] are also shown and display pronounced softness – clearly polydomains can deform softly and the requirement of compatibility between domains does not appreciably harden response.

### 5.2.4 NEMATIC GENESIS POLYDOMAINS

We expect the coefficient of non-ideality,  $\alpha$ , to be much higher for nematic genesis polydomains because the cross-linking state is not isotropic and distinguishes the direction of the nematic director,  $\hat{\mathbf{n}}_0$ . It will probably have a similar magnitude to that observed in monodomain elastomers where  $\alpha \sim 0.1$ . However, although non-ideality will be larger, it is conceptually less important because already the ideal part of the energy will contribute significantly to the stress. This is because even an ideal nematic genesis polydomain is not expected to have any soft modes. Soft modes are generated by symmetry breaking spontaneous distortions from an isotropic reference state. Locally an individual domain does have an isotropic reference configuration, which is reached by applying the inverse spontaneous deformation  $\underline{\underline{\gamma}} = \underline{\underline{\ell}_0}^{-1/2}$ , but the spatially-dependent deformation  $\underline{\underline{\gamma}}(\mathbf{x}) = \underline{\underline{\ell}_0}^{-1/2}(\mathbf{x})$  will not be mechanically compatible, so it is impossible to apply a deformation that places the whole sample in the isotropic reference state simultaneously. The reason for this large difference between nematic and isotropic genesis polydomains is that there are very few deformation patterns of the form  $\underline{\lambda}(\mathbf{x}) = \underline{\underline{\ell}_0}^{-1/2}(\mathbf{x})$  that are compatible deformations, and no nematic disclination patterns are compatible deformations. An isotropic genesis polydomain is forced to undergo such a deformation on cooling to the nematic after cross-linking, so it must choose one of the deformation patterns that is mechanically compatible and these, as we have seen in the previous section, allow for macroscopic movement across the QCH. In contrast the nematic-genesis polydomain undergoes its “spontaneous-distortion” in the melt where there are no conditions of compatibility because adjacent regions can flow past each other, a deformation which would result in a fracture in a solid network. One consequence of this is that when a nematic genesis polydomain is heated to what would be its “isotropic” state, it is

unable to undergo its energy minimizing contraction  $\underline{\gamma}(\mathbf{x}) = \underline{\underline{\ell}}_0^{-1/2}(\mathbf{x})$  everywhere because this is not a compatible deformation. This will result in the high temperature state being internally stressed, and may lead to elevation of the transition temperature.

We can bound the ideal nematic genesis free energy in the same way we bounded the isotropic genesis non-ideal free energy. An upper bound is provided by a test strain field. The simplest test field would be a constant strain throughout the sample, giving a Taylor bound. However, we can find a tighter upper bound by applying the same strain to each domain, but allowing each domain to form textured deformations that average to the strain imposed on it; this is what we termed in the previous section a “Taylor-like bound”. Consequently, if the strain imposed macroscopically is  $\underline{\lambda}$ , the free energy density of each domain will be  $F_{Ii}^r(\underline{\lambda} \cdot \underline{\ell}^{1/2})$ , where  $F_{Ii}^r(\underline{\lambda})$  is the relaxed energy for an ideal monodomain in [27] given by eq. (5.6) and is attained by texturing (by laminates). The factor of  $\underline{\ell}^{1/2}$  in the argument of  $F_{Ii}^r$  is appropriate because the function  $F_{Ii}^r(\underline{\lambda})$  is written in terms of deformations from the isotropic reference state, whereas the domains in the nematic genesis polydomain are already in the elongated nematic state. The deformation  $\underline{\ell}^{1/2}$  is the deformation the isotropic state would have to undergo to reach the nematic state that the domain was cross-linked in, and the component  $\underline{\lambda}$ , of the compound deformation in the argument of  $F_{Ii}^r$ , is the deformation from this nematic state. A lower bound can be found using the Sachs constant stress limit. However, since the elastomer is ideal, the individual domains can deform softly. This means that, in the constant stress limit where compatibility of the deformations between the different domains is not required, the elastomer can deform completely softly. We can calculate the end of the soft plateau in the Sachs bound analytically in the same way we did for the isotropic-genesis case. Since one considers a

spontaneous contraction  $\underline{\underline{\ell}}_0^{-1/2}$  in going from the nematic state to an isotropic reference state, followed by a spontaneous elongation  $r^{1/3}$  in elongating to the nematic state along  $\hat{\mathbf{n}}$ , the end softness in the Sachs bound will occur at  $\langle |r^{1/3} \underline{\underline{\ell}}_0^{-1/2} \mathbf{x}| \rangle$  which evaluates to

$$\langle |r^{1/3} \underline{\underline{\ell}}_0^{-1/2} \mathbf{x}| \rangle = \frac{1}{2} \left( 1 + \frac{r \tan^{-1} \sqrt{r-1}}{\sqrt{r-1}} \right). \quad (5.14)$$

This limits to  $1 + \epsilon/4$  for small anisotropy  $r = 1 + \epsilon$ , and to  $\sqrt{r}\pi/4$  for large  $r$ .

The two bounds on the energy (calculated numerically) are both plotted in Fig. 5.6. These bounds on the energy are not very good — there is a large gap between them. The Sach's limit displays complete ordering of the elastomer at zero stress while the test strain field shows hard elasticity and finite modulus ( $\sim \mu$ ) at all extensions. This is because nematic genesis polydomains are strongly heterogeneous materials, and good methods for finding stress strain curves for such materials have yet to be developed at large deformations that are required here. Taylor (affine) and Sach's (constant stress) bounds on heterogeneous materials are independent of the domain structure of the material, meaning the Taylor bound gives an upper bound on the energy of the hardest possible domain structure, and Sach's gives a lower bound on the energy for the softest possible domain structure. Unfortunately there exist vanishingly unlikely domain structures which are indeed completely soft, namely the textured-deformation domain structures realized by the isotropic genesis polydomains. There also exist domain structures which certainly have no macroscopic soft modes - fig. 5.5. Since the domain structures in nematic polydomains will certainly not be of the compatible double laminate type — they will be disclination textures which are not mechanically compatible — the lower bound is of little physical significance. Therefore, we estimate the stress strain

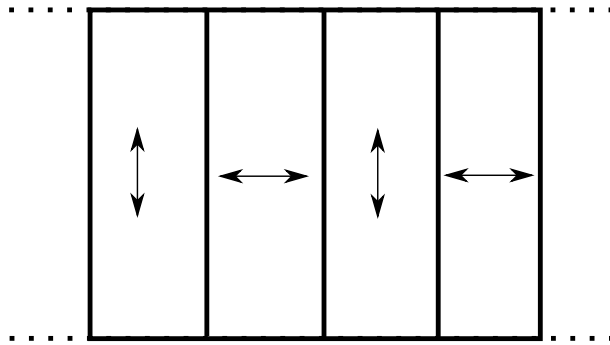


Figure 5.5: An example of a possible director pattern at cross-linking in a nematic genesis polydomain that certainly doesn't have any macroscopic soft modes. This can be seen by considering a line element along the boundary in the plane of the diagram - all soft modes of the vertical stripes require this element to contract while all soft modes of the horizontal stripes require it to extend or not deform, so there are no macroscopic soft deformations.

relation for these polydomains by simply taking the derivative of the upper bound on the energy. The resulting stress-strain curve, shown in Fig. 5.7, matches the experimentally observed completely hard behavior.

The inclusion of non-ideality in the nematic genesis model will elevate the Sach's limit to a plateau of height  $\propto \alpha$  but will not alleviate the fundamental difference between the soft elasticity seen in the Sachs and the hard elasticity seen in the Taylor-like limit.

### 5.3 SMECTIC POLYDOMAINS

Smectic liquid crystal phases are phases in which the rods not only have orientational order but are also layered. Liquid crystal elastomers can exhibit smectic ordering [31], and monodomains with both SmA ordering [33] (in which the liquid crystal director is parallel to the layer normal) and SmC ordering [9] (in which the liquid crystal di-

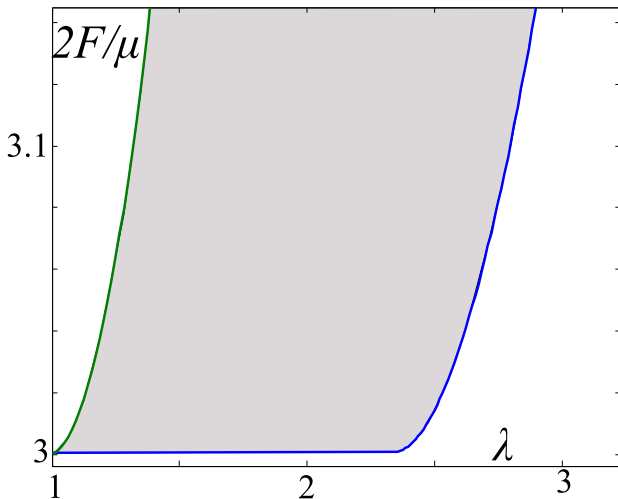


Figure 5.6: Bounds on the free energy density of an ideal nematic genesis polydomain with  $r = 8$ . Upper curve (green) — upper bound using a test strain field. Lower curve (blue) — lower bound using a constant stress. There is a very large gap between the two bounds. Note that the ideal system displays hard elastic response for purely geometrical reasons stemming from compatibility requirements.

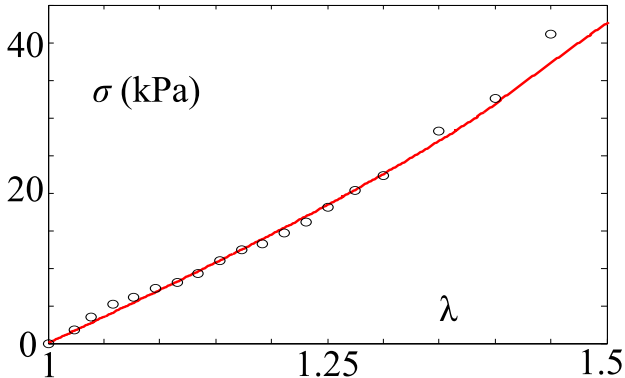


Figure 5.7: Estimate of stress vs strain for an ideal nematic genesis polydomain elastomer with  $r = 1.65$  and  $\mu = 37000$ , obtained by differentiating the upper bound on the energy. The circles are stress-strain data for a real sample, the exact analogue of the sample used in fig. 5.4 but cross-linked in the nematic polydomain state. We thank K. Urayama for permission to reproduce this data. We note that the fitting parameter  $r$  is the same but a slightly higher value of  $\mu$  is needed. This probably reflects the fact that in reality nematic genesis polydomains have a significant non-ideal term ( $\alpha \sim 0.1$ ) which will slightly harden the system.

rector makes a constant angle  $\theta$  with the layer normal) have been synthesized. SmC phases in which all the rods have the same chirality (SmC\* phases) are particularly interesting because they have electrical polarizations along the cross product of the layer normal and the director. The introduction of these phases significantly increases the total number of polydomains that can be considered since there are now four distinct states — isotropic, nematic, SmA and SmC — and polydomains can be made that have been cross-linked in any one of these states then cooled or heated to any other of the states.

In strongly coupled elastomers, smectic behavior is usually modeled by assuming that the layers deform affinely under deformations (so that a layer normal  $\mathbf{k}$  becomes  $\underline{\underline{\gamma}}^{-T} \cdot \mathbf{k}$  after a deformation  $\underline{\underline{\gamma}}$  has been applied) and then adding terms to the underlying nematic free energy that penalize changing the inter-layer spacing and rotating the director away from its preferred angle with the layer normal. This means that although SmA elastomers have the same cylindrical symmetry as nematics they do not have any soft elastic modes since the layers deform affinely (they cannot translate or rotate relative to the rubber matrix) and rotation of the director away from the layer normal costs energy. SmC elastomers could still exhibit soft modes since their director can rotate in a cone around the layer normal without changing the inter-layer spacing or deviating from the preferred tilt angle.

(i) *Isotropic Genesis:* The modeling assumptions outlined above are well established for monodomain smectic elastomers but they seem rather strange for polydomain elastomers crosslinked in the isotropic state. In particular, the assumption that the layers move affinely seems appropriate if the layers have been embedded into the elastomer at crosslinking. But if, for isotropic genesis, they have appeared after crosslinking as the result of a symmetry-breaking isotropic-SmA tran-

sition, then they could equally well have formed in any other direction so one would expect them to be able to rotate through the sample. Indeed, since the isotropic-SmA transition will be accompanied by a spontaneous deformation that is a stretch along the director and hence also the layer normal, a deformation that returns the elastomer to its isotropic configuration and then stretches it by the same amount in a different direction must, on symmetry grounds, be soft and must cause the layers to rotate. With this view, the isotropic cross-linked SmA polydomains are no different to the isotropic cross-linked nematic polydomains since the spontaneous deformations at the transitions are of exactly the same form and break the same symmetry. Accordingly we expect exactly the same macroscopic soft elastic response. SmC polydomains cross-linked in the isotropic state will also behave in the same way. However, although this simple symmetry argument cannot be circumvented in equilibrium, it is possible that non-equilibrium kinetic effects prevent the elastomer from realizing this soft elasticity on experimentally accessible time scales and that the layers, though really free to rotate through the sample, are effectively frozen in at the transition to the layered state. This freezing would result in a complete hardening of SmA elastomers since, while the layers are deforming affinely, there are no local soft modes. Equally, affine layer deformations imposed by the freezing-in of layers would make the SmC polydomain much like the nematic genesis nematic polydomain case since it would possess local soft modes but there would be no compatibility between the soft modes of adjacent domains so these cannot be used to make macroscopic soft modes.

(ii) *SmA or SmC Genesis:* Most of the other routes to smectic polydomains will result in macroscopically hard elasticity, for example cross-linking directly in a SmA state will lead to a polydomain with no local soft modes, cross-linking in a SmC polydomain state will result in a

system analogous to the nematic cross linking nematic polydomain.

### 5.3.1 SOFT POLYDOMAIN SMECTIC ELASTICITY

To recover macroscopically soft elasticity, we need the elastomer to break a symmetry at a transition after cross-linking in such a way that if it had happened to break it in the same way in every domain a monodomain would have formed. One interesting system that has this property is a SmA monodomain that is cooled without any external influences into a SmC polydomain. Crosslinking in the SmA monodomain state guarantees that the smectic layers are permanently embedded in the elastomer and will subsequently deform affinely and that, since the layers are embedded as a monodomain, after cooling the system can access fully aligned SmC monodomain states without having to rotate the layers through the elastomer. To discuss this case will take the SmA cross-linking state as the reference state and use a set of axes such that the SmA layer normal  $\mathbf{k} = (0, 0, 1)$  while  $(0, 1, 0)$  and  $(1, 0, 0)$  are perpendicular vectors in the SmA layer plane, see Fig. 5.8. The local spontaneous deformations at the SmA-SmC transition

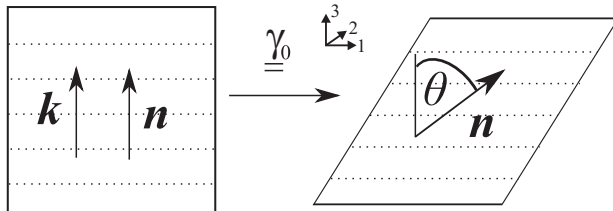


Figure 5.8: A SmA elastomer (left) with director  $\mathbf{n}$  aligned along the layer normal  $\mathbf{k}$  cools and undergoes a deformation  $\underline{\gamma}_0$  to form a SmC elastomer (right) in which the director forms an angle  $\theta$  with the layer normal. The deformation typically includes a contraction along  $\mathbf{k}$  since the rods have tilted which reduces the inter-layer spacing.

if the director tilts in the  $\mathbf{k} - (1, 0, 0)$  plane will be

$$\underline{\underline{\gamma}}_0 = \begin{pmatrix} \gamma_{11} & 0 & \gamma_{13} \\ 0 & 1/\gamma_{11}\gamma_{33} & 0 \\ 0 & 0 & \gamma_{33} \end{pmatrix} \quad (5.15)$$

where all the components of this deformation have fixed values determined by the microscopic details of the elastomer. This transition is illustrated in Fig. 5.8. Elastomers have been synthesized with values of  $\gamma_{13}$  as large as 0.4 [37].

In the SmA phase there is nothing to distinguish any direction in the  $(0, 1, 0) - (1, 0, 0)$  plane, so the above deformation would also have been soft if it had been applied at any other angle in the  $(0, 1, 0) - (1, 0, 0)$  plane, so the full set of soft deformations,  $K_{SmC}^0$ , is all deformations that can be written in the form  $\underline{\underline{R}} \cdot \underline{\underline{\gamma}}_0 \cdot \underline{\underline{R}}_k$ , where  $\underline{\underline{R}}$  is a rotation and  $\underline{\underline{R}}_k$  is a rotation about  $\mathbf{k}$ . The full set of deformations that can be made soft by constructing textures out of such deformations is known to be [3]

$$K_{SmC}^{qc} = \{ \underline{\underline{\lambda}} \in \mathbb{M}^{3 \times 3} : \text{Det}(\underline{\underline{\lambda}}) = 1, |\underline{\underline{\lambda}} \cdot \mathbf{k}|^2 \leq \gamma_{13}^2 + \gamma_{33}^2, \\ |\underline{\underline{\lambda}}^{-T} \cdot \mathbf{k}|^2 \leq 1/\gamma_{33}^2, f_1(\underline{\underline{\lambda}} \cdot \underline{\underline{\lambda}}_i) \geq 1 \}, \quad (5.16)$$

where the function  $f_1$  returns the smallest principal value of its argument and the deformation  $\underline{\underline{\lambda}}_i = \text{diag}(\gamma_{11}\gamma_{33}, \gamma_{11}\gamma_{33}, \rho)$  where

$$\rho = \frac{1 - \gamma_{11}^4\gamma_{33}^2}{\gamma_{13}^2 + \gamma_{33}^2 - \gamma_{13}^4\gamma_{33}^4}. \quad (5.17)$$

The set  $K_{SmC}^{qc}$  is fairly complicated, but the four conditions in it each have a simple interpretation. The determinant condition  $\text{Det}(\underline{\underline{\lambda}}) = 1$  requires that the elastomer have the same volume after deformation as it did in the SmA state. A line element in the  $\mathbf{k}$  direction of the SmA

is stretched by a factor of  $\sqrt{\gamma_{13}^2 + \gamma_{33}^2}$  by any of the local spontaneous deformations in  $K_{SmC}^0$ , so the longest a line element in the  $\mathbf{k}$  direction can be after deformation is  $\sqrt{\gamma_{13}^2 + \gamma_{33}^2}$  (which occurs when every local spontaneous deformation is the same), imposing the first inequality. The second inequality can be understood in an analogous way — a vector area along  $\mathbf{k}$  has its area increased by a factor of  $1/\gamma_{33}$  by any of the local spontaneous deformations but its direction may be rotated. The average of all these vector areas,  $\underline{\lambda}^{-T} \cdot \mathbf{k}$ , cannot be larger than the sum of the areas that make it up so  $|\underline{\lambda}^{-T} \cdot \mathbf{k}|^2 \leq 1/\gamma_{33}^2$ . The final inequality is the analog of  $f_1(\underline{\lambda}) \geq r^{-1/6}$  in the ideal nematic case, requiring that the elastomer cannot be compressed so much in any direction that it is thinner than the natural width of the thinnest direction of the underlying chain distribution.

The set  $K_{SmC}^{qc}$  is much richer than its ideal nematic counterpart, in particular uniaxial deformations of the form  $\underline{\lambda} = \text{diag}(1/\sqrt{\lambda}, 1/\sqrt{\lambda}, \lambda)$ , which are stretches by  $\lambda$  along the original layer normal, are in  $K_{SmC}^{qc}$  provided that  $\gamma_{33}^2 \leq \lambda^2 \leq \gamma_{33}^2 + \gamma_{13}^2$ . This means that there is a whole set of textured SmC polydomain states whose deformation with respect to the parent SmA state is a simple stretch along the SmA layer normal. All of these SmC polydomain states have the same macroscopic cylindrical symmetry as the SmA state. When the SmA sample is cooled to the SmC state it could form any of these states, so the resting configuration of a SmC polydomain may have a uniaxial stretch relative to the SmA state. This was not the case in the isotropic genesis nematic polydomains because there was only one textured state with the full isotropic symmetry of the cross-linking state.

In the ideal SmC case our inability to uniquely identify one polydomain state with cylindrical symmetry makes no difference to the analysis at all since every state in  $K_{SmC}^{qc}$  is an energy minimizing state and deformations that move the polydomain between them are perfectly

soft. The addition of a non ideal term, which must be small since it breaks both the homogeneity and symmetry of the cross-linking state by energetically favoring a single director orientation, will have a very similar effect to its addition in the nematic case. Non-ideality will break the complete energy degeneracy of  $K_{SmC}^{qc}$  placing some states (those near the boundary where there is less freedom to choose between different textures to minimize the non-ideal energy) slightly higher in energy so that small but finite stresses are needed to allow the elastomer to explore the complete set. The lack of a single unique state with cylindrical symmetry means that we can not be sure what the energy minimizing state is, indeed which state it is will depend on the precise functional and spatial form of the non-ideal term included, so it may depend on the chemical nature of the elastomer.

### 5.3.2 ELECTROMECHANICAL SWITCHING OF SOFT POLYDOMAIN SmC\* ELASTOMERS

Interest in SmC elastomers is mostly driven by their potential for electrical actuation. Chiral SmC\* liquids exhibit an (improper) ferroelectric polarization along the cross product of their director and layer normal [45]. Being chiral there is a twist of the tilt direction (and hence of the polarization) about  $\mathbf{k}$  on advancing along the layer normal direction. There is accordingly no macroscopic electrical polarisation unless the twist is undone by external fields or by boundary effects [19]. On crosslinking in the SmA state and cooling to the SmC\* state with domains, this twist is largely suppressed. Twist of  $\hat{\mathbf{n}}$  about  $\mathbf{k}$  means the  $\gamma_{13}$  spontaneous shear direction in eqn. (5.15) rotates from layer to layer, giving rise to elastic incompatibility. The effect of such incompatibility on texture formation has been discussed in detail in connection with mechanical switching of SmC monodomains [2].

Without twist, domains accordingly develop a net polarisation so that, when an electric field is applied, energy is minimized by domain re-orientation so that polarization is parallel to the applied field. Our inability to specify which point deep in the interior of  $K_{SmC}^{qc}$  is the lowest energy resting state of SmA monodomain genesis SmC\* poly-domains does not prevent us from analyzing their electrical actuation since the most extreme actuation is achieved by making the elastomer traverse the whole set  $K_{SmC}^{qc}$  (from boundary to boundary). If an electrical field is applied in the  $(0, 1, 0)$  direction to such a SmC poly-domain then this will cause it to form a state with its polarization vector uniformly in the  $(0, 1, 0)$  direction which it can do by forming a monodomain with its director and layer normal both in the  $(1, 0, 0) - (0, 0, 1)$  plane. The deformation of this monodomain with respect to the parent SmA state,  $\underline{\underline{\gamma}}_1$ , is of the form of eqn (5.15). If the electric field is then reversed the elastomer will flip into the opposite state which still has the director and layer normal both in the  $(1, 0, 0) - (0, 0, 1)$  plane but with the director on the other side of the layer normal so that their cross-product (and hence the polarization) is reversed. This state has a deformation with respect to the SmA

$$\underline{\underline{\gamma}}_2 = \begin{pmatrix} \gamma_{11} & 0 & -\gamma_{13} \\ 0 & 1/\gamma_{11}\gamma_{33} & 0 \\ 0 & 0 & \gamma_{33} \end{pmatrix}. \quad (5.18)$$

The full deformation undergone by the elastomer when the electric field is reversed is  $\underline{\underline{\lambda}} = \underline{\underline{\gamma}}_2 \cdot \underline{\underline{\gamma}}_1^{-1}$ , giving

$$\underline{\underline{\lambda}} = \begin{pmatrix} 1 & 0 & -2\gamma_{13}/\gamma_{33} \\ 0 & 1 & 0 \\ 0 & 0 & 1 \end{pmatrix}, \quad (5.19)$$

simply a reversal of the spontaneous shear. Since the discrepancy in energy between different states in  $K_{SmC}^{qc}$  is driven entirely by the addition of non-ideality which expected to be small, the electric fields required to perform this very large actuation will also be small — smaller than the fields used to perform similar actuations on SmC\* monodomain samples which have large non-ideal fields cross-linked into them to make them form monodomains. This suggests that SmA monodomain genesis SmC\* polydomains are probably better candidates for electrical actuation than their monodomain counterparts.

## 5.4 CONCLUSIONS

There is a fundamental difference between those polydomain liquid crystal elastomers cross-linked in a high symmetry state then cooled to a low symmetry state and those crosslinked directly in the low symmetry state. The former will be extremely soft macroscopically while the latter will be mechanically hard. We have analyzed two completely soft examples, nematic polydomains cross-linked in the isotropic state and SmC polydomains cross-linked in the SmA monodomain state and one hard example - nematic polydomains cross-linked in the nematic state. This distinction between soft and hard polydomains has not previously been appreciated, but very recent experiments confirm that it is correct [56]. The recognition of softness in some polydomain systems makes the fabrication of useful LCE soft actuators more likely since polydomains are much easier to synthesize and are not limited to thin film geometries. Our results suggest that a SmC\* polydomain cross-linked in a SmA monodomain state would be a good choice for low field electrical actuation.

LCE's are very analogous to martensitic metals since both systems exhibit symmetry-breaking transitions coupled to deformations.

In the martensitic case the symmetries that are broken are discrete whereas in LCE's they are continuous. However, drawing analogies between LCE polydomains and martensite polycrystals is quite subtle. The soft polydomain LCE's with homogeneous high temperature cross-linking states are analogous to single crystal martensite systems. However, single martensite crystals are difficult to prepare because, even if they are prepared in the high symmetry state, they are not isotropic so the crystal can form with different orientations at different points in space. This is in marked contrast to isotropic genesis LCE polydomains where, because the cross-linking state is completely isotropic, cross-linking in a spatially homogeneous state is trivial. There is no satisfactory martensite analog of cross-linking in the low symmetry polydomain state since martensite poly crystals are formed in a poly crystalline high symmetry state, so they access a stress-free high symmetry state, whereas the low symmetry cross-linked elastomers cannot. There is one, albeit rather contrived, LCE system, not analyzed here, that is directly analogous to a martensite polycrystal — an elastomer cross-linked in the SmA polydomain state then cooled to a SmC polydomain state. Such an elastomer would, on heating, return to a stress-free SmA polydomain state, and has local soft modes in the SmC state generated by the symmetry breaking SmA-SmC transition.

# Chapter 6

## EPILOGUE

I HOPE THE WORK presented in this thesis stands on its own as an advance, albeit an incremental one, in our collective understanding of liquid crystal elastomers. That said, there can be no doubt that there is much interesting work left to be done, and that this thesis raises some interesting questions that it does not answer. In this final section I will simply draw attention to those avenues which I think may be particularly fruitful in the coming years.

### 6.1 ACTUATION OF POLYDOMAIN ELASTOMERS

Although actuation of polydomain elastomers seems at first sight completely hopeless because they do not change shape when they pass through their phase transitions, in fact actuation of soft polydomains is a very real possibility. This is quite simply because, since soft polydomains can access a large range of shapes at approximately the same energy, it should be possible to move the elastomer between these shapes using external stimuli such as electric fields, magnetic fields or light. Even simpler, if a polydomain is subject to mechanical stress that causes it to stretch to the limit of the set of soft deformations then heated to the high symmetry state, it will be forced to retract back to the center of the set, forming a simple temperature-driven actuator.

Indeed, a polydomain under an external load is essentially completely equivalent to a normal semi-soft monodomain elastomer, but without the associated difficulties in the synthesis and the restriction to thin films.

## 6.2 LENGTH SCALES IN ISOTROPIC GENESIS POLYDOMAIN NEMATIC ELASTOMERS

Our analysis of polydomain nematic elastomers did not explicitly resolve the length scale of the domains. As discussed in chapter 5, the domains must form because some underlying random field, probably originating in the cross-links of the network, cause the nematic director to locally prefer one direction, and it ought to be possible to trade the gain of alignment with the random field against the costs of gradients in the director to infer a characteristic domain size. Traditionally such trade-offs are made using the celebrated Imry-Ma [38] analysis, which shows that even asymptotically weak random fields destroy long range order if the symmetry that has been broken by the ordered phase is continuous. Nematic polydomains would certainly appear to be in the Imry-Ma limit since the domains contain many many sources of disorder (cross-links), but it is unclear how to complete the analysis while retaining the condition of elastic compatibility. Comparing the results for simple Imry-Ma calculations [34, 54] with the experimental domain size of  $1\mu\text{m}$ , it is clear that the condition of elastic compatibility must considerably increase the domain size, as would be qualitatively expected since it restricts the minimization over director patterns to those director patterns consistent with elastic compatibility.

### 6.3 EXTREMELY SOFT POLYDOMAIN ELASTOMERS

Continuing with the above theme, it would also be interesting to study the microscopic origin of the  $\alpha$  term in isotropic polydomain elastomers because it might allow the design of mechanisms to soften their elasticity still further. The picture that  $\alpha$  is caused by rod-like cross-links that favor orientation of the nematic director with the cross-link suggests that point like cross-links could have a dramatic softening effect, while if we believe that the cross-linking state, although macroscopically isotropic, has local and temporal correlations that give rise to the random field in some other way, then cross-linking slowly in a very hot state may have a softening effect.

### 6.4 ELASTOMERS WITH IMPRINTED DIRECTOR PATTERNS

Historically it has not been possible to prepare elastomers that are not in either fully aligned monodomains or completely uncontrolled polydomains, but the rise of UV cross-linking techniques raises the possibility of samples cross-linked in the nematic state in which a high degree of control over the exact director pattern can be exercised. Such elastomer could be designed to be either hard or soft, depending on whether the pattern chosen corresponded to a mechanically compatible deformation, but perhaps more interestingly, they could also be prepared to undergo unusual and complex shape changes at the isotropic-nematic transition.

### 6.5 IMPRINTING OF ELECTRIC ORDER

Nematic liquids never exhibit ferro-electric order, but the individual rods can themselves have electrical and shape dipoles, so para-electric order can be forced on an nematic liquid by the application of an

external vector such as an electrical field. A nematic elastomer cross-linked by polar rod-like cross-links might be able to retain a electric order because the cross-links cannot rotate after cross-linking, leading to the formation of a rubber with a permanent electric dipole but no chiral components.

## Bibliography

- [1] J. Adams. On the polarization of chiral main-chain liquid-crystalline elastomers. *Eur. Phys. J. E*, 14(3):277–285, 2004.
- [2] J. Adams and M. Warner. Mechanical switching of ferroelectric rubber. *Phys. Rev. E*, 79:061704, 2009. doi: 10.1103/PhysRevE.79.061704.
- [3] J. M. Adams, S. Conti, and A. DeSimone. Soft elasticity and microstructure in smectic c elastomers. *J. Cont. Mech. Ther.*, 18:319, 2006.
- [4] J. M. Adams, S. Conti, A. DeSimone, and G. Dolzmann. Relaxation of some transversally isotropic energies and applications to smectic a elastomers. *Math. Models Methods Appl. Sci.*, 18:1–20, 2008.
- [5] J. M. Adams and M. Warner. Elasticity of smectic-a elastomers. *Phys. Rev. E*, 71(2):021708, Feb 2005.
- [6] R. Atkin and N. Fox. *An Introduction to the theory of elasticity*. 1980. London: Longman, 1990.
- [7] J. M. Ball. Convexity conditions and existence theorems in nonlinear elasticity. *Arch. Rational Mech. Anal.*, 63:337, 1976.
- [8] J. M. Ball and R. D. James. Fine phase mixtures as minimizers of energy. *Arch. Rat. Mech. Anal.*, 100:13, 1987.
- [9] I. Benne, K. Semmler, and H. Finkelmann. Second harmonic generation on mechanically oriented SmC\* elastomers. *Macromol. Rapid. Comm.*, 15(4):295–302, 1994.

- [10] K. Bhattacharya. *Microstructure of Martensite*. Oxford University Press, Oxford, 2003.
- [11] J. S. Biggins. Strain-induced polarization in non-ideal chiral nematic elastomers. *Proc. R. Soc. A*, 465(2105):1361, 2009.
- [12] J. S. Biggins. Textured deformations in liquid crystal elastomers. *Liquid Crystals*, 99999(1):1–18, 2009.
- [13] J. S. Biggins and K. Bhattacharya. Characterization of soft stripe-domain deformations in sm-c and sm-c\* liquid-crystal elastomers. *Phys. Rev. E*, 79(6):061705, Jun 2009.
- [14] J. S. Biggins, E. M. Terentjev, and M. Warner. Semisoft elastic response of nematic elastomers to complex deformations. *Phys. Rev. E*, 78:041704, 2008.
- [15] J. S. Biggins, M. Warner, and K. Bhattacharya. Elasticity of Polydomain Liquid Crystal Elastomers. *Arxiv preprint arXiv:0911.3513*, 2009.
- [16] J. S. Biggins, M. Warner, and K. Bhattacharya. Supersoft elasticity in polydomain nematic elastomers. *Phys. Rev. Lett.*, 103(3):037802, Jul 2009.
- [17] P. Bladon, E. M. Terentjev, and M. Warner. Transitions and instabilities in liquid crystal elastomers. *Phys. Rev. E*, 47(6):R3838–R3840, Jun 1993.
- [18] H. R. Brand. Electrochemical effects in cholesteric and chiral smectic liquid-crystalline elastomers. *Die Makromol. Chemie. Rap. Comm.*, 10(9):441–445, 1989.
- [19] N. Clark and S. Lagerwall. Submicrosecond bistable electro-optic switching in liquid crystals. *Appl. Phys. Lett.*, 36:899, 1980.
- [20] N. A. Clark and R. B. Meyer. Strain-induced instability of monodomain smectic a and cholesteric liquid crystals. *Appl. Phys. Lett.*, 22:493, 1973.

## BIBLIOGRAPHY

- [21] S. M. Clarke, A. Hotta, A. R. Tajbakhsh, and E. M. Terentjev. Effect of crosslinker geometry on equilibrium thermal and mechanical properties of nematic elastomers. *Phys. Rev. E*, 64(6):061702, Nov 2001.
- [22] S. M. Clarke and E. M. Terentjev. Slow stress relaxation in randomly disordered nematic elastomers and gels. *Phys. Rev. Lett.*, 81(20):4436–4439, Nov 1998.
- [23] S. M. Clarke, E. M. Terentjev, I. Kundler, and H. Finkelmann. Texture evolution during the polydomain-monodomain transition in nematic elastomers. *Macromolecules*, 31:4862, 1998.
- [24] S. Conti. Quasiconvex functions incorporating volumetric constraints are rank-one convex. *Journal de Mathmatiques Pures et Appliqués*, 90(1):15 – 30, 2008.
- [25] S. Conti, A. DeSimone, and G. Dolzmann. Semisoft elasticity and director reorientation in stretched sheets of nematic elastomers. *Phys. Rev. E*, 66(6):061710, Dec 2002.
- [26] P. G. de Gennes and J. Prost. *the Physics of Liquid Crystals*. Oxford University Press, USA, New York, 2nd ed. edition, 1995.
- [27] A. DeSimone and G. Dolzmann. Macroscopic response of nematic elastomers via relaxation of a class of  $\text{so}(3)$ -invariant energies. *Arch. Rational Mech. Anal.*, 161:181, 2002.
- [28] A. DeSimone and L. Teresi. Elastic energies for nematic elastomers. *Euro. Phys. J. E*, 29(2):191–204, 2009.
- [29] A. Donald, A. Windle, and S. Hanna. *Liquid crystalline polymers*. Cambridge Univ Pr, 2006.
- [30] J. L. Erickson. Continuous martensitic transitions in thermoelastic solids. *J. Therm. Stres.*, 1981.
- [31] H. Finkelmann, H. Kock, and G. Rehage. Investigations on liquid crystalline polysiloxanes 3. Liquid crystalline elastomers - a new type of liquid crystalline material. *Makromol. Chem., Rap. Comm.*, 2:317–322, 1981.

- [32] H. Finkelmann, I. Kundler, E. M. Terentjev, and M. Warner. Critical stripe-domain instability of nematic elastomers. *J. de Phys II*, 7:1059, 1997.
- [33] P. Fischer, C. Schmidt, and H. Finkelmann. Amphiphilic liquid-crystalline networks-phase behavior and alignment by mechanical fields. *Macromol. Rapid. Comm.*, 16(6):435–447, 1995.
- [34] S. V. Fridrikh and E. M. Terentjev. Polydomain-monodomain transition in nematic elastomers. *Phys. Rev. E*, 60(2 Pt B):1847, 1999.
- [35] E. Fried and S. Sellers. Incompatible strains associated with defects in nematic elastomers. *The Journal of Chemical Physics*, 124:024908, 2006.
- [36] L. Golubovic and T. C. Lubensky. Nonlinear elasticity of amorphous solids. *Phys. Rev. Lett.*, 63:1082, 1989.
- [37] K. Hiraoka, W. Sagano, T. Nose, and H. Finkelmann. Biaxial shape memory effect exhibited by monodomain chiral smectic C elastomers. *Macromolecules*, 38(17):7352–7357, 2005.
- [38] Y. Imry and S. Ma. Random-field instability of the ordered state of continuous symmetry. *Phys. Rev. Lett.*, 35(21):1399–1401, 1975.
- [39] I. Kundler and H. Finkelmann. Strain induced director reorientation in nematic single crystal elastomers. *Macromol. Chem. - Rapid Comm.*, 16:679, 1995.
- [40] I. Kundler and H. Finkelmann. Director reorientation via stripe-domains in nematic elastomers: influence of cross-link density, anisotropy of the network and smectic clusters. *Macromol. Chem. Phys.*, 199:677, 1998.
- [41] J. Küpfer and H. Finkelmann. Nematic liquid single crystal elastomers. *Makromol. Chem. Rap. Comm.*, 12(12):717, 1991.

## BIBLIOGRAPHY

- [42] J. K  pfer and H. Finkelmann. Liquid crystal elastomers: Influence of the orientational distribution of the crosslinks on the phase behaviour and reorientation process. *Makromol. Chem. Phys.*, 195:1353, 1994.
- [43] L. Landau and E. Lifshitz. *Elasticity theory*. 1967.
- [44] A. Menzel, H. Pleiner, and H. Brand. Response of pre-stretched nematic elastomers to external fields. *Euro. Phys. J. E*, 30(4):371–377, 2009.
- [45] R. Meyer, L. Liebert, L. Strzelecki, and P. Keller. Ferroelectric liquid crystals. *J. de Phys. Lett.*, 36:L69, 1975.
- [46] E. Nishikawa and H. Finkelmann. Smectic-a liquid single crystal elastomers - strain induced break-down of smectic layers,. *Macromol. Chem. Phys.*, 200:312–322, 1999.
- [47] E. Nishikawa, H. Finkelmann, and H. R. Brand. Smectic A liquid single crystal elastomers showing macroscopic in-plane fluidity. *Macromol. Rap. Comm.*, 18(2):65–71, 1997.
- [48] P. Olmsted. Rotational invariance and goldstone modes in nematic elastomers and gels. *J. Phys. II (France)*, 4:2215, 1994.
- [49] R. Pelcovits and R. Meyer. Piezoelectricity of cholesteric elastomers. *J. Phys. II France*, 5:877–882, 1995.
- [50] A. Petelin and M.   opi  . Observation of a soft mode of elastic instability in liquid crystal elastomers. *Phys. Rev. Lett.*, 103(7):077801, Aug 2009.
- [51] O. Stenull and T. C. Lubensky. Unconventional elasticity in smectic-*a* elastomers. *Phys. Rev. E*, 76(1):011706, Jul 2007.
- [52] E. Terentjev and M. Warner. Piezoelectricity of chiral nematic elastomers. *Eur. Phys. J. B*, 8(4):595–601, 1999.
- [53] E. M. Terentjev. Phenomenological theory of non-uniform nematic elastomers: Free energy of deformations and electric-field effects. *Europhys. Lett.*, 23(1):27, 1993.

- [54] N. Uchida. Soft and nonsoft structural transitions in disordered nematic networks. *Phys. Rev. E*, 62(4):5119–5136, 2000.
- [55] K. Urayama, S. Honda, and T. Takigawa. Deformation coupled to director rotation in swollen nematic elastomers under electric fields. *Macromolecules*, 39(5):1943–1949, 2006.
- [56] K. Urayama, E. Kohmon, M. Kojima, and T. Takigawa. Polydomain- monodomain transition of randomly disordered nematic elastomers with different cross-linking histories. *Macromolecules*, 42:4084, 2009.
- [57] G. Verwey and M. Warner. Soft rubber elasticity. *Macromolecules*, 28:4299–4302, 1995.
- [58] G. Verwey and M. Warner. Compositional fluctuations and semisoftness in nematic elastomers. *Macromolecules*, 30(14):4189–4195, 1997.
- [59] G. Verwey and M. Warner. Nematic elastomers cross-linked by rigid rod linkers. *Macromolecules*, 30(14):4196–4204, 1997.
- [60] G. C. Verwey, M. Warner, and E. M. Terentjev. Elastic instability and stripe domain in liquid crystalline elastomers. *J. Phys. II France*, 6:1273–1290, 1996.
- [61] M. Warner, P. Bladon, and E. M. Terentjev. Soft elasticity-deformation without resistance in liquid crystal elastomers. *J. Phys. II (France)*, 4:93, 1994.
- [62] M. Warner, K. Gelling, and T. Vilgis. Theory of nematic networks. *J. Chem. Phys.*, 88:4008, 1988.
- [63] M. Warner and E. M. Terentjev. The coupling of chiral chains to mechanical distortions in elastomers. *Proc. R. Soc. A*, 455(1990):3629–3644, 1999.
- [64] M. Warner and E. M. Terentjev. *Liquid Crystal Elastomers*. Oxford University Press, Oxford, 2nd ed. edition, 2007.

## BIBLIOGRAPHY

- [65] F. Ye and T. C. Lubensky. Phase diagrams of semisoft nematic elastomers. *J. Phys. Chem. B*, 113(12):3853–3872, 2009.
- [66] F. Ye, R. Mukhopadhyay, O. Stenull, and T. C. Lubensky. Semisoft nematic elastomers and nematics in crossed electric and magnetic fields. *Phys. Rev. Lett.*, 98(14):147801, 2007.